SCALE EFFECTS ON CAVITATION

by

Swamy Sundaram, B.E.(Hons.)

Thesis submitted for the degree of Ph.D.
to the Faculty of Engineering,
The University of Glasgow.

March, 1966.

WATER

Nothing is lovelier than moving water,
The diamond element, innumerable jewel,
Brittle and splintering under the sharp sun,
Yet softer than doves' feathers, and more smooth
Than down of swan.
Nothing is lovelier than water lying still,
When the Moon takes that stillness for her glass.

- Gerald Bullett (1957)

ACKNOWLEDGEMENTS

The Author's thanks are extended to Professor T.R.F. Nonweiler, Dr. A.S. Thom and Mr. P.H. Tanner of the Department of Aeronautics and Fluidmechanics for their advice and encouragement throughout the present work.

The Author wishes to record his thanks and deep appreciation to Mr. P.H. Tanner for his invaluable help in assembling the apparatus. He would also like to express his gratitude to the Commonwealth Scholarship Commission in the United Kingdom for having granted him a Scholarship to pursue further studies.

ABSTRACT

Scale effects on cavitation can broadly be defined as the deviations from the classical law of similarity of cavitation. The classical similarity law takes into consideration only pressure and inertia forces of the flow, while cavitation is a complex phenomenon involving hydrodynamic aspects of fluid flow, molecular forces and thermodynamic properties of the fluid. The scale effects on cavitation are therefore classified under three headings:-

(a) Scale effects on the minimum pressure that occurs in the flow;

(b) Scale effects on the inception of cavitation;

(c) Scale effects on the growth of cavitation bubbles.

In his work the author has collected all the available information to date on scale effects on cavitation under the above-mentioned classifications.

It appears, besides many other factors, that the cavitation parameter is a function of Reynolds, Froude and Prandtl numbers. In order to analyse the effect of Prandtl number on cavitation, a cavitation rig without a resorber was designed and erected. Cavitation experiments were done on a valve which was primarily designed to dissipate the pressure generated by the centrifugal pump of the circuit. Aqueous solutions of pluracol V-10 of different concentration were used as the working media. Various properties of pluracol V-10 solutions such as

viscosity, specific heat, conductivity were obtained experimentally. There is some experimental evidence to conclude qualitatively that the tendency of the fluid to cavitate decreases with increasing Prandtl number.

NOMENCLATURE

A	Area of cross-section normal to the direction of flow.
a	Velocity of propagation of pressure wave in a fluid.
a_1, a_2	Numerical constants.
al	Area of cross-section.
av	Effective area of vapour removal.
C	Temperature coefficient for determining changes in the enthalpy of the liquid during vaporisation.
Cpl	Specific heat of a fluid.
C_H	Heat transfer coefficient.
C_Q	Volume entrainment coefficient.
D	Characteristic dimension of model or structure.
d	Diameter of cavitation nuclei
F	Froude number.
H	Pressure head across a hydraulic machinery.
Hsv	Suction head above vapour pressure.
h	Pressure head or height of roughness as the case may be
K, K_d	Desinent cavitation number.
K_i	Incipient cavitation number.
K_M	Thoma's cavitation number for a hydraulic machine.
k	Thermal conductivity of a fluid.
L	Loss of head across the valve.
l	Valve travel.
M	Mach number.
N	Speed of pump shaft or number of gram mols as the case may be.
p	Static pressure.

p_v, p_1, p_2	Vapour pressure of fluid.
Pr	Prandtl number $= (\frac{C_{pl}.\mu}{k})$
R	Reynolds number or radius of bubble.
S	Suction specific speed.
T	Absolute temperature.
V	Velocity of flowing fluid.
vg	Specific volume of saturated vapour.
vl	Specific volume of liquid.
W	Weber number.
Z	Axial length of conical section of the valve.
z	Height of elevation with respect to a fixed datum.
α	Air content of water (expressed as ml/l, reduced to 0°C and 760 mm. pressure).
α_s	Air content of fully saturated water at atmospheric conditions.
δ	Local boundary layer thickness.
θ	Semi-angle of cone.
λ	Latent heat of vaporisation.
μ	Absolute viscosity of a fluid.
ν	Kinematic viscisity of a fluid.
ρ	Mass density of a fluid.
σ_i	Cavitation number of turbine.
σ_s	Surface tension of liquid.
ϕ	A function of design and operating point of a pump.

Suffixes and other symbols are explained as they occur in the text.

CONTENTS

CHAPTER 1

CAVITATION IN GENERAL

1.1 Introduction.

In the last twenty years, no other aspect of hydraulic machinery design and operation has received as much attention as cavitation. Cavitation is a complicated phenomenon involving hydrodynamic and thermodynamic aspects, and even today it escapes thorough understanding. In order to cope with the problem of cavitation in hydraulic machines, experimental and theoretical studies are carried out universally on hydrodynamic machines such as pumps and on apparatus without moving parts such as venturi-shaped bodies in water tunnels[1,2,3]. The amount of knowledge available on cavitation today is immense.

1.2 The Phenomenon of Cavitation.

Cavitation, in general, is a dynamic phenomenon controlled by hydrodynamics of flow and the thermodynamic properties of the fluid. Cavitation is broadly defined as the local vaporization of liquid due to local pressure reductions. In general a liquid is said to cavitate when vapour or gas-filled bubbles are formed while under motion. The bubbles thus formed move from low pressure to high pressure zones of hydraulic machinery and implode, generating high pressure waves. These high pressure waves impinge violently on the walls or vanes of the

hydraulic machinery, thereby producing noise, vibration, erosion and deterioration in hydraulic performance.

1.3 Aim of the present work.

Model testing is becoming increasingly important as the sizes of the prototype machines are growing bigger. Further, since water is available in abundance and at low cost, the hydraulic models are being tested with water and the results are being extrapolated or deducted for fluids other than water. Hence, the aim of the present work is to review the literature available today on scale effects on cavitation and to conduct some experiments with water and solutions of water with a viscosity additive in order to observe the scale effects produced by the thermodynamic properties of fluid.

The original idea was to conduct these experiments on a medium sized centrifugal pump and hence a small 4 in. cavitation-rig was set up, with a non-cavitating valve to dissipate the head developed by the pump. But unfortunately, the non-cavitating valve started cavitating before the pump did and therefore the so-called non-cavitating valve was used as the device for producing cavitation.

CHAPTER 2

PRESENT DAY THEORY OF CAVITATION INCEPTION

2.1 Tension in Liquids.

It has been proved theoretically and experimentally that "pure liquids" can sustain tension for a short time. But the estimates of tensile strength of liquids, based on the assumption of simultaneous separation of all atomic bonds, give very high values which do not at all correspond with experimental results[4,5]. The experimental data have been reciewed by Temperley and Chembers[4]. They point out clearly the discrepancies between the results of different workers. Further they add that there are good reasons to neglect the extremes values and using their experimental values, they conclude that the tensile strength of water in presence of glass is equivalent to about 30 to 50 atmospheres; for water in presence of steel it is about 2 atmospheres minimum and 23 atmospheres maximum. R.M. Davies et al[6], by using "double-piston" method and "pressure bar" method arrive at an average value of about 10 atmospheres for water.

2.2 "Nuclei" or "weak-spots" in liquid

However, when a liquid is subjected to tension, it is in a meta-stable condition and bubbles are observed to grow from extremely small nuclei, submicroscopic in size. It is now generally well- established

theory that the inception of cavitation in liquids is triggered by the nuclei containing vapour, undissolved gas or both. These nuclei are present either within the liquid or on suspended particulate matter or in crevices on bounding walls. Existence of such nuclei has been demonstrated experimentally[7,8]. Further, tensile strengths of liquids calculated from nucleation theory agree satisfactorily with the maximum experimental values[9]. Using the fact that air cavities present in water absorb sound energy, M. Strasberg[10] has made some measurements using an ultrasonic device and suggests the following:

N_R is the smallest number of delectable bubbles per cm^3 of water with radii ranging from $\frac{1}{2}$ to $\frac{3}{2}$ R_f where R_f is the radius of resonant bubble.

Frequency (kc/sec)	R_f (cm)	N_R
150	2.2×10^{-3}	1 bubble/200 cm^3
250	1.3×10^{-3}	1 bubble/30 cm^3
550	6×10^{-4}	1 bubble/2 cm^3
1100	3×10^{-4}	8 bubbles/cm^3

2.3 Stability and Growth of Nuclei

2.3.1 Even though it is well established that the nuclei present in liquids are responsible for the inception of cavitation, there is still some difficulty in establishing their presence and stability.

If there is pressure balance between the pressure p' within the bubble and the pressure p outside it, then

$$p' = p + \frac{2\sigma_s}{R} \qquad (2.3.1)$$

where R is the radius of the bubble and σ_s is the surface tension. The pressure p' inside the bubble is the sum of vapour pressure p_v of the liquid and partial pressure p_g of entrained gas. From the above equation one can derive the minimum value of $p - p_v = p_{min.}$ occurring at a radius

$$R_{min} = \frac{-4\sigma_s}{3(p - p_v)} \qquad (2.3.2)$$

One can further observe that the critical pressure to trigger cavitation is below vapour pressure and if the pressure p is slightly decreased, the bubble being unstable would grow without bounds. When the bubble is stable, it will dissolve by diffusion of air into the surrounding liquid[11]. The effect of surface tension should be nullified in some way in order that these nuclei can exist. Eisenberg[7] suggests that these nuclei are stabilized on microscopic dust particles present in liquids or on the crevices present on bounding walls. Another hypothesis is that an organic skin formed by the contaminants in liquid stabilizes the bubble. Further experiments in this field are highly desirable.

2.3.2 Theoretical and experimental analysis of growth of a nucleus is very complicated. Rayleigh (1917) examined theoretically the behaviour of an incompressible fluid in which he imagined a spherical void to be suddenly formed. In his analysis however, he neglected the surface tension effects and the pressure of liquid vapour in the bubble. More recently Noltingk and Neppiras[12], Plesset et al[13,14] have analysed the

growth of nuclei taking into consideration viscous effects, surface tension and thermal effects. A bubble may grow to visible size in two ways (a) by the relatively slow diffusion of dissolved air out of the liquid into the nucleus or (b) by its sudden explosive expansion into a large cavity. The former process is generally called "gaseous cavitation" while the latter is known as "vaporous cavitation". In fact the bubble may grow by gaseous diffusion and evaporation of the liquid. It is possible that a nucleus originally too small to undergo vaporous cavitation at the existing pressure could grow by gas diffusion until it became large enough to trigger vaporous cavitation. Strasberg[10] has treated the growth of a bubble by gaseous diffusion and vaporous cavitation separately and his results are shown in Fig.2.3.2.1. It may be concluded from the work of Notlingk and Neppiras[12] that inception of growth of nuclei depends only slightly on the duration of pressure while the maximum size to which nuclei will grow depends upon duration of pressure application. Plesset[13] treats the growth of a nucleus as the growth of a vapour bubble in superheated liquid. The factors which affect the rate of bubble growth are the surface tension, the liquid inertia and the pressure difference between the pressure within the bubble and the ambient pressure. He concludes that the initial growth of the bubble will be slow but is accelerated with increase in size because of the reduction in surface tension. When the rate of bubble growth becomes appreciable the temperature and hence the pressure within the bubble drops and the rate of growth is decreased. The reduction of the temperature within the bubble is a consequence of

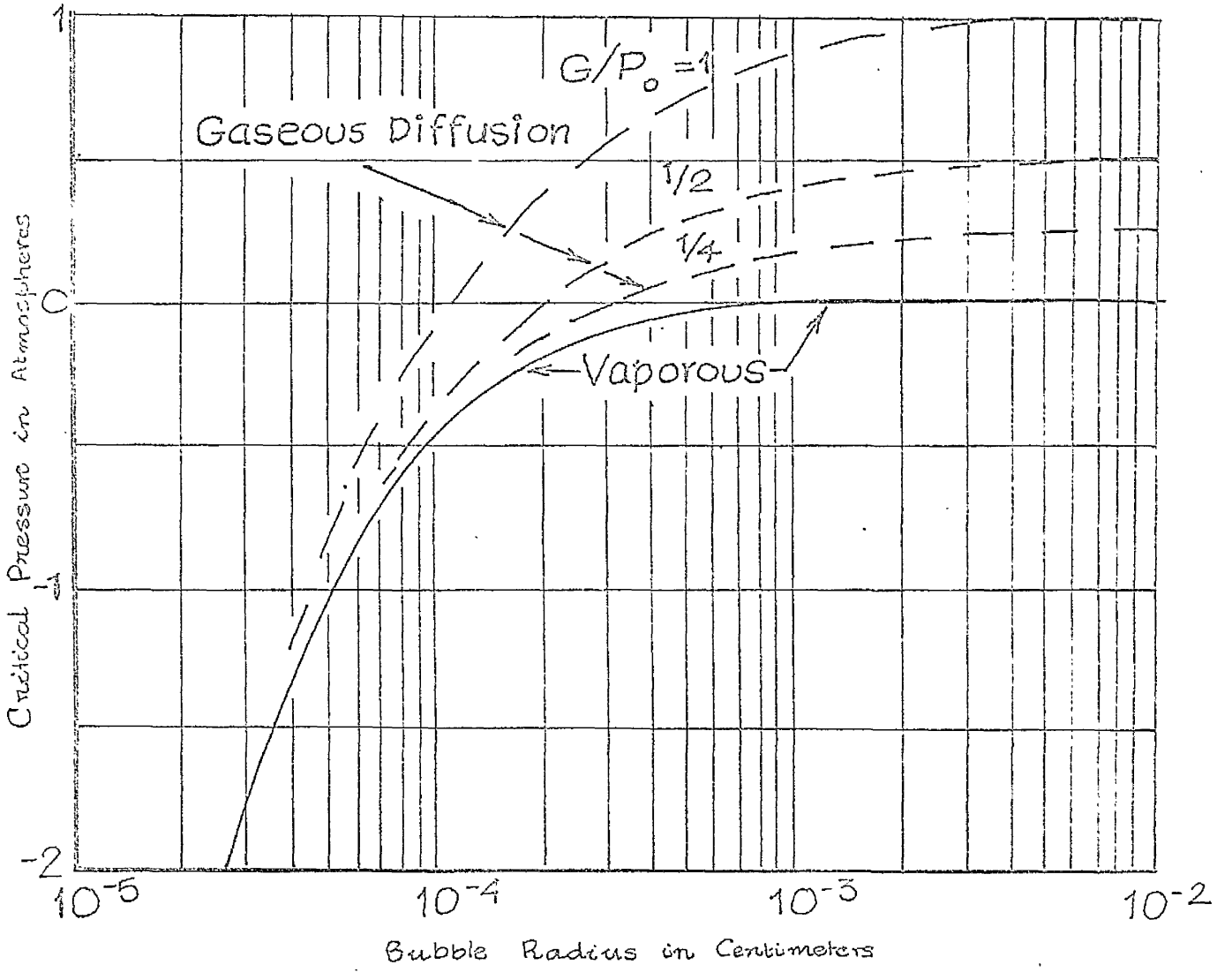

FIG 2.3.2.1. The Critical pressure for cavitation as a function of the radius of air bubble nucleus The indicated values of critical pressure are relative to vapour pressure so that zero corresponds to vapour pressure. G/P_o is the ratio of gas saturation pressure to ambient pressure. (After Strasberg).

the latent heat requirement of the evaporation which takes place at the vapour-liquid interface as the bubble grows. Plesset and Zwick[13] have calculated the growth of vapour bubbles by taking into account approximately the heat transfer in a small "boundary layer" at the bubble wall. Their theory compares very favourably with experiments done by Dergarabedian[15]. Figs. 2.3.2.2 and 2.3.2.3 show some of their results.. One can observe that the effect of local cooling around the bubble in retarding growth is marked.

2.4 Cavitation Number

It is generally assumed that cavitation starts in fluid when the minimum pressure at any point reaches the vapour pressure p_v of the liquid corresponding to the ambient temperature. In a flowing liquid the parameter which describes the pressure conditions for similarity for cavitating flow is called cavitation number or cavitation parameter. If p_o denotes the static pressure and Vo the uniform flow velocity of the liquid at a great distance from the cavitating body, then the general character of the flow in so far as cavitation is concerned is expressed by the cavitation parameter

$$K = \frac{p_o - p_v}{\frac{1}{2} \rho V_o^2} \qquad (2.4.1)$$

where ρ is the mass density of the flowing fluid. But usually, in order to avoid the friction losses that occur in flowing liquid, p_o and Vo are replaced by the pressure p_m which is the minimum pressure measurable along the cavitating body or structure and the corresponding velocity at that point. Hence equation (2.4.1) becomes

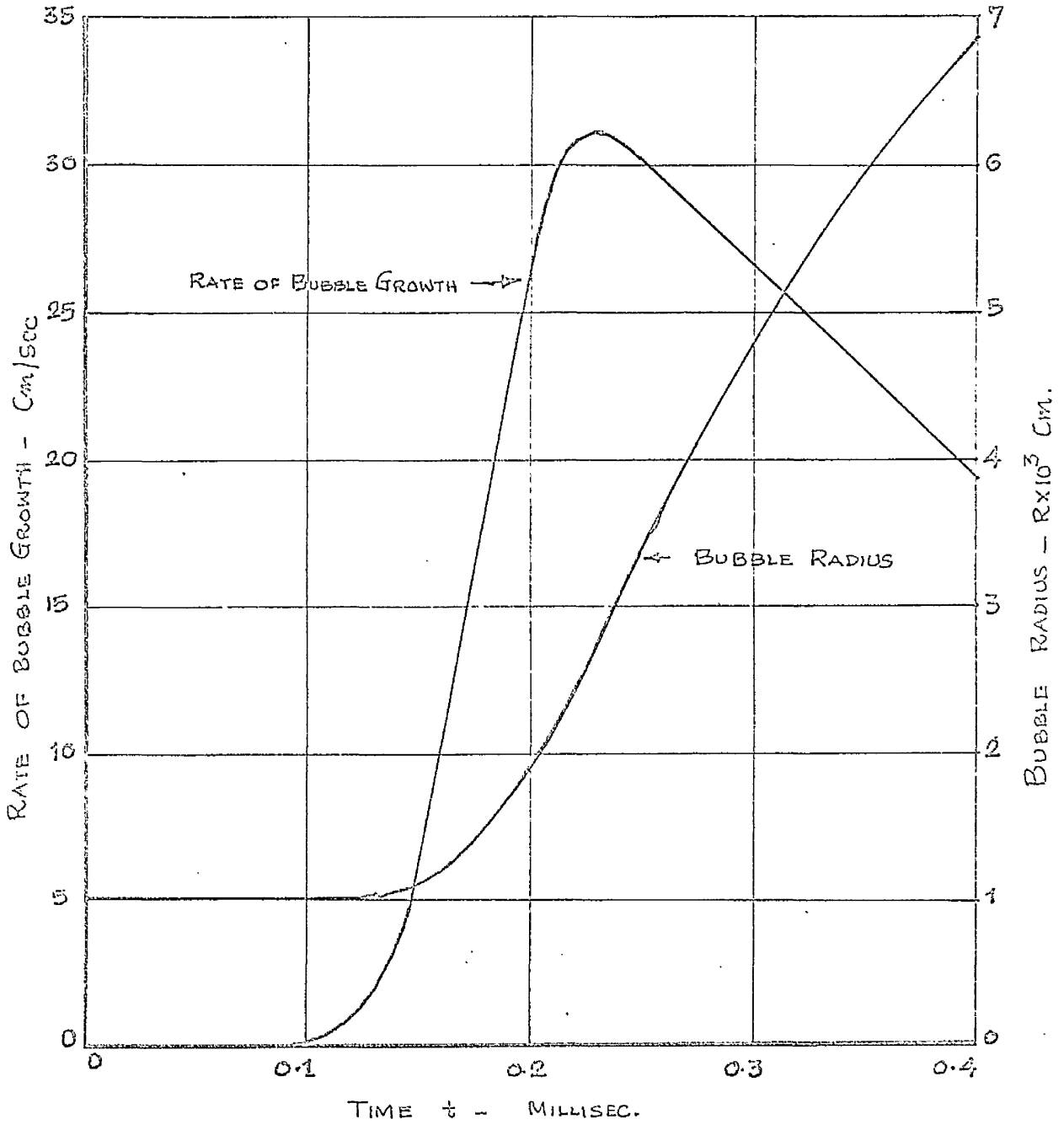

FIG. 2.3.2.2. Theoretical radius and radial velocity curves for the growth of a pure vapour bubble in water at 1 atm. external pressure, superheated to 103°C. (After Plesset)

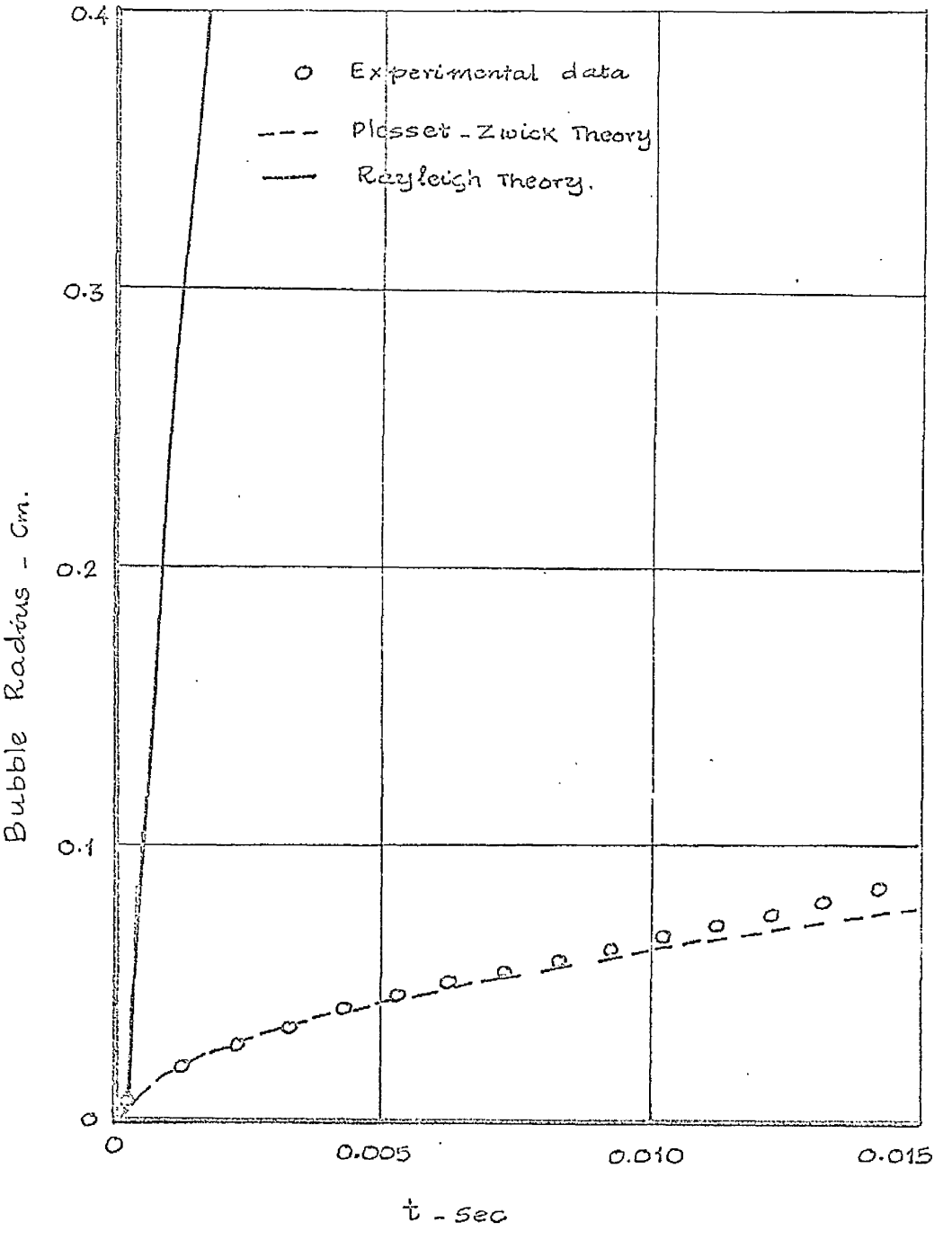

FIG. 2.3.2.3. Effect of heat transfer on bubble growth. Comparison of theoretical bubble radius - time values with experimental values for water at 1 atm. external pressure, superheated to 105.1°C. (After Dergarabedian).

$$K = \frac{p_m - p_v}{\frac{1}{2} \rho V^2} \qquad (2.4.2)$$

where p_m is the minimum observed pressure and V is the velocity of the fluid at the point where minimum pressure is measured.

In the present work, the author has used only the equation (2.4.2). The pressure distribution along the valve was obtained and the minimum pressure p_m measured; the corresponding velocity V was used to calculate the cavitation parameter K.

CHAPTER 3

SCALE EFFECTS ON CAVITATION

3.1 The Classical Cavitation Number

As mentioned in the previous chapter, the most elementary relationship between the velocities, pressures and fluid properties pertaining to cavitation is the equation (2.4.2) which states that the cavitation number

$$K = \frac{p_m - p_v}{\frac{1}{2}\rho V^2} = \text{constant} \qquad (3.1.1)$$

where p_m is the minimum measured pressure in the flow in the cavitating structure or past the object, V is the velocity at the corresponding point, p_v is the vapour pressure of the liquid at the ambient temperature and ρ is the mass density of the fluid.

The above equation can be modified to suit hydrodynamic machines, Thoma's law of similarity for cavitation is given by

$$K_M = \frac{Hsv}{H} = \text{constant} \qquad (3.1.2)$$

where H is the total head across the machine and Hsv is its total suction head above vapour pressure. Thus the classical theory expressed by equations (3.1.1) and (3.1.2) states that the form and extent of cavitation voids will be similar if and only if the cavitation parameter K or Thoma's number K_M have the same values for the two flows compared or the two hydrodynamic machines compared. Generally speaking,

so far this classical cavitation parameter has served very well but still we are unable to predict accurately the cavitation characteristics of the prototype from model tests. Research workers and designers in this field have observed in the past some significant departures from the classical law of similarity for cavitation. Since cavitation is a complicated phenomenon, involving the hydrodynamic aspects of the flow and the fluid properties such as number of nuclei present, their size and distribution, vapour pressure, latent heat, termperature, viscosity, surface tension, thermal conductivity and specific heat of the fluid, one can clearly observe the inadequacy of the classical similarity law of cavitation which takes into consideration only pressures and velocities. Nevertheless, the cavitation parameter K has been very useful till today and at present many research workers in various research laboratories throughout the world are trying to find out "the scale effects on cavitation".

Scale effects on cavitation are broadly defined as the departures from the classical similarity relation expressed by equation (3.1.1) when the model size, flow velocity and fluid properties are changed. In spite of the growing knowledge and understanding of the physics of the process of cavitation, the treatment is still far from quantitative. When we extrapolate model test results to prototype conditions, such as rivers or the oceans or fluids other than water, so little is known about the size and number of nuclei available which are extremely responsible for cavitation. Further, we know that the thermodynamic properties of the fluid such as latent heat, specific heat, thermal

conductivity are also important factors governing the process of cavitation, yet we are unable to express their effects quantitatively. Although today we have elaborate theory and the differential equations for the bubble growth, it appears that no useful scaling laws can be derived. A review of the literature available to date on scale effects in cavitation is given below.

3.2 Scale Effects on Cavitation.

3.2.1 Departures or deviations from the classical law of similarity as expressed by equation (3.1.1) are defined as Scale Effects on Cavitation and so it is worthwhile to analyse the fundamental assumptions on which the above law of similarity is based. These are[16] as follows:-

(a) All other forces except inertia forces are neglected or assumed negligible. The pressure differences in the flow of fluid are proportional to inertia forces i.e. proportional to ρv^2. Besides, the effect of surface irregularities are neglected or the geometric similarity is automatically assumed to include surface irregularities of the cavitating structures or models.

(b) In spite of the fact that many research workers have observed tension in liquid before cavitation started, it is assumed that the pressure at which the cavitation begins is the vapour pressure of the liquid corresponding to the ambient temperature.

(c) Cavitation is assumed basically to be vaporisation of the liquid and hence cavitation takes place instantaneously as soon as the pressure drops down to the vapour pressure. All "the time effects" or "the delay'

is neglected.

(d) Although it is well known today that the nuclei present in a liquid are responsible for the inception of cavitation, and their size and distribution vary from one fluid to the other, the classical law of similarity assumes the effect of nuclei in all liquids is the same.

The above mentioned assumptions, strictly speaking, are not really valid, since the first assumption completely neglects the friction, gravity and viscous forces which exist in flow of real fluids. In other words it is based on flow of "ideal fluid". The remaining assumptions are connected with the mechanism of cavitation inception which even today is not thoroughly understood.

3.2.2 General Classification of Scale Effects.

Scale effects on cavitation can broadly be classified into three categories, as follows:

(1) Scale effect on the flow: These are the hydrodynamic factors which are responsible for the minimum pressures that occur in the flow of fluid.

(2) Scale effect on inception of cavitation: These are the effects produced by microscopic nuclei present in the fluid which are responsible for the inception of cavitation.

(3) Scale effect on the growth of cavitation bubbles: These are the thermodynamic factors which are responsible for the rate of growth of cavitation bubbles and the maximum size to which they can grow.

In the following pages, the author discusses the above classificati

in detail with the results published by the other workers in this field.

3.3 Scale Effects on the Flow:

Considering the flow of fluid in which cavitation is about to start or just at the point of inception of cavitation, one can assume that the pressure distribution along the structure or model is the same as that which exists in a non-cavitating flow. From hydrodynamic principles the following laws of similarity governing the minimum pressure can be derived.

3.3.1 In order to maintain the same ratio of inertia to viscous forces, the Reynolds number must be kept constant, i.e.

$$R = \frac{V.D}{\nu} = \text{Constant} \qquad (3.3.1)$$

where V is the velocity of the flow, D is characteristic dimension and ν is the kinematic viscosity of the fluid. Kermeen et al[17] and Holl[16] in their papers discuss in detail the effect of Reynolds number. Kermeen et al come to the conclusion from their experimental results that the incipient cavitation number varies with free stream velocity and model scale. For smooth, streamlined bodies the incipient cavitation number increases with model size and free stream velocity. Further they add that the incipient cavitation number approaches the magnitude of minimum pressure coefficient on the body tested. The Fig.3.3.1.1 shows the variation of incipient cavitation number with Reynolds number for three symmetrical Joukowski Hydrofoils tested by them. Fig.3.3.1.2 shows the

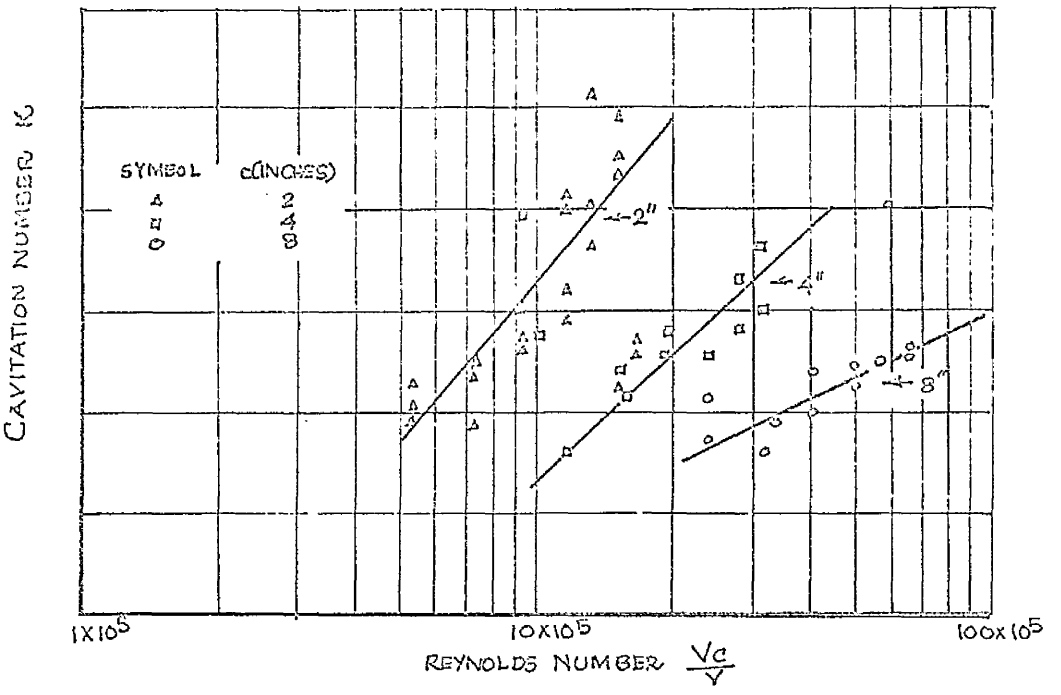

FIG. 3.3.1.1. Cavitation Number Versus Reynolds number for three Symmetrical Joukowski Hydrofoils (After Parkin)

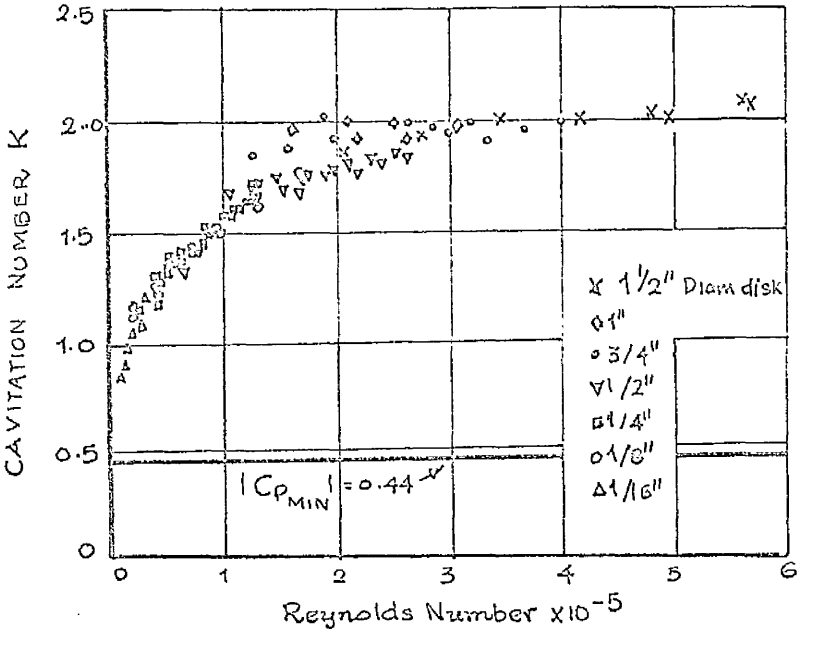

FIG. 3.3.1.2. Cavitation number Versus Reynolds number for a series of disks (After Parkin)

variation of cavitation number with Reynolds number for various sharp-edged disks tested. They conclude that for their disk experiments, the incipient cavitation number did not approach any limiting value as the Reynolds number was increased and the incipient cavitation number was always greater than the magnitude of minimum pressure coefficient on the body. It is relevant to mention here that the term "incipient cavitation number", as used by Kermeen et al, is defined as the state of liquid flow at which cavitation just disappears or at which small wisps of cavitation are seen only intermittently as the static pressure of the system is slowly increased at constant free-stream velocity.

Holl and Wislicenus[16] come to the conclusion in their paper that there exists a most distinct difference between cavitation attached to the surface of a body and cavitation away from the wall and/or travelling with the flow. Surface attached cavitation shows an increase in cavitation number with increasing Reynolds number while travelling cavitation or cavitation away from a solid wall shows an increase in cavitation number with increasing size and either slower increase or no change or a decrease with increasing velocity or Reynolds number. This particular character of not-attached or travelling cavitation, Holl and Wislicenus conclude, may be explained by the effect of a limited number of nuclei plus the effect of a characteristic velocity of cavitation, Vc, which increases slower than the free stream velocity V. Fig.3.3.1.3 shows the decrease in cavitation number for a cavitation process away from the wall.

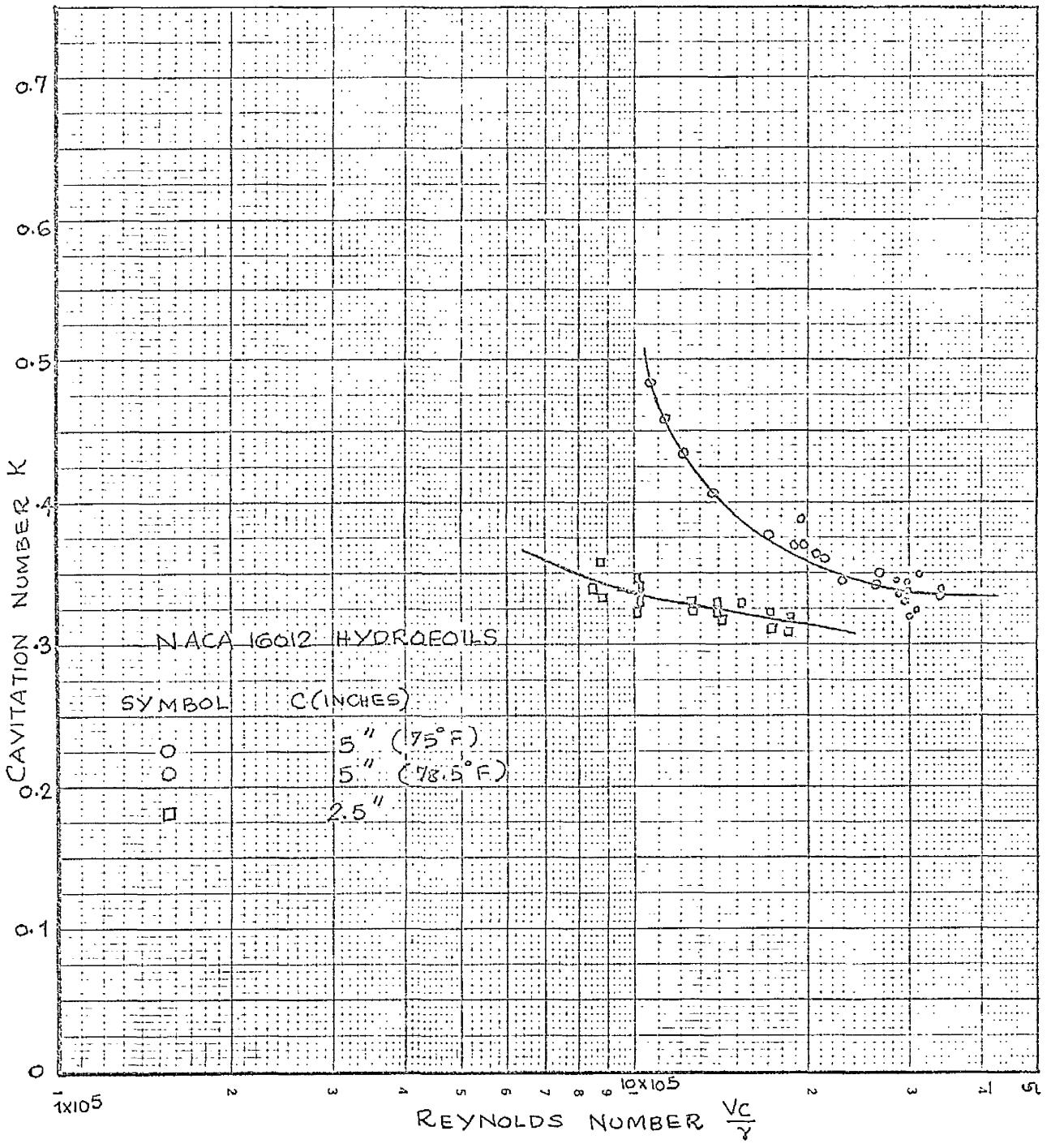

FIG. 3.3.1.3. Cavitation Number as a function of Reynolds number (After Holl)

3.3.2 In order to maintain the same ratio of inertia to gravitational forces, the Froude number must be kept constant

$$F = \frac{V}{\sqrt{gD}} = \text{Constant} \qquad (3.3.2)$$

Till today there are no available experimental results showing the effect of Froude's number. However, Gerber in his paper[18] discusses the relative importance of maintaining the same Froude's number between the model and the prototype tests, especially pertaining to cavitation. Fig.3.3.2.1. is taken from Gerber's paper and it shows a pronounced effect of test head H on efficiency. In this figure, the cavitation parameter K is defined as follows:-

$$K = \frac{H_B - Hd - Hs}{H} \qquad (3.3.2a)$$

where H_B is the atmospheric pressure, Hd is the vapour pressure of water at the corresponding temperature, Hs is the static suction head for the machine and H is the total or net head across the machine. In the particular case shown in the figure (3.3.2.1), it seems that the full scale turbine was installed using the cavitation tests results under H = 22.5 metres, But the full scale turbine of more than 1000 h.p. gave unsatisfactory results under full load. The only explanation was the occurrence of cavitation. The model test was then repeated with a head of 10 metres which showed clearly that the fall in efficiency due to cavitation was feasible.

Pierre Danel and Jacques Duport[21] have presented a valuable discussion of various considerations applying to model testing of large hydrodynamic machinery, pertaining to cavitation. Regarding turbine

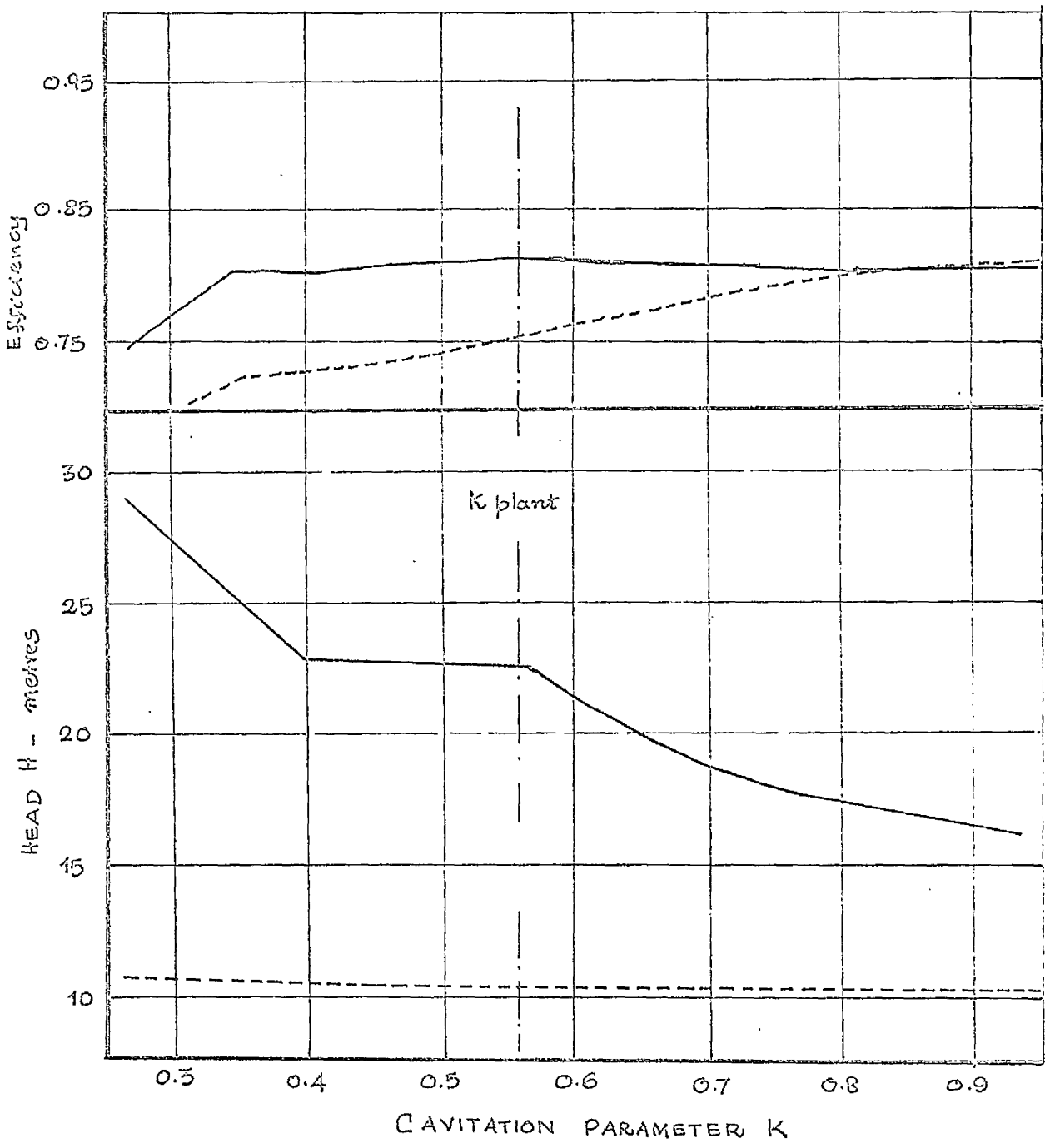

FIG. 3.3.2.1. Efficiency as a function of K.
Pronounced effect of test head H on efficiency.
(After Gerber).

model testing for cavitation, they derive the following equation relating cavitation number σ_i with pressure heads of the machine:-

$$\left(\frac{h - h_{cr}}{H}\right) = \sigma_i - Z\left(D/H\right) - Km(Z) \qquad (3.3.2.1)$$

where h is the absolute pressure head at the point under consideration; h_{cr} is the critical pressure head at which cavitation starts; $\sigma_i = \frac{h_a - h_s - h_{cr}}{H}$ is the plant cavitation number, where h_a is the atmospheric pressure head, h_s suction head, H is the total head across the machine $Z = z/D$ is the relative elevation of the point under consideration with respect to the runner diameter D and Km is a factor which depends upon the operating conditions of the turbine and upon the location of the point under consideration. They further conclude that the factor $\frac{h - h_{cr}}{H}$ can be expressed as the difference between the ordinates of the straight line Δ (Fig.3.3.2.2) with equation $y = \sigma_i - Z\left(D/H\right)$ which depends only on σ_i and D/H and the ordinates of the curve $y = Km\,(Z)$ which depends only on the design of the turbine and conditions under which it operates. From Fig. (3.3.2.2), it can be seen the limiting value of σ_i is the value at which $y = \sigma_i - Z\left(D/H\right)$ is tangent to the curve Km (Z). From this, they conclude that, for turbines having the same design and operating conditions, the critical value of cavitation number $\sigma_{i_{cr}}$ will be the same only if the values of $\left(H/D\right)$ are equal and hence it is necessary to conform to the Froude similitude conditions. However, there exist many practical disadvantages of applying the Froude similitude criterion to scale model tests of hydraulic turbines such as the very

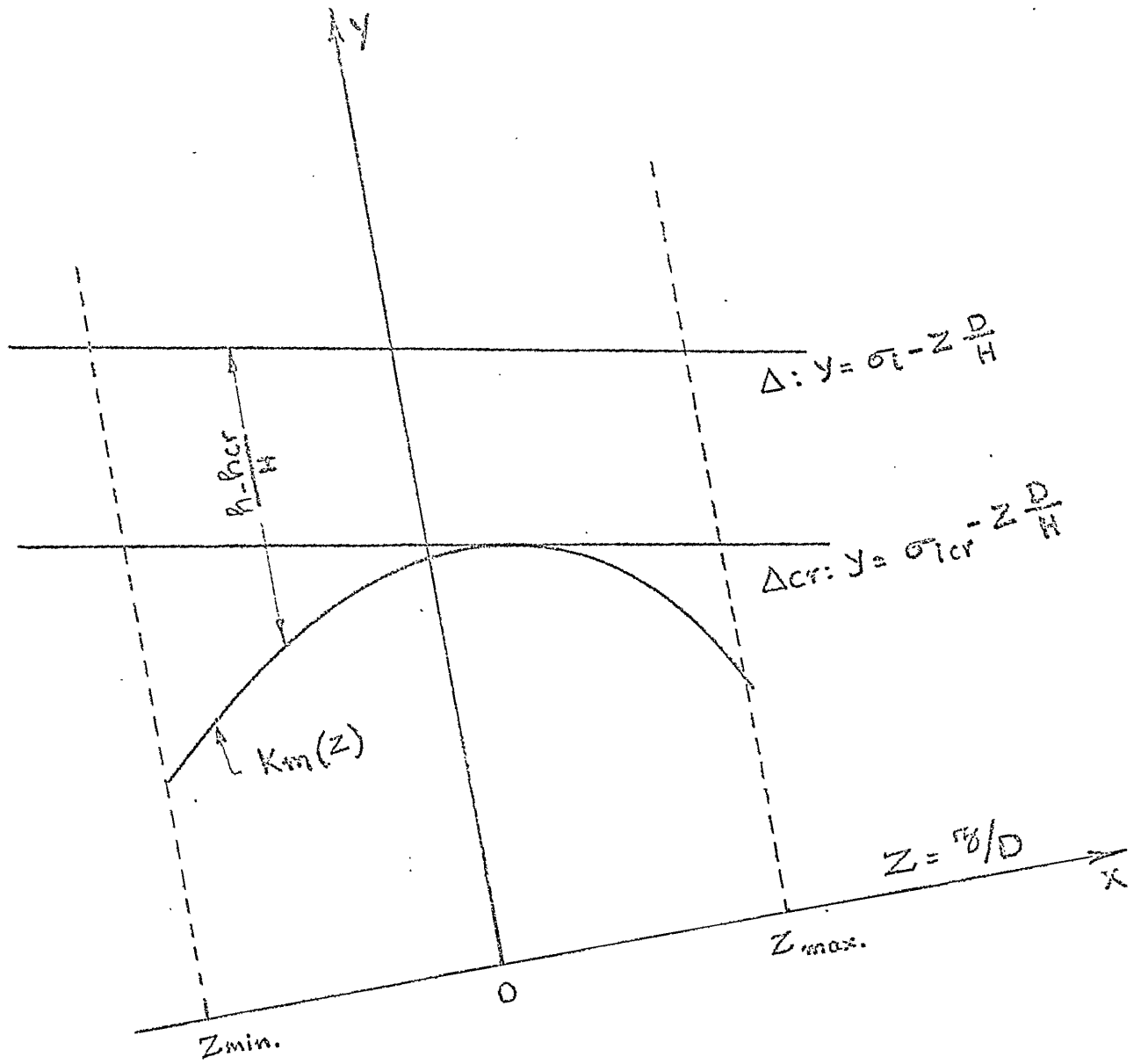

FIG. 3.3.2.2. COMPUTATION OF $\left(\frac{h-h_{cr}}{H}\right)$.

low test heads requiring high vacuum at the inlet side resulting in diffusion of air from the water throughout the model which interferes with both performance and cavitation phenomena. Nevertheless, several European manufacturers have recently built new laboratories where it is possible to run model tests in accordance with Froude's similarity.

3.3.3 In order to maintain similar effects of compressibility, Mach number should be kept constant, i.e.

$$M = \frac{V}{a} = \text{Constant} \qquad (3.3.3)$$

where "a" is the velocity of propagation of pressure wave within the flowing fluid. To some extent, the liquids can be treated as nearly incompressible and hence the effect of Mach number can be neglected. When we consider the inception or the initial appearance of cavitation bubbles, the ratio of vapour to liquid is negligible. But in the case of "super-cavitating flow", we are dealing with a mixture of liquid and vapour and this mixture can have a very low accoustic velocity. Hence the Mach number is important.

3.3.4 In order to maintain the same kind of pressure distribution in the model and prototype, we have to maintain strict geometrical similarity. Geometric similarity of the cavitating boundaries here includes all surface roughness or finish and other irregularities. This is extremely difficult condition to satisfy.

The pressure distribution, especially the minimum pressure on

the body, is greatly affected by surface finish or irregularities. Surface irregularity, which is always present, can significantly lower the minimum pressure from that which would be predicated for a smooth surface on a submerged body. Hence the cavitation number for a rough surface is always greater than for a smooth surface for the same geometric body.

Shal'ner[19] and Holl[20] have conducted experiments to investigate the effect of surface irregularities on the inception of cavitation. These investigations show that very small surface irregularities can produce significant local pressure reductions. Holl concludes that the onset of cavitation for a surface irregularity in a turbulent boundary layer depends on the following parameters (a) Relative height of roughness h/δ where h is the height of roughness, δ the local boundary layer thickness (b) The boundary layer shape parameter H (c) The roughness Reynolds number R_h. Although these three parameters affect the inception of cavitation, it appears from his results that the relative height of roughness h/δ is the most important factor governing the inception of cavitation on a rough surface. The fig. (3.3.4.1) shows the effect of surface irregularities on cavitation inception.

3.3.5 Boundary layer and turbulence to some extent affect the inception of cavitation. Kermeen et al[17] have investigated the effect of boundary layer on cavitation inception for smooth stream lined bodies and for bluff bodies. Their work has thrown considerable light on the

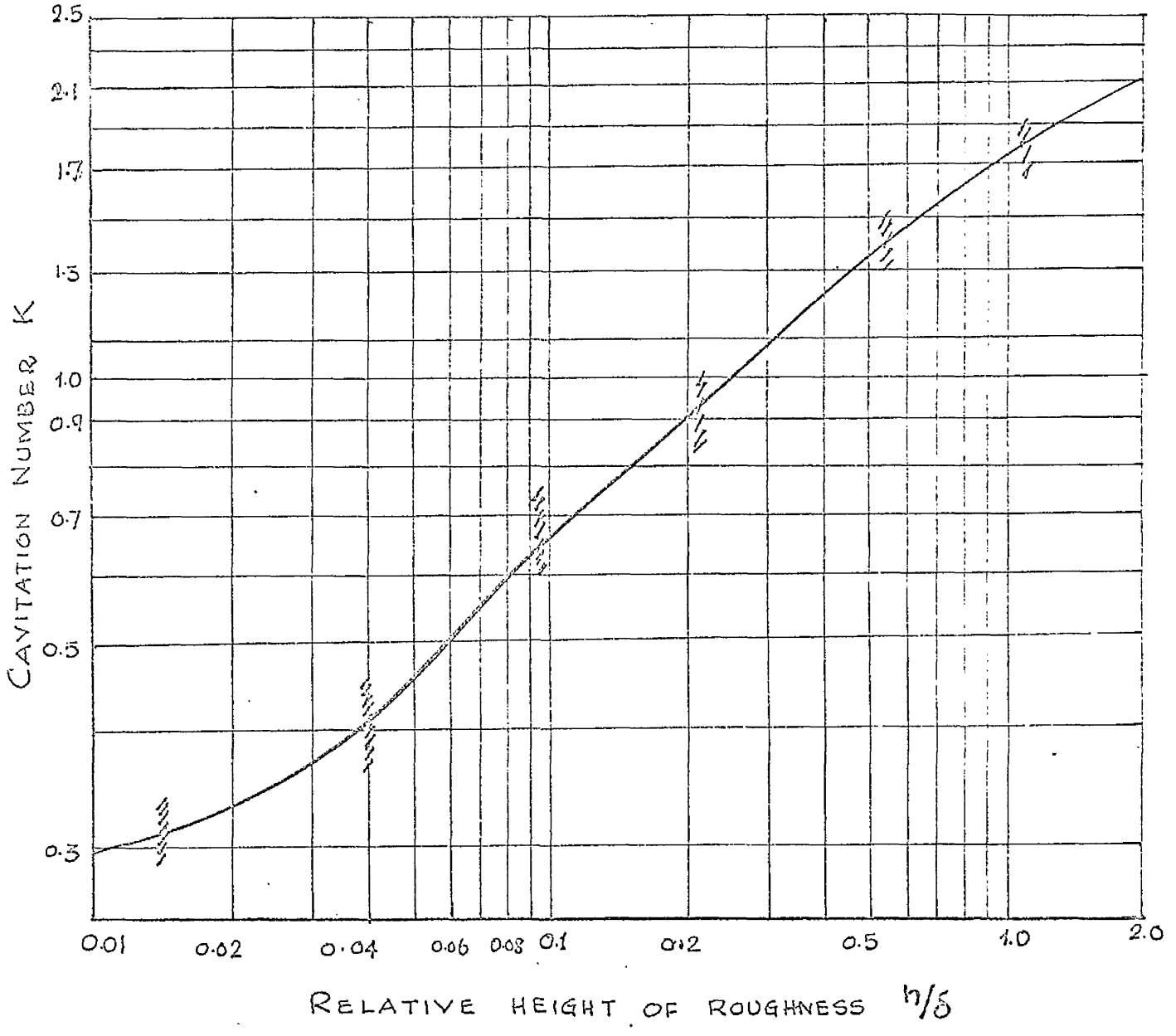

FIG. 3.3.4.1. Effect Of Surface Irregularities on Cavitation Inception. (After Holl)

mechanism of cavitation inception. From their photographic investigations, it can be concluded that microscopic bubbles grow in the boundary layer and travel with less than free stream velocity. This inception of cavitation is called "microscopic cavitation". As these bubbles reach the turbulent boundary layer zone they suddenly grow into bubbles which are visible to the unaided eye and this phase of the cavitation is called "macroscopic cavitation". Thus, it is now well established that in laminar boundary layers cavitation will occur first at the boundary on which the nuclei are established in crevices. In experiments with turbulent boundary layers in a rectangular nozzle Daily and Johnson[22] found that the observed onset of cavitation corresponded to a pressure drop, due to turbulence, of the order of 0.40 to 0.57 ft. of water. Of all the cavities observed only about 1½% were found in the 10% of the boundary layer nearest the wall, while the majority of bubbles were located in the central portion of the boundary layer. Further the boundary pressure was found to be greater than the vapour pressure even when relatively severe cavitation was occurring. The pressure at which the larger nuclei (0.02 inch diameter) became unstable was about 0.5 ft of water above the vapour pressure. Daily and Johnson conclude that the nuclei originated initially at boundary cracks and crevices. Such bubbles emerging in the pressure of the high velocity gradient near the wall would experience hydrodynamic lift. As these bubbles grow further, the drag forces would accelerate them to the fluid velocity. Vortical eddies are present in the turbulent boundary layer and the majority of free nuclei would be transported

toward the centre of the large vortical eddies formed. This qualitative picture of the boundary layer to some extent explains why the majority of cavitation bubbles were observed in the central portion of the boundary layer. From the pressure drop due to boundary shape ρ_{wmin}, the local turbulence pressure drop ρ_t and the critical pressure ρ^x for the nuclei to become unstable and grow, Daily and Johnson derive the following equation

$$\frac{p_o - p_v}{\frac{1}{2}\rho V_o^2} = \frac{p_o - p_{wmin}}{\frac{1}{2}\rho V_o^2} + \frac{p_t}{\frac{1}{2}\rho V_o^2} - \frac{p^x}{\frac{1}{2}\rho V_o^2} \qquad (3.3.5.1)$$

or

$$K_i = C_p + K_t - \frac{p^x}{\frac{1}{2}\rho V_o^2} \qquad (3.3.5.2)$$

where K_i is the incipient cavitation index, C_p is the boundary pressure drop coefficient and K_t is the pressure drop coefficient due to the local turbulence. Since the intensity of turbulence in the boundary layer is dependent on Reynolds number, some change in the index K_t can be expected with change in Reynolds number. Little data are available on the magnitude of the turbulent pressure fluctuations and nothing much can be concluded on the effects of turbulence on the inception of cavitation.

3.4 Scale Effects on inception of Cavitation

3.4.1 Cavitation hysteresis and Cavitation delay-time

Cavitation parameter K is generally used to describe the nature of cavitating flow. Usually, the cavitation experiments are done by

varying the absolute pressure of the system while the free stream velocity is held constant. While doing so, three kinds of flow regime are observed.

(a) At large values of K, non-cavitating flow is observed around the model or structure being tested.

(b) As the value of K is decreased, at a certain value of it, a number of macroscopic bubbles are observed in the flow. This particular phase of cavitation is broadly classified as the inception of cavitation.

(c) When the value of K is further decreased the number and size of cavitation bubbles increase until finally one large cavity appears and completely encloses a portion of the model or structure under study. This kind of flow is called the "cavity flow". The study of "cavity flow" is well developed today and this comes under "Helmholtz motions"[23].

The state at which macroscopic cavitation bubbles appear in a flow may be called "limited cavitation". Limited cavitation can be produced in a flow either by decreasing the absolute pressure of the system gradually till macroscopic cavitation starts or by first establishing a cavity flow and then increasing the pressure until cavitation disappears. The former process is called "incipient cavitation" while the latter is known as "desinent cavitation". It is found that the pressure p_i at which incipient cavitation occurs is less than or equal to the pressure p_d at which cavitation disappears. This phenomenon is referred to as "cavitation hysteresis". However, the desinent cavitation pressure is found to be the upper limit of the incipient cavitation pressure. Thus in general,

$$p_i \leq p_d \qquad (3.4.1.1)$$

and $K_i \leq K_d$

Besides the cavitation hysteresis, another strange phenomenon is also observed while conducting cavitation experiments. Sometimes, even when the pressure of the free stream is kept at the inception pressure p_i, the liquid sustains for several seconds this pressure and then it suddenly explodes into cavitation flow. This time-delay is called the cavitation-delay time.

Holl and Treaster[24] have recently conducted some investigations into cavitation hysteresis. From their results only tentative and qualitative conclusions can be derived. Cavitation hysteresis is a random phenomenon. The cavitation delay time tends to decrease with increasing velocity, size and dissolved air content. Further cavitation delay time is also influenced by the surface characteristics of the model and the pressure history of the fluid.

3.4.2 Effects of dissolved air content

It is now well established that nuclei present in the liquid or trapped on the crevices on the surface of the body are responsible for the inception of cavitation. But to date only very little is known about the relationship between the amount of gas dissolved in a liquid and entrained gas content. Further, the size and distribution of these nuclei in various liquids are not known today.

Crump[25] has investigated the effects which air content in water have on the inception of cavitation. He observed a significant

dependence of inception of cavitation on total air content. Further, he observed that in fully aerated water, cavitation first appeared at the boundary in the form of small vapour cavity. In de-aerated fresh water the cavitation first appeared in the form of individual bubbles which did not necessarily form at the boundary. Williams and McNulty[31] have also observed that the inception of cavitation in flowing water is affected by the amount of air present in the water. Kanellopoulos[32] has conducted some cavitation experiments on a small centrifugal pump and has found, in spite of the considerable scatter in the results, a pronounced effect of total gas content on the inception of cavitation. Strasberg[10] with his experiments on ultrasonically induced cavitation, has derived a functional relation

$$p_c = a_1 G - a_2 p_m \qquad (3.4.2.1)$$

where p_c is the critical pressure, G is the equilibrium or saturation pressure of the air dissolved in the water, p_m is the maximum external water pressure to which the cavity has been subjected and a_1 and a_2 are numerical constants, whose values are unknown to date except that $a_2 + 1 > a_1 > 1$. Till the relationship between the amount of dissolved and entrained gas content of a liquid is established it is extremely difficult to predict the effect of gas content on the inception of cavitation quantitatively.

3.4.3 Surface tension, nuclei size and distribution effects

Cavitation nuclei are assumed to be pockets of undissolved gas

trapped in the crevices on the surface of the model or structure or on hydrophobic solids. Since the walls of the crevices are unwetted the gas pressure is less than the water pressure due to the effect of surface tension. So, for cavitation taking place on the surface of the hydraulic structures or model, the following condition for law of similarity can be obtained

$$\text{Weber Number} = W = \frac{\rho V^2 D}{\sigma_s} = \text{Constant} \qquad (3.4.3.1)$$

where ρ is the mass density of the fluid, V is the velocity of flow, D is the characteristic dimension of the model, σ_s is the surface tension of the fluid at the ambient temperature.

However, considering the number of nuclei present in the flowing fluid, we can also derive another condition for similarity of cavitation nuclei i.e.,

$$\text{Weber Number of Nuclei} = W_n = \frac{\rho V^2 d}{\sigma_s} = \text{Constant} \qquad (3.4.3.2)$$

where d is the diameter of the nuclei.

The number of nuclei present in unit volume of the fluid may be important only when the cavitation is taking place away from solid boundaries. Besides, the number of nuclei is significant only when it is sufficiently small for every nucleus to act as the centre of cavitation inception. Since the number, the size and the distribution of these nuclei are still unknown even for ordinary liquids such as tap water, river waters and ocean waters, the above condition is

extremely difficult to fulfil. Although there is some experimental evidence today showing the effect of Weber Number, one cannot be conclusive due to the fact these experimental results have been obtained by keeping the surface tension constant (i.e. water at the same temperature) and varying the velocity of the flow. However, it is important to recognise the existence of Weber number of nuclei as another possible factor on the scale effects of cavitation.

While discussing the effect of turbulent pressure fluctuation on the inception of cavitation(refer 3.3.5) we obtained the equation

$$Ki = Cp + Kt - \frac{p^x}{\frac{1}{2}\rho Vo^2}$$

In the above equation, the term $\frac{p^x}{\frac{1}{2}\rho Vo^2}$ depends on surface tension and the size of nuclei present. If the origin of these nuclei is the surface of the model, the size of the nuclei would mainly depend upon the surface tension, fluid density, velocity, model size and the characteristic of the surface and the boundary layer. Daily[22] suggests that the size of the nuclei created at the surface of the model to some extent depends on the characteristics of the boundary layer, whose thickness, in general, is inversely proportional to Vo^n where n is less than unity. Hence p^x can be written proportional to Vo^n or

$$\frac{p^x}{\frac{1}{2}\rho Vo^2} = \frac{A\,Vo^n}{\frac{1}{2}\rho Vo^2} = \frac{B}{Vo^m} \quad (m > 1) \qquad (3.4.3.3)$$

From this, we can see that the effect of the parameter depending on

surface tension and nuclei size can be reduced by operating at high velocities. Daily adds further that the effect of the parameter $\frac{p^x}{\frac{1}{2}\rho V_o^2}$ on cavitation inception can be reduced by introducing into the test water large nuclei and operating at velocities greater than 30 ft/Sec.

3.5 Scale Effects on the Growth of Cavitation Bubbles

When a vapour bubble grows inside a liquid - here the growth of bubble by the diffusion of gas is neglected - evaporation of the liquid takes place at the surface of the bubble. Plesset and Zwick[13] have investigated this phenomenon theoretically and they have found that because of the latent heat requirement for evaporation, a change in bubble size must be accompanied by a heat transfer across the bubble wall. Due to heat transfer, the liquid surrounding the bubble is subjected to cooling. Since the vapour pressure at the bubble wall is dependent upon the temperature there, a decrease in the vapour pressure inside the bubble is brought about by the resultant cooling of the surrounding liquid due to heat transfer and this causes a decrease in the rate of bubble growth. Fig.(3.5.1) taken from Plesset and Zwick's paper, shows theoretical radius and bubble wall temperature curves for the growth of a pure vapour bubble in water at 1 atmosphere external pressure, superheated to 103°C. Referring to Fig.(2.3.2.2) one can note the marked effect upon the rate of growth of a vapour bubble due to cooling of the surrounding liquid which provides the heat necessary for evaporation.

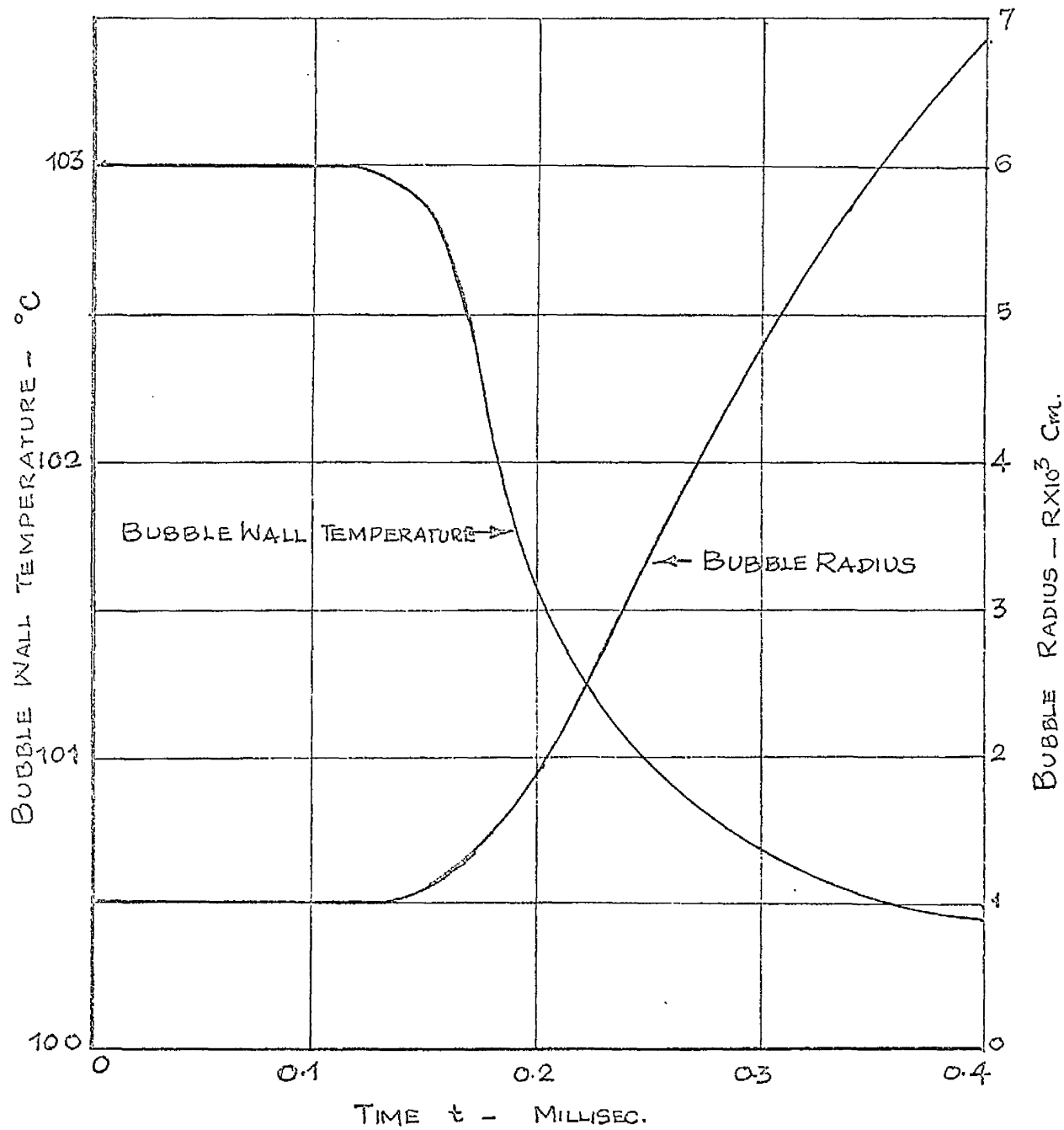

FIG. 3.5.1. Theoretical radius and bubble wall temperature curves for a pure vapour bubble in water at 1 atm. external pressure, superheated to 103°C (After Plesset & Zwick.)

3.5.1. Stahl and Stepanoff[33] first tried to derive a simple approximation by which this cooling effect could be taken into consideration while predicting the suction head requirements for suppressing cavitation in centrifugal pumps operating in different fluids. Jacobs[34] continued this work further and derived the following equations for centrifugal pumps.

$$(NPSH)_2 = (NPSH)_1 + \left\{ \frac{\lambda\, vl}{vg} \quad \frac{\phi}{1 - \frac{C}{vl}\left(\frac{dT}{dp}\right)} \right\}_1 - \left\{ \frac{\lambda\, vl}{vg} \quad \frac{\phi}{1 - \frac{C}{vl}\left(\frac{dT}{dp}\right)} \right\}_2 \qquad (3.5.1.1)$$

$$(NPSH)_2 = (NPSH)_1 \frac{\left\{ \frac{\lambda\, vl}{vg} \quad \frac{\phi}{1 - \frac{C}{vl}\left(\frac{dT}{dp}\right)} \right\}_1}{\left\{ \frac{\lambda\, vl}{vg} \quad \frac{\phi}{1 - \frac{C}{vl}\left(\frac{dT}{dp}\right)} \right\}_2} \qquad (3.5.1.2)$$

where NPSH is net positive suction head required to suppress cavitation in a centrifugal pump

ϕ = A function of design and operating point of pump

λ = latent heat of vaporisation

vl = specific volume of liquid

vg = specific volume of vapour at ambient temperature

C = Temperature coefficient for determining change in the enthalpy of the liquid during vaporisation

$\frac{dT}{dp}$ = slope of vapour pressure curve

1, 2 are used to identify fluids.

The term on the right hand side of equation (3.5.1.2) excluding (NPSH), is generally known as the "Cavitation tendency ratio". Boretz[35] derives an equation relating the cavitation tendency ratio to suction specific speed as follows:

$$\text{Cavitation Tendency Ratio} = \text{CTR} = \left(\frac{S_2}{S_1}\right)^{4/3} \qquad (3.5.1.3)$$

where S is the suction specific speed of a pump which is equal to $\frac{N_o Q^{\frac{1}{2}}}{(Hsv)^{\frac{3}{4}}}$, N = speed of pump Q = discharge Hsv = net positive suction head above vapour pressure.

In view of the discrepancies existing between theoretical and experimental cavitation tendency ratios further investigations are required, and the qualitatively accurate predictions of the cavitation tendency ratio suggest further evaluation and refinement of this concept.

3.5.2 A simple similarity relation for the effect of vaporisation and heat transfer can be derived in the following manner[16]. The amount of heat transferred to the nuclei

$$\text{for evaporation} = C_H \left(\frac{al\ V}{vl}\right) Cpl\ (\Delta T) \qquad (3.5.2.1)$$

where C_H is the heat transfer coefficient which is a function of Reynolds, Prandtl and Froude numbers.

al is area of cross-section through which fluid is passing at velocity V

vl is specific volume of the fluid.

Cpl is the specific heat of the fluid

and ΔT is the change in temperature.

The amount of heat required for the evaporation

$$= C_Q \cdot \frac{av\ V}{vg} \cdot \lambda \qquad (3.5.2.2)$$

where C_Q is the volume entrainment coefficient which is a function of at least Reynolds and Froude numbers.

av is effective area of vapour removal

V is velocity of vapour removal which is assumed to be the same as free stream velocity

λ is latent heat of vaporisation

and vg is specific volume of vapour

From the above equations we obtain

$$\Delta T = \frac{C_Q}{C_H} \cdot \frac{av}{al} \cdot \frac{vl}{vg} \cdot \frac{\lambda}{Cpl} \qquad (3.5.2.3)$$

Using Clapeyron's equation, we can obtain the change in vapour pressure Δp_v due to cooling as

$$\Delta p_v = \frac{C_Q}{C_H} \cdot \frac{av}{al} \cdot \frac{vl}{vg} \cdot \frac{1}{(vg - vl)} \cdot \frac{\lambda^2}{Cpl\ T} \qquad (3.5.2.4)$$

Therefore, the non-dimensional factor expressing the effect of cooling due to evaporation is

$$\frac{\Delta p_v}{\frac{1}{2}\rho V^2} = \frac{1}{\frac{1}{2}\rho V^2} \cdot \left(\frac{C_Q}{C_H}\right) \cdot \frac{av}{al} \cdot \frac{vl}{vg} \cdot \frac{1}{(vg - vl)} \cdot \frac{\lambda^2}{Cpl\ T} \qquad (3.5.2.5)$$

or

$$\frac{\Delta p_v}{\frac{1}{2}\rho V^2} = \frac{C_Q}{C_H} \cdot \frac{av}{al} \cdot \frac{vl}{vg} \cdot \frac{1}{\left(\frac{vg}{vl} - 1\right)} \cdot \frac{\lambda^2}{\frac{V^2}{2g}\ T\ Cpl} \qquad (3.5.2.6)$$

$$\text{or} \quad \frac{\Delta p_v}{\frac{1}{2}\rho V^2} = f(R, F, Pr)\left(\frac{av}{al} \cdot \frac{vl}{vg}\frac{1}{\left(\frac{vg}{vl} - 1\right)}\right)\left(\frac{\lambda^2}{\frac{V^2}{2g}\, T\ Cpl}\right) \quad (3.5.2.7)$$

Therefore the condition for similarity of reduction in vapour pressure is

$$\frac{\Delta p_v}{\frac{1}{2}\rho V^2} = \text{constant} \quad (3.5.2.8)$$

But it is extremely difficult to satisfy all the conditions of equation (3.5.2.7). However it is worthwhile to note that the effect of change in vapour pressure due to local cooling depends on Prandtl number and the parameter $\frac{\lambda^2}{V^2/2g\ Cpl\ T}$ besides other factors.

3.6 Summary of scale effects on cavitation

The following Table.1. gives a summary of the present day knowledge of scale effects on cavitation.

Table.1.

General Characteristics	Forces of Parameters	General Law of Similarity
Ideal Flow	Inertia forces only	$K = \frac{p - p_v}{\frac{1}{2}\rho V^2}$ = Constant
Scale effects on the flow (or minimum pressure)	Viscosity & Inertia forces	$R = \frac{VD}{\mu/\rho}$ = Constant
	Gravity & Inertia forces	$F = \frac{V}{\sqrt{gD}}$ = Constant
	Elasticity & Inertia forces	$M = \frac{V}{a}$ = Constant (Can be neglected in "limited cavitation")
	Surface irregularities	h/L = Constant or $(\frac{h}{\delta})$ = Constant
	Boundary Layer & Turbulence	$\frac{p_t}{\frac{1}{2}\rho V^2}$ = Constant (= pressure fluctuation due to turbulence)
Scale effects on the inception of cavitation	Cavitation hysteresis & delay-time	Either Desinent or Incipient Cavitation pressure is measured throughout the experiment thereby reducing the scatter in results
	Dissolved air Content	$\frac{\alpha}{\alpha_s}$ = constant (α = Amount of dissolved air; α_s = Amount of dissolved air under saturation condition.)
	Surface tension, nuclei size and inertia forces	$W = \frac{\rho V^2 d}{\sigma_s}$ = constant or $W = \frac{\rho V^2 D}{\sigma_s}$ = constant
Scale effects on the growth of cavitation bubbles	Heat transfer, vaporisation and cooling due to growth of bubbles	$\frac{C_l}{C_H} \frac{av}{al} \frac{vl}{vg} \frac{1}{(\frac{vg}{vl} - 1)} \frac{\lambda^2}{\frac{V^2}{2g} T\, Cpl}$ = Const

3.7 Object of the present work

One can observe from Table 1. that the laws of similarity for the inception of cavitation are indeed severe and it is practically impossible to fulfil all the conditions set forth. However, some factors affecting the inception of cavitation can be neglected by comparing their relative importance.

Throughout the present work, only desinent cavitation pressures were measured, i.e. cavitating flow was first established by lowering the absolute pressure of the system and then the pressure was gradually increased to a point where the cavitation bubbles just disappeared. The absolute pressure of the system when the cavitation just disappeared was noted and this pressure was used to calculate the cavitation parameter K. This particular procedure was used throughout the experiments of the present work so as to reduce the scatter produced in the results by the "hysteresis" effect of cavitation.

Therefore, using the information given by Table 1, one can write that

$$K = f\left[R,\ F,\ M,\ \frac{h}{L},\ \frac{pt}{\frac{1}{2}\rho V^2},\ \frac{\alpha}{\alpha_s},\ W,\ P_n,\ \left(\frac{av}{al}\ \frac{vl}{vg}\ \frac{1}{(vg/vl - 1)}\right)\ \frac{\lambda^2}{\frac{V^2}{2g}\,T.Cpl}\right] \qquad (3.7.1)$$

(a) Mach Number Effect

As described above, only desinent cavitation pressures were observed throughout. Therefore, we can safely assume that at the

point of cavitation the number of bubbles of observable size is almost nil and hence it is a flow of liquid, not that of a mixture of liquid and vapour (or gas). Since liquids are nearly incompressible, the effect of changes in Mach Number can be neglected.

(b) Effects of Surface irregularities and boundary-layer turbulence

Cavitation experiments in the present work were done on the valve and the same valve with a particular fixed opening was used throughout. Hence it is assumed that the effect of surface irregularities on the inception of cavitation was the same.

Since sufficient theoretical or practical knowledge is not yet available to calculate the pressure fluctuations pt due to turbulence, the effects of boundary layer and turbulence were neglected.

(c) Effect of dissolved air Content

Preliminary experiments with fully saturated water (100% air-content) and water with 40.5% air-content showed almost no change or effect of dissolved air content on cavitation inception. This proves that the dissolved air content of water is an important factor only when there are insufficient nuclei to trigger cavitation. Further, the present experiments were conducted with fluids fully saturated with air under atmospheric conditions. It is assumed therefore, that the effect of dissolved air-content was the same throughout.

(d) Effect of Weber Number

Although there are some experimental results showing the effect

of Weber Number, one cannot derive any positive conclusion from these. It can however, be remarked that probably Weber number of nuclei is an important factor only when almost all the nuclei present in the fluid act as the source of inception of cavitation. The distribution, size and number of nuclei present in various fluids such as ordinary tap water, river and ocean waters are still to be determined. Further, it is not yet known in what way the amount of total dissolved gas content and entrained gas in nuclei are related with each other.

The cavitation rig used to conduct the experiments of the present work does not have a resorber and further, the preliminary experiments revealed that cavitation occurred only on the surface of the plug of the valve. Hence it was assumed that there were always more than sufficient nuclei present in the fluid to trigger cavitation and therefore the effect of Weber number of nuclei was neglected.

(e) From the above statement, we can say that the cavitation parameter

$$K = f_1 \left(R, F, Pr, \left(\frac{av}{al} \quad \frac{vl}{vg} \quad \frac{1}{\left(\frac{vg}{vl} - 1 \right)} \quad \frac{\lambda^2}{\frac{V^2}{2g} T.Cpl} \right) \right) \qquad (3.7.e.1)$$

Let us now consider the factor $\left(\frac{av}{al} \cdot \frac{vl}{vg} \cdot \frac{1}{\left(\frac{vg}{vl} - 1 \right)} \quad \frac{\lambda^2}{\frac{V^2}{2g} T.Cpl} \right)$ alone.

This factor consists of a term involving volume ratio $\left(\frac{av}{al} \quad \frac{vl}{vg} \quad \frac{1}{\left(\frac{vg}{vl} - 1 \right)} \right)$ and the term $\frac{\lambda^2}{\frac{V^2}{2g} T.Cpl}$. Assuming further that the ratio $\left(\frac{\varepsilon v}{al} \right)$ is constant for the same form of cavitation, the volume ratio can be

simplified to $(vl^2/_{vg}2)$ since $vg \gg vl$. In the present work, the properties of the working fluid (water) were changed by adding a substance called polyoxyalkaline polyol, generally known as pluracol V-10 (see next chapter). This additive brought about an enormous change in viscosity of the solution, while the change in vapour pressure was almost negligible. The changes in specific volume of liquid and vapour were also negligible. Hence the effect of parameter $(vl^2/_{vg}2)$ was neglected. Further, for constant velocity, the term

$$\frac{\lambda^2}{\frac{V^2}{2g}\ T.Cpl}$$

varied only about 10-12% while Prandtl number varied from 6 to about 160. Hence the effect of the parameter $\frac{\lambda^2}{\frac{V^2}{2g}\ T.Cpl}$ was also neglected.

It is therefore concluded that the change observed in cavitation parameter K is due to change in Reynolds number and Prandtl number, while Froude number is kept constant as far as possible. We obtain therefore that

$$\text{cavitation parameter } K = F\left(R, F, Pr\right) \qquad (3.7.g.2)$$

The aim of the present work is to conduct cavitation tests on the valve with a fixed opening under constant Froude number. It was originally intended to obtain a functional relationship between Reynolds and Prandtl number with respect to cavitation parameter K. Unfortunately a sever limitation was imposed on the flow velocity by the centrifugal pump in the cavitation rig since the rig was designed and erected with the idea to conduct experiments on the pump. However

experiments were conducted on the valve under constant Froude number while Reynolds and Prandtl numbers were varied. The effects of Reynolds and Prandtl number on cavitation were obtained.

Chapter 4

PROPERTIES OF WATER-PLURACOL SOLUTIONS

4.1 General

Water is the common liquid which is used universally to test hydraulic machinery and the results are extrapolated to liquids other than water. In some cases petroleum products such as heavy fuel oil, light lubricating oil are used to test hydraulic machines. It is common practice to use glycerol in various concentration in water to analyse the effect of viscosity on the performance of hydraulic machines. In the present work the author has used liquid polyoxyalkylene polyol, generally known as pluracol V-10 in different concentration in water to observe the effect of Reynolds and Prandtl numbers on the inception of cavitation. Pluracol V-10 is a new product and was specifically developed for improving the viscosity of aqueous-systems. Pluracol V-10 is a high molecular weight (average molecular weight 42,000 $\pm$ 1,000) liquid, polyoxyalkylene polyol, with a very high viscosity. It is non-volatile and thermally stable below 450^{o}F. This product is obtainable commercially from Wyandotte Chemical International Inc., London.

4.2 Physical Properties of Pluracol V-10 and its solutions in water

4.2.1 Specific Gravity

The specific gravity 60/60°F of pure Pluracol V-10 is 1.14. The variation of specific gravity of pluracol V-10 and water solution at different concentrations is shown in Fig.(4.2.1.1). This obtained by using a Westphal Balance[36]. Fig.(4.2.1.2) gives the density of pluracol solutions of different concentration at different temperatures. This graph is obtained by using a pyknometer[36]. Fig.(4.2.1.3) gives a comparative study of densities of aqueous solutions of glycerol and pluracol.

4.2.2 Solubility

Pluracol V-10 is soluble in water in all proportions below 170°F. Above this temperature its solubility decreases with increasing temperature.

4.2.3 Viscosity

The outstanding physical property of Pluracol V-10 polyol is its extremely high viscosity. The viscosity of other fluids such as glycol-water type, fire-resistant hydraulic fluids can be controlled by addition of this viscous polyol. It has excellent resistance to shear and will not hydrolyze or degrade under most conditions. The high viscosity of Pluracol V-10 is of economic importance because less is needed in the solution to obtain the desired viscosity. Fig.(4.2.3.1)

shows the viscosity of aqueous solutions of pluracol and glycerol[37]. Figures (4.2.3.2, 4.2.3.3 and 4.2.3.4) show the viscosity of pluracol-water solutions of different concentration (by weight) at different temperatures. Aqueous solutions of pluracol V-10 have Newtonian properties similar to those of petroleum oils. Pure pluracol V-10 has a kinematic viscosity of 45,000 centistokes at 100°F and 6,000 centistokes at 210°F. The results shown in Figures (4.2.3.1 to 4.2.3.4) are obtained by using British Standards Capillary tube viscometers.

4.2.4 Specific Heat

Fig. (4.2.4.1) gives the specific heat of pluracol solution at different concentration. A calorimeter in which the liquid can be electrically heated was used and the results are believed to be accurate to ± 1%.

4.2.5 Conductivity

Solutions of water and pluracol V-10 up to 15% concentration by weight were tested in the glass and brass radial heat flow Conductivity Cell at the Mechanical Engineering Research Annexe by Mr. J.E. Venart. Tests were made on two isotherms, 16.5°C and 41.5°C. These results are believed to be accurate to ± 2%. The results are presented in Figures 4.2.5.1 and 4.2.5.2. Figure (4.2.5.3) gives the Prandtl number of pluracol solutions of different concentration between 15° and 50°C temperatures.

4.2.6 Vapour pressure, Specific volume of vapour and Latent heat of vaporisation

In the present work, the author has used pluracol V-10 and water solutions of up to 15% concentration by weight. The average molecular weight of pluracol V-10 is 42,000. Hundred grams of a solution of 15% concentration by weight contains $\frac{15}{42,000} = 0.000357$ gram mols of pluracol V-10 and $\frac{85}{18} = 4.725$ gram mols of water. Since the number of gram mols of pluracol V-10 is very small compared to the gram mols of water, the solution is dilute. For dilute solutions, the change in vapour pressure is given by the formula[38].

$$\frac{P_1 - P_2}{P_1} = \frac{N_2}{N_1 + N_2} \qquad (4.2.6.1)$$

where P_1 is the vapour pressure of the solvent at a certain temperature, P_2 is the vapour pressure of the solution at the same temperature, N_2 and N_1 are gram mols of the solute and solvent respectively. From the above equation, the change in vapour pressure of a pluracol V-10 and water solution of 15% concentration by weight is equal to 0.00755%, which is negligible. We can therefore, conclude that the addition of up to 15% of pluracol V-10 to water does not change the vapour pressure of water.

Pluracol V-10 is a non-volatile substance and the vapour given off by a solution of a non-volatile substance is composed entirely of the solvent. Hence the vapour of pluracol V-10 solution is purely water vapour. Since the vapour pressure of pluracol V-10 solution

is the same as that of water, we can conclude that the specific volume of saturated vapour of pluracol solution is the same as that of water. Fig.(4.2.6.1) gives the vapour pressure of water at different temperatures.

The Clausius - Clapeyron equation states

$$\lambda \simeq (T\ vg)\ \left(\frac{dp}{dT}\right) \qquad (4.2.6.1)$$

where λ is Latent heat of vaporisation, T is absolute temperature vg is the specific volume of saturated vapour and $\left(\frac{dp}{dT}\right)$ is the slope of vapour pressure curve at temperature T. Since the specific volume vg of saturated vapour and $\left(\frac{dp}{dT}\right)$ the slope of vapour pressure curve of pluracol V-10 solution are exactly the same as that of water, the latent heat of vaporisation of pluracol V-10 solution is equivalent to that of water.

4.2.7 Other important properties of Pluracol V-10

Appearance	Light coloured, clear, viscous liquid
Pour point	4.5°C
Flash point	265.5°C
Fire point	279.4°C
Thermal stability	Decomposes above 248°C

non-gumming

non-carbonizing

non-corrosive

non-separating

non-hydrolizing

non-rancidifying

not subject to bacterial action

4.3 Properties of Pluracol-water Solutions used.

The authbr in the present work has used five pluracol V-10 and water solutions of different concentration in addition to water. The Table 2 gives the properties of various solutions used.

See next page for ..... Table 2

Table.2.

Fluid	Conc. of Pl.V.10 by wt.	Sp. Gravity $^{17}/_{17}{}^{o}C$	Kinematic Viscosity	Specific Heat	Thermal Conductivity	Prandtl Number
Water	0%	1.0000	Fig.(4.3.1)	1.000	Fig.(4.3.7)	Fig.(4.3.
Solution No. 1	2.13%	1.0022	Fig.(4.3.2)	0.994	Fig.(4.3.8)	Fig.(4.3.
2	5.5%	1.0090	Fig.(4.3.3)	0.980	Fig.(4.3.9)	Fig.(4.3.
3	8.5%	1.0125	Fig.(4.3.4)	0.966	Fig.(4.3.10)	Fig.(4.3.
4	11%	1.0160	Fig.(4.3.5)	0.954	Fig.(4.3.11)	Fig.(4.3.
5	12.75%	1.0192	Fig.(4.3.6)	0.944	Fig.(4.3.12)	Fig.(4.3.

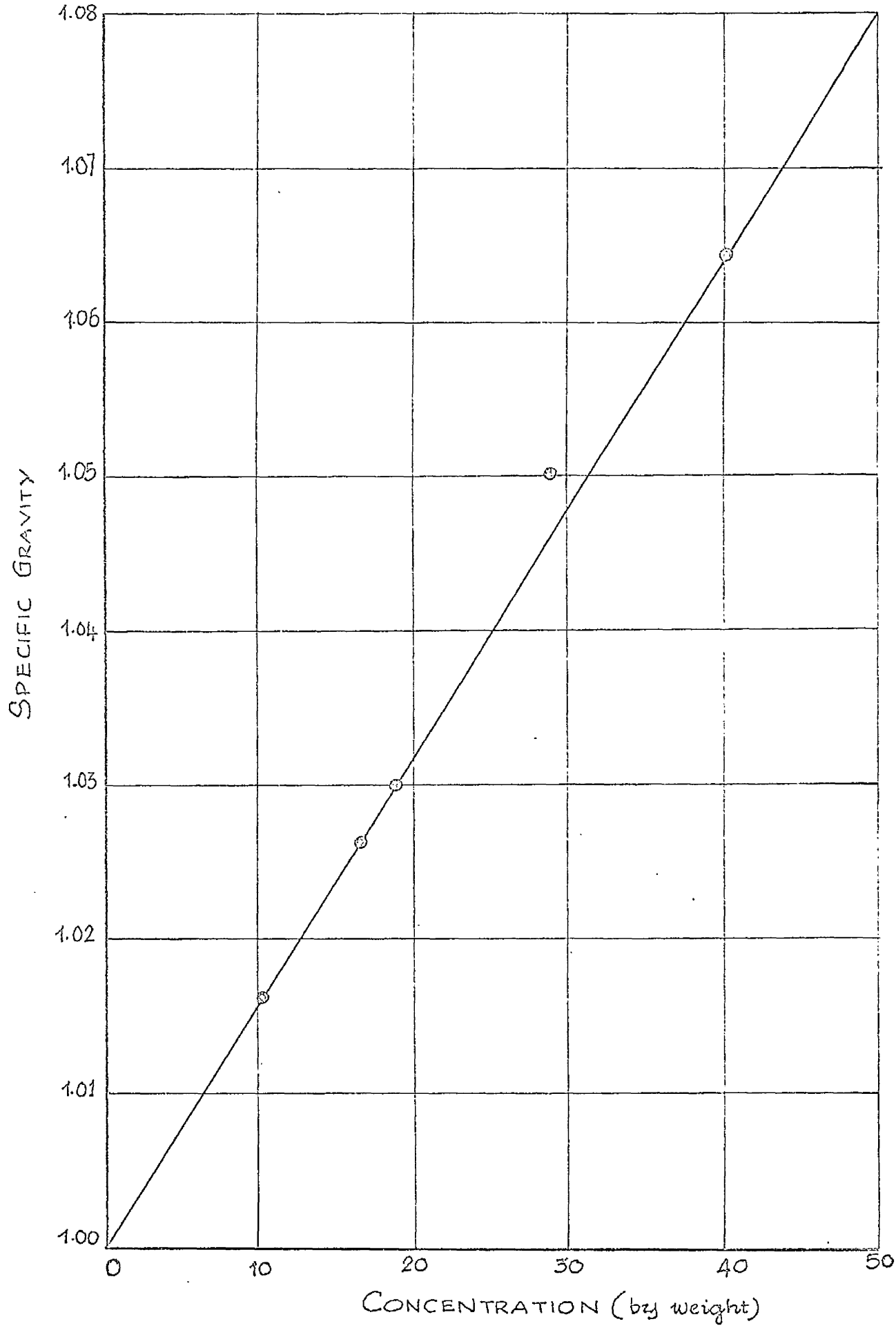

FIG. 4.2.1.1. Specific Gravity of aqueous pluracol V-10 solution at 17°C

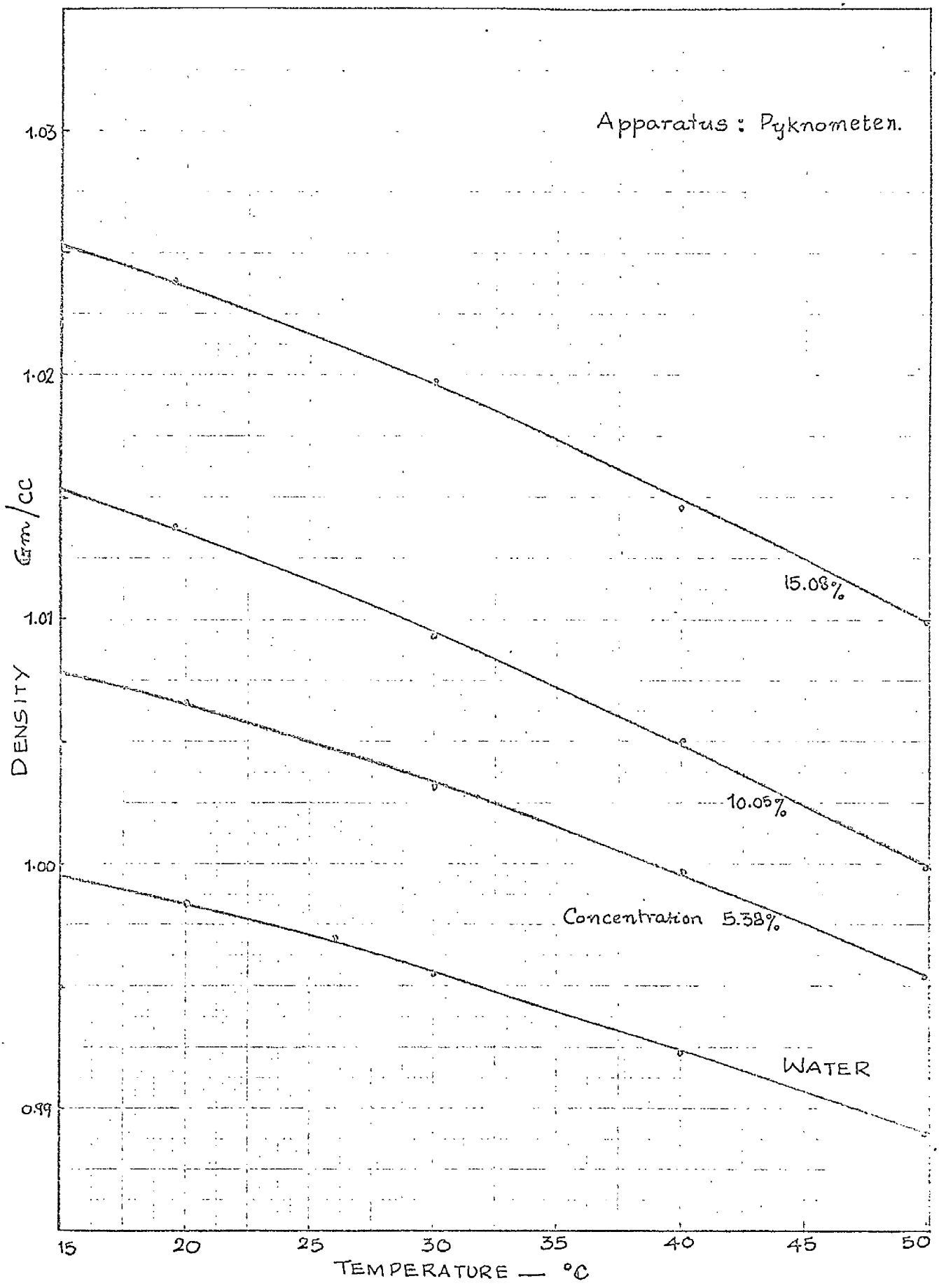

FIG. 4.2.1.2. Density of Pluracol solutions at different temperatures.

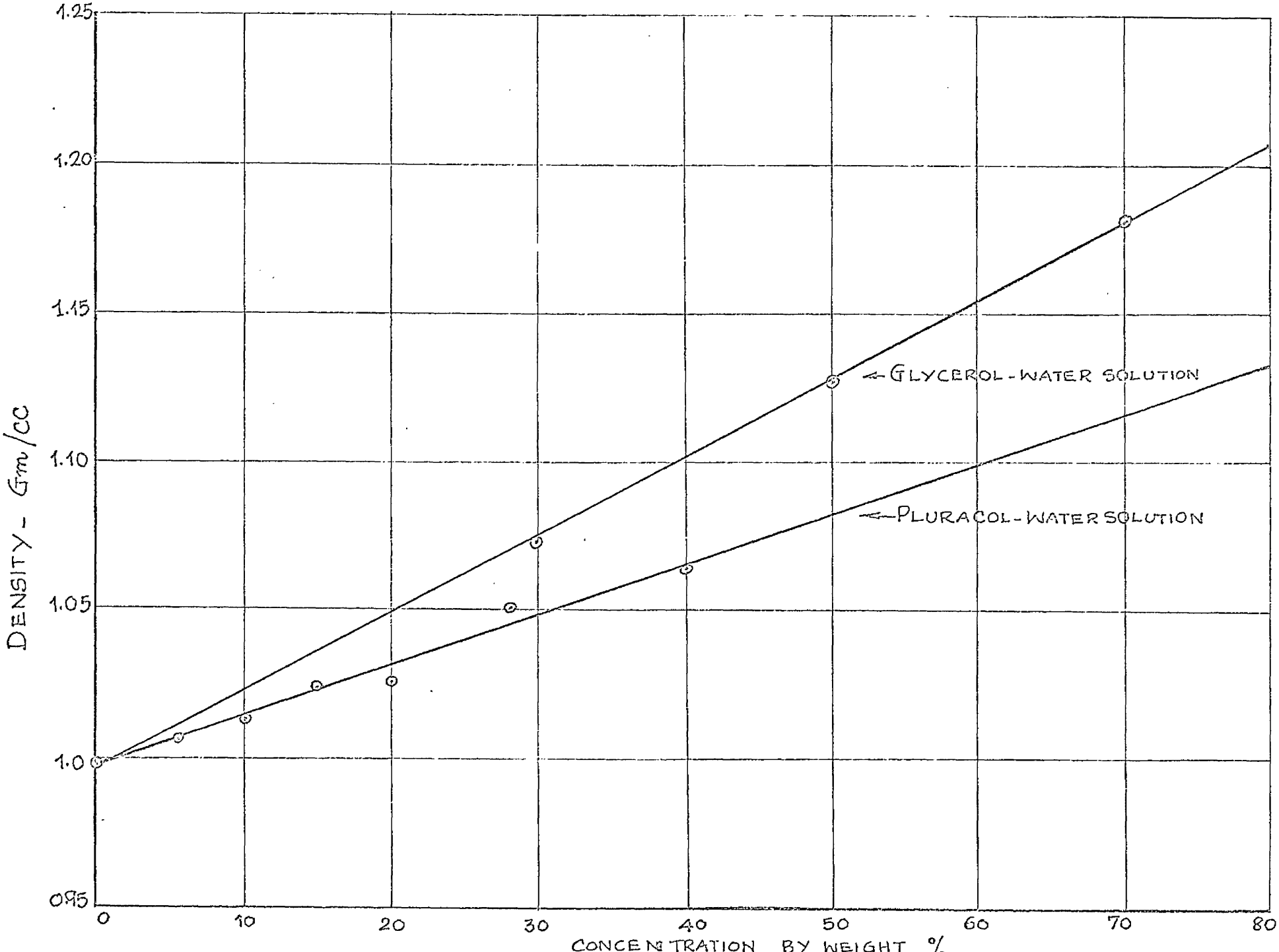

FIG. 4.2.1.3. DENSITIES OF PLURACOL GLYCEROL SOLUTIONS AT 20°C

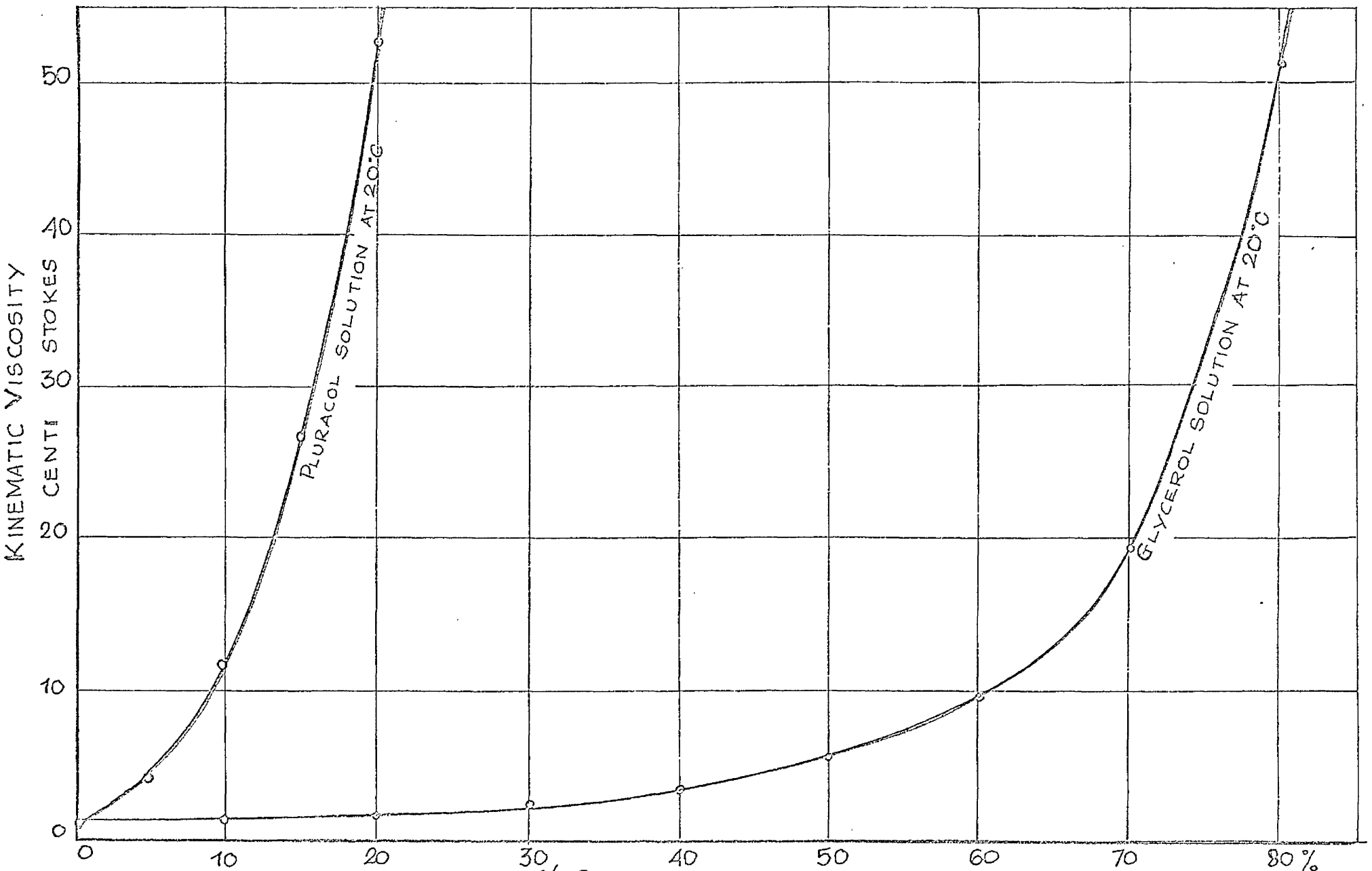

FIG. 4.2.3.1. VISCOSITY OF PLURACOL AND GLYCEROL SOLUTIONS AT 20°C.

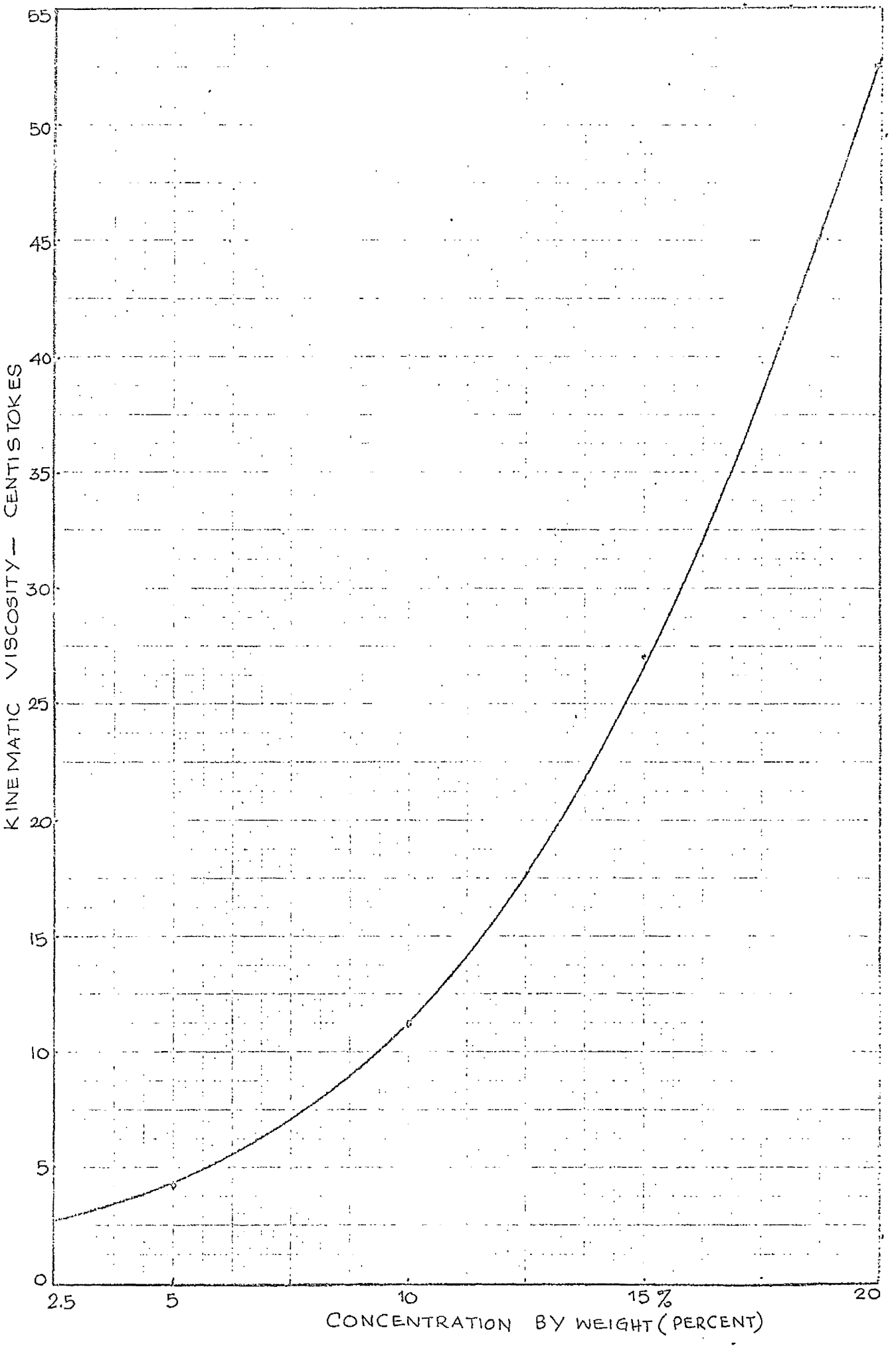

FIG. 4.2.3.2. Kinematic Viscosity of Pluracol Solution at 20°C

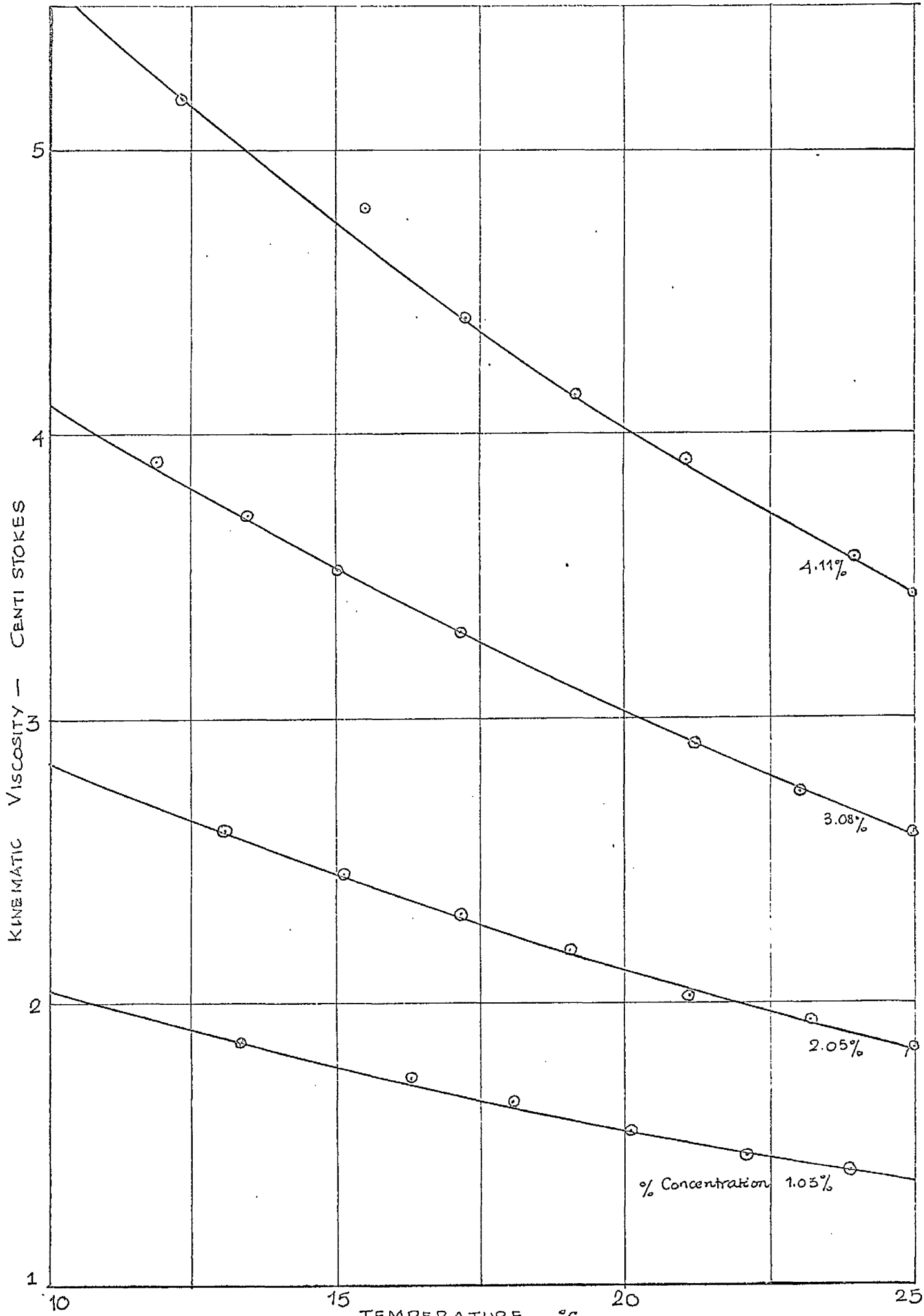

FIG. 4:2.3.3. KINEMATIC VISCOSITY OF PLURACOL SOLOTION

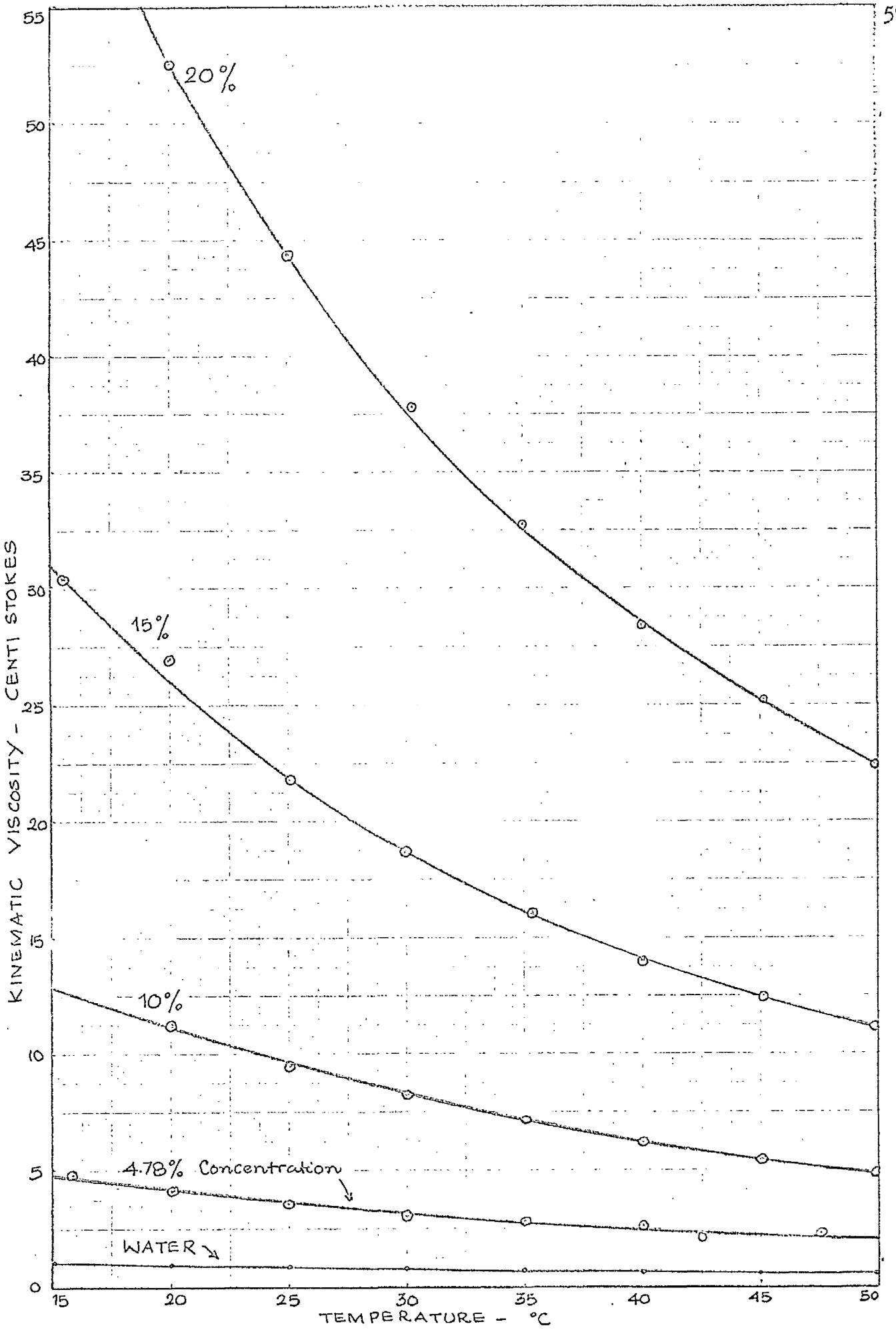

FIG. 4.2.3.4. Kinematic Viscosity of Pluracol Solution.

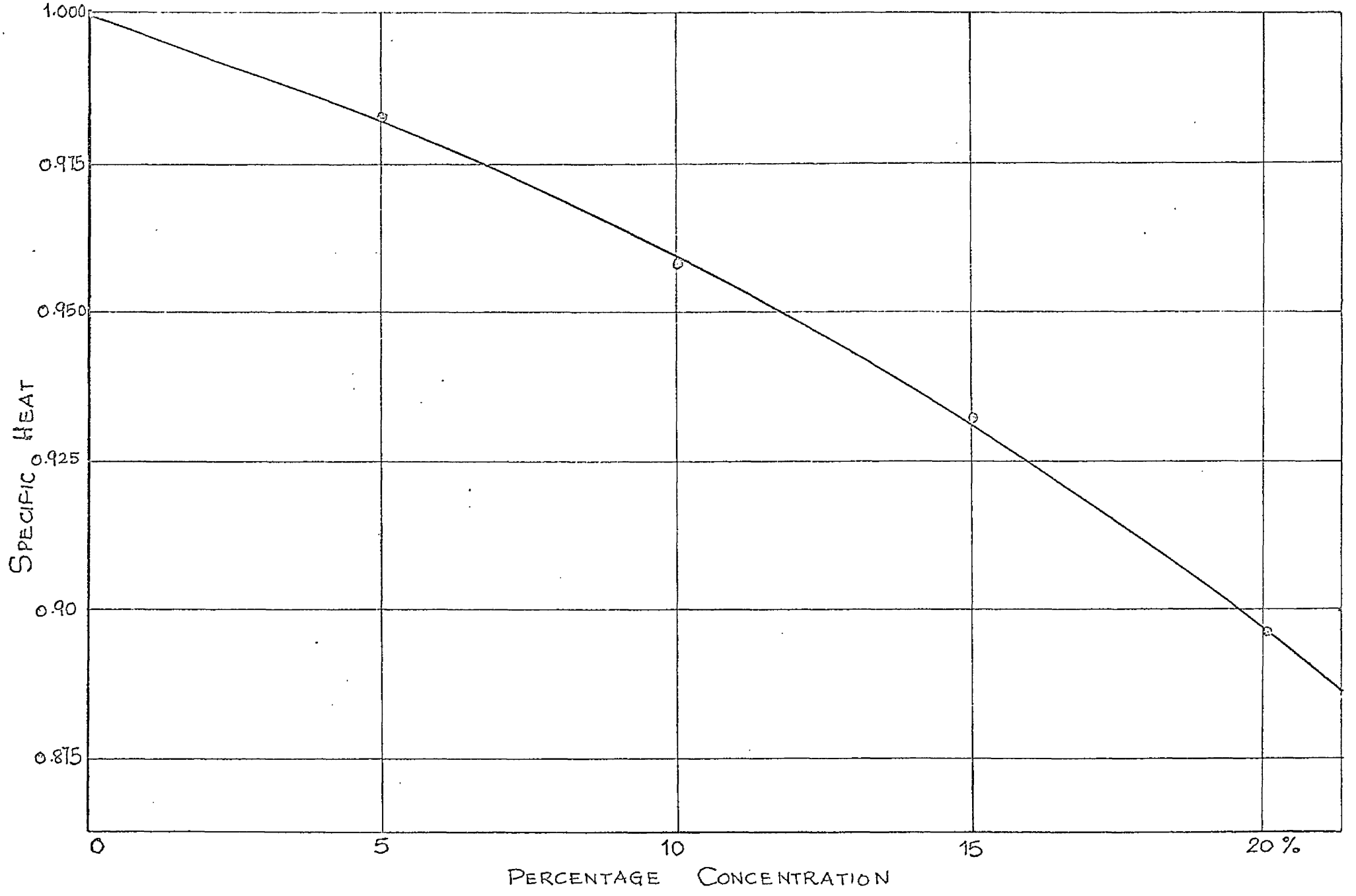

FIG. 4.2.4.1. SPECIFIC HEAT OF PLURACOL SOLUTION.

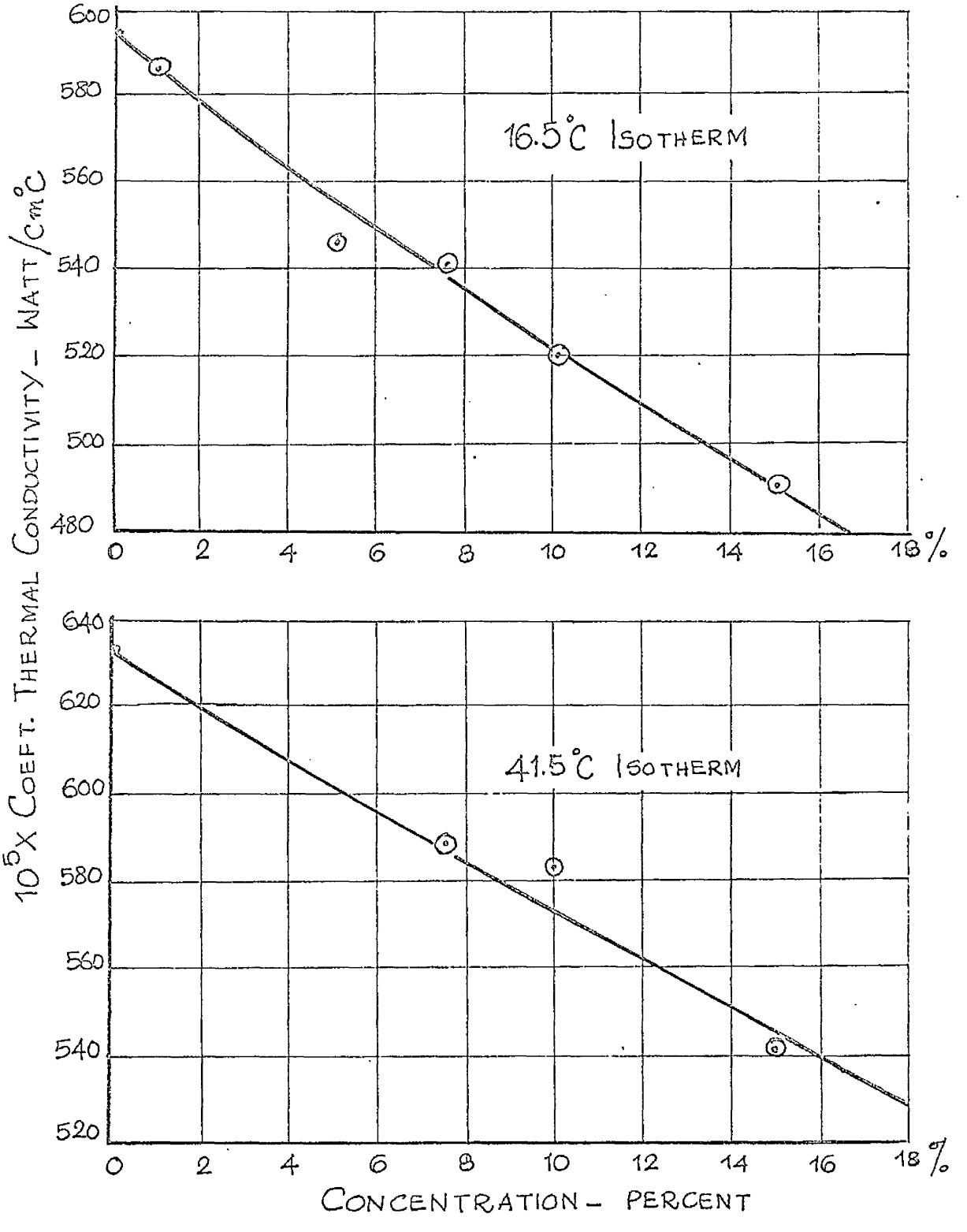

FIG. 4.2.5.1. THERMAL CONDUCTIVITY OF PLURACOL SOLUTION.

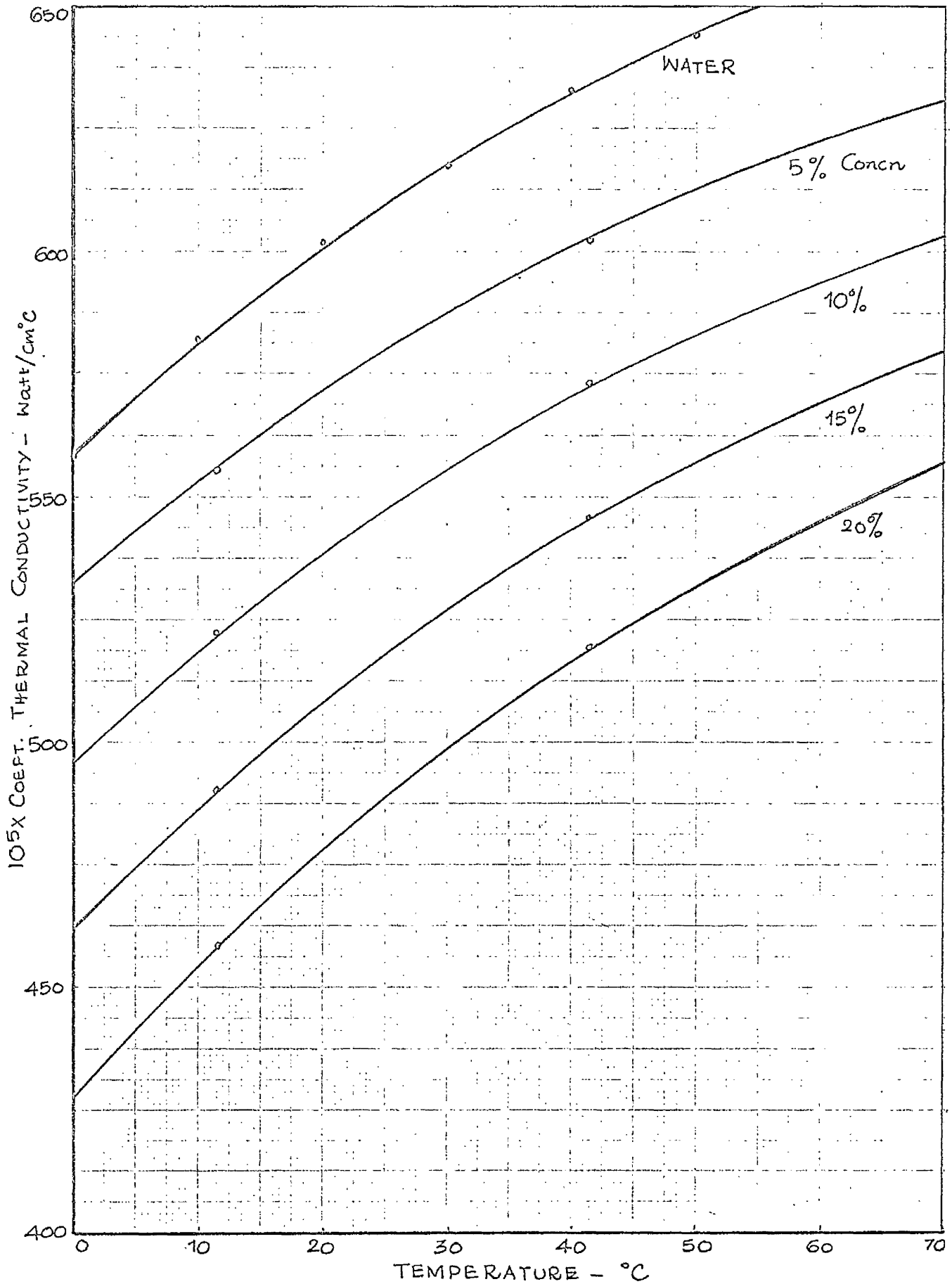

FIG. 4.2.5.2. THERMAL CONDUCTIVITY OF PLURACOL SOLUTION

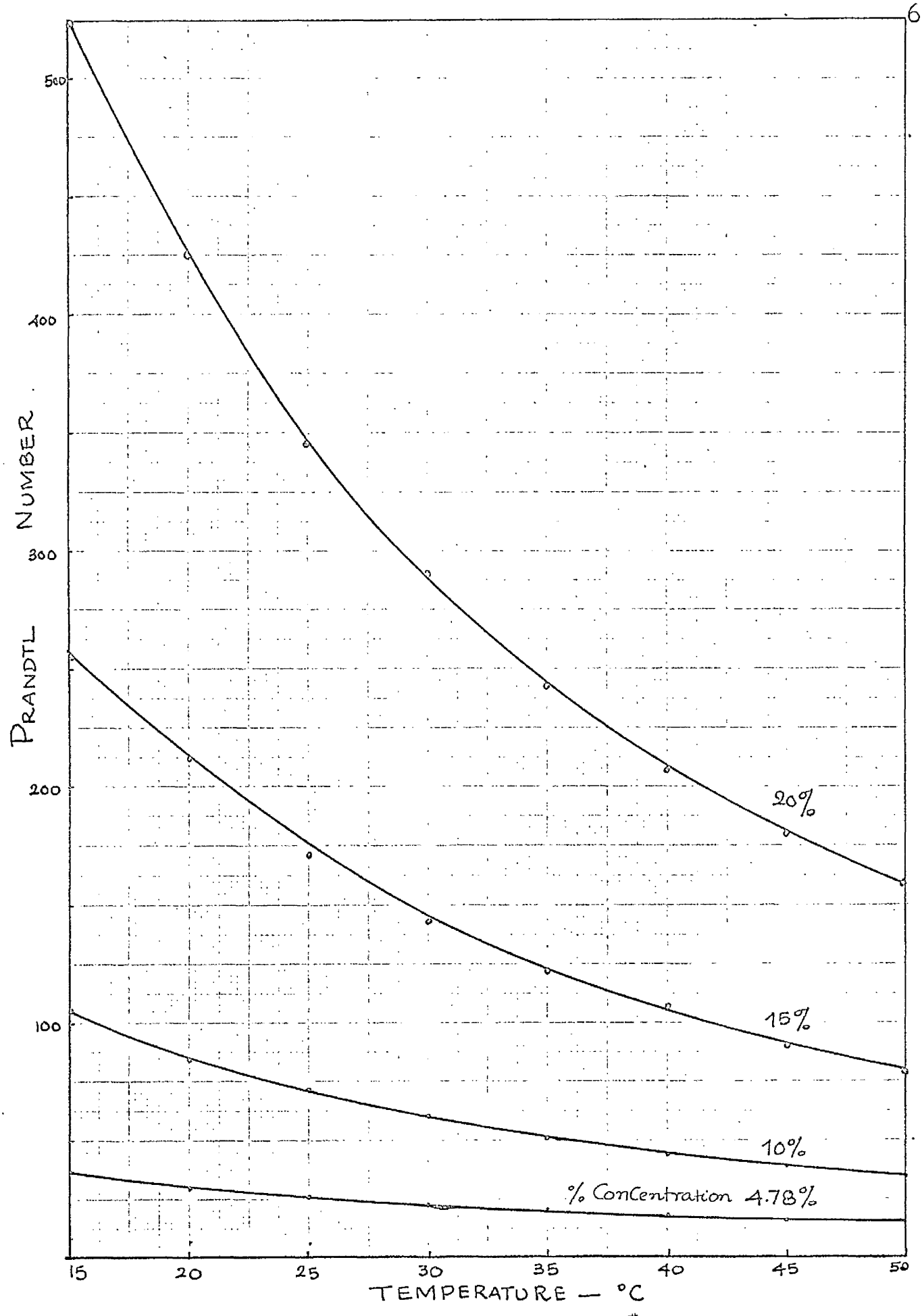

FIG. 4.2.5.3. PRANDTL NUMBER OF PLURACOL SOLUTION.

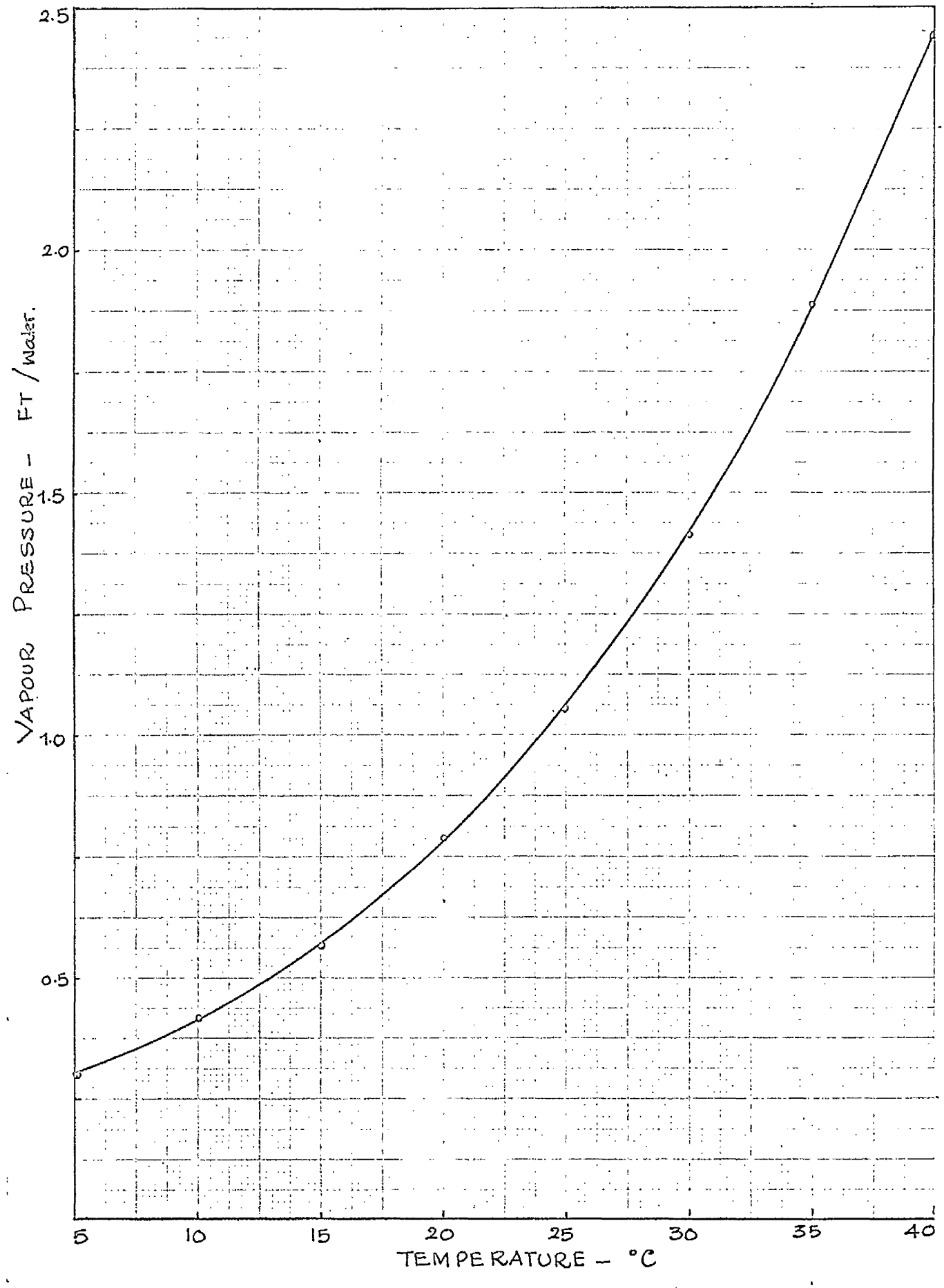

FIG. 4.2.6.1. VAPOUR PRESSURE OF WATER.

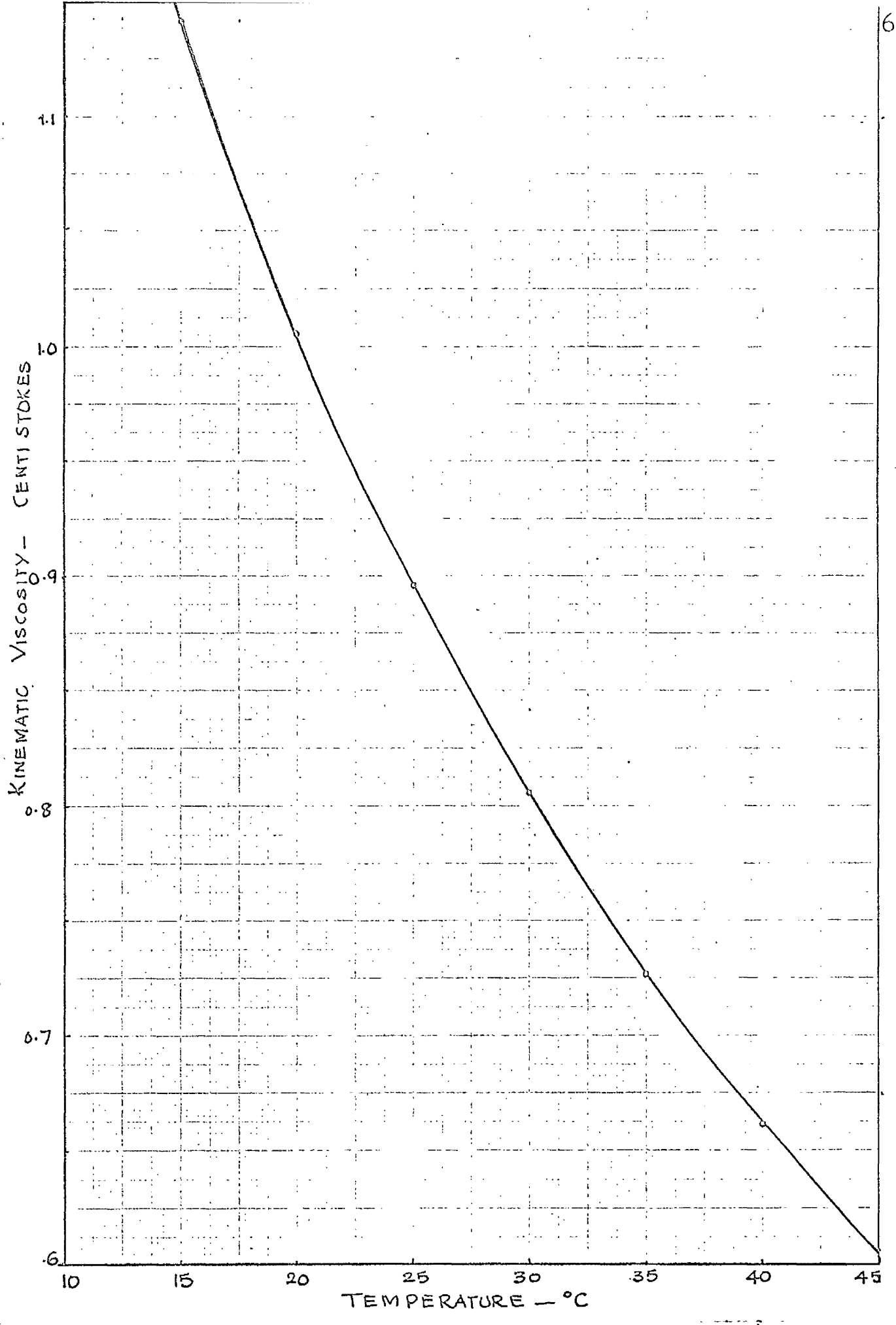

FIG. 4.3.1. KINEMATIC VISCOSITY OF WATER.

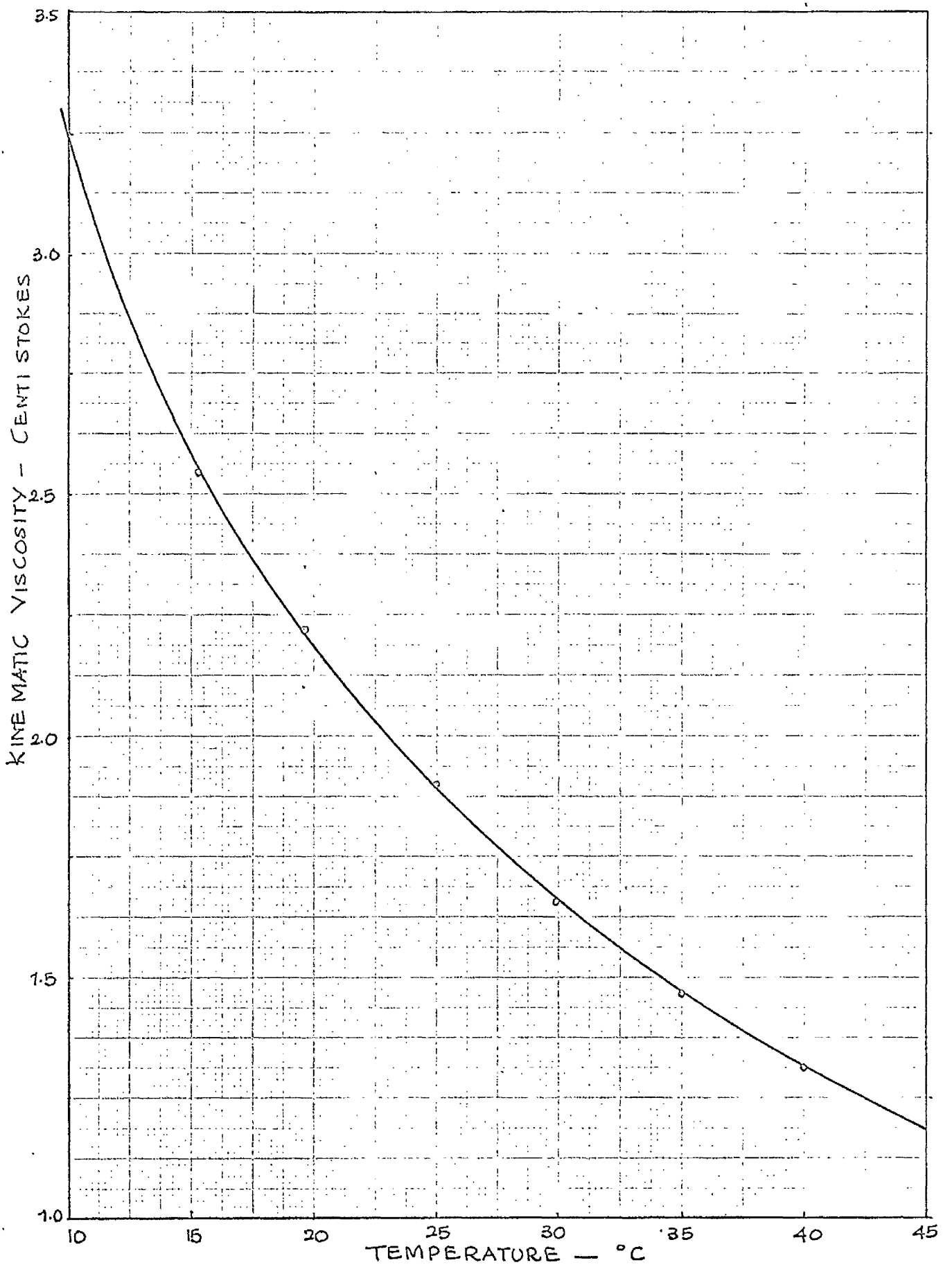

FIG. 4.3.2. KINEMATIC VISCOSITY OF PLURACOL SOLUTION No:1.

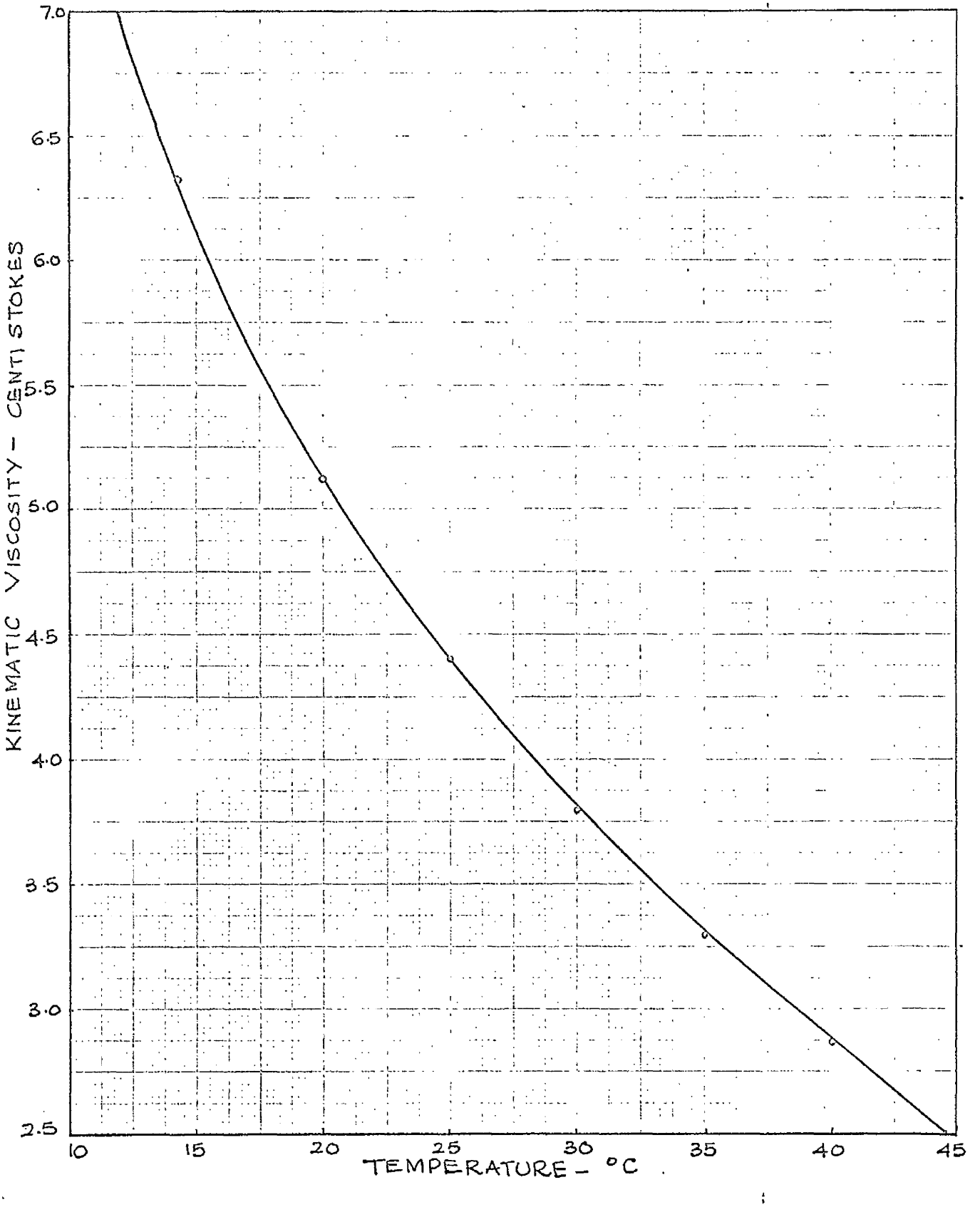

FIG. 4.3.3. KINEMATIC VISCOSITY OF PLURACOL SOLUTION NO: 2.

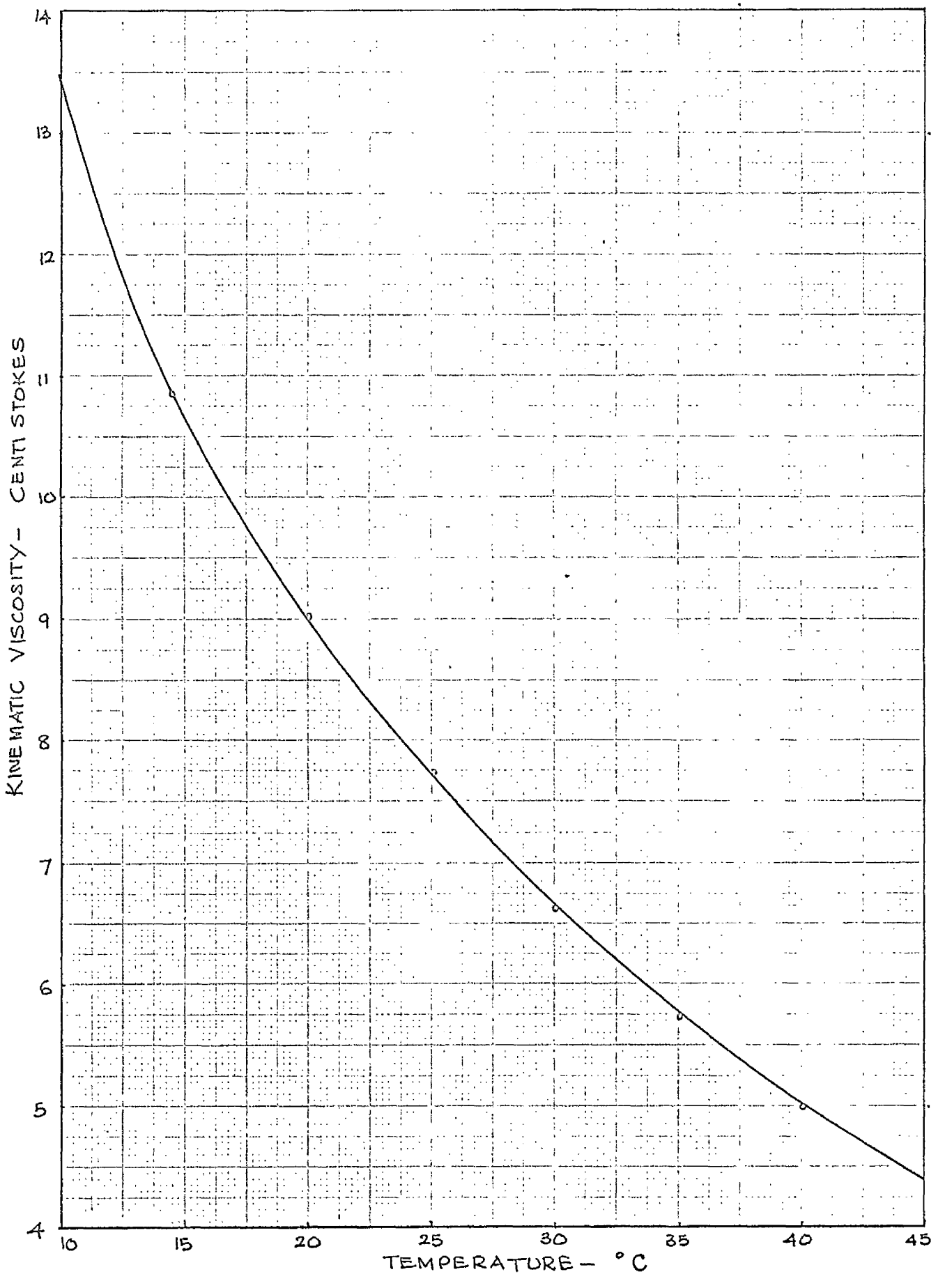

FIG. 4.3.4. KINEMATIC VISCOSITY OF PLURACOL SOLUTION NO: 3.

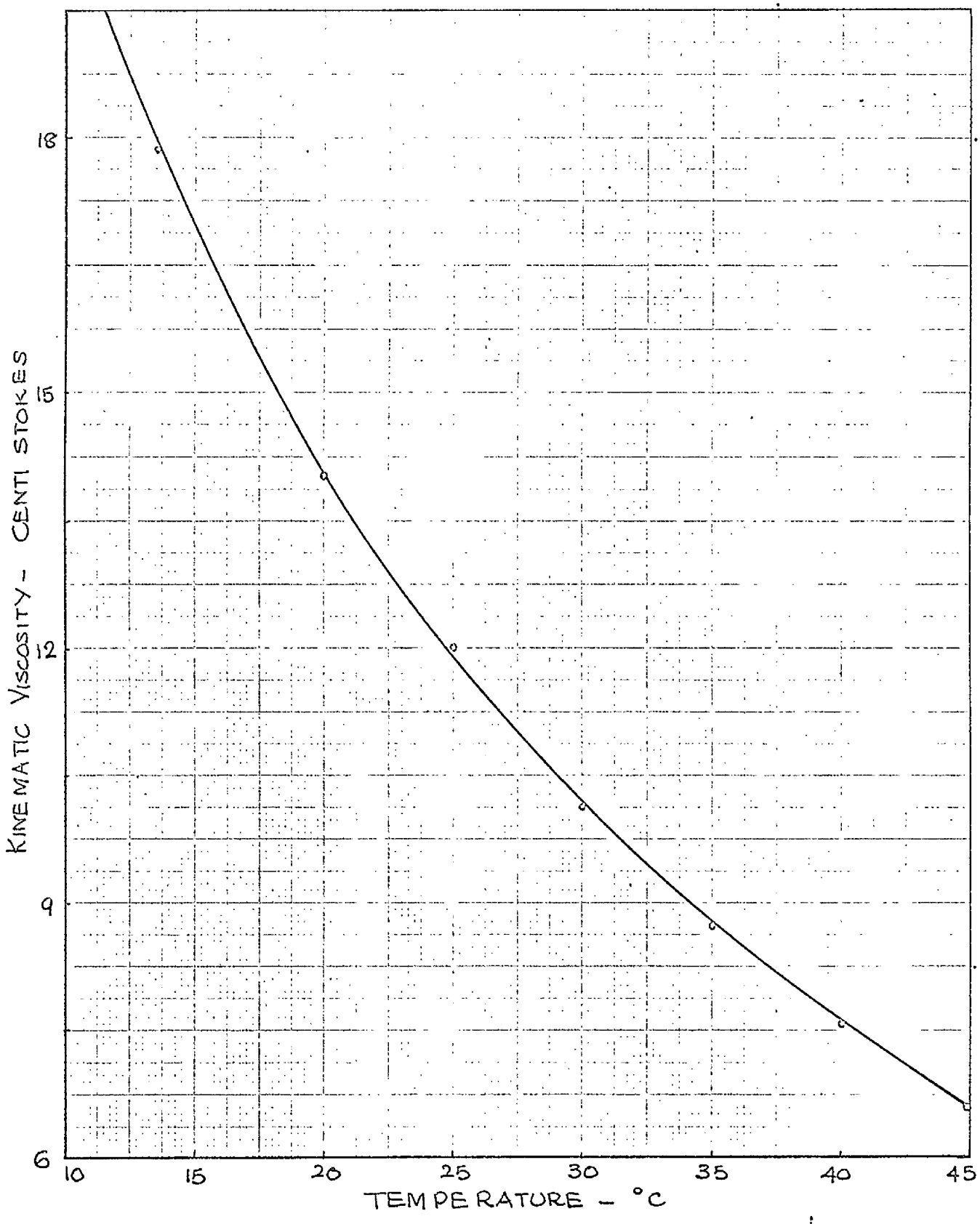

FIG. 4.3.5. KINEMATIC VISCOSITY OF PLURACOL SOLUTION NO: 4.

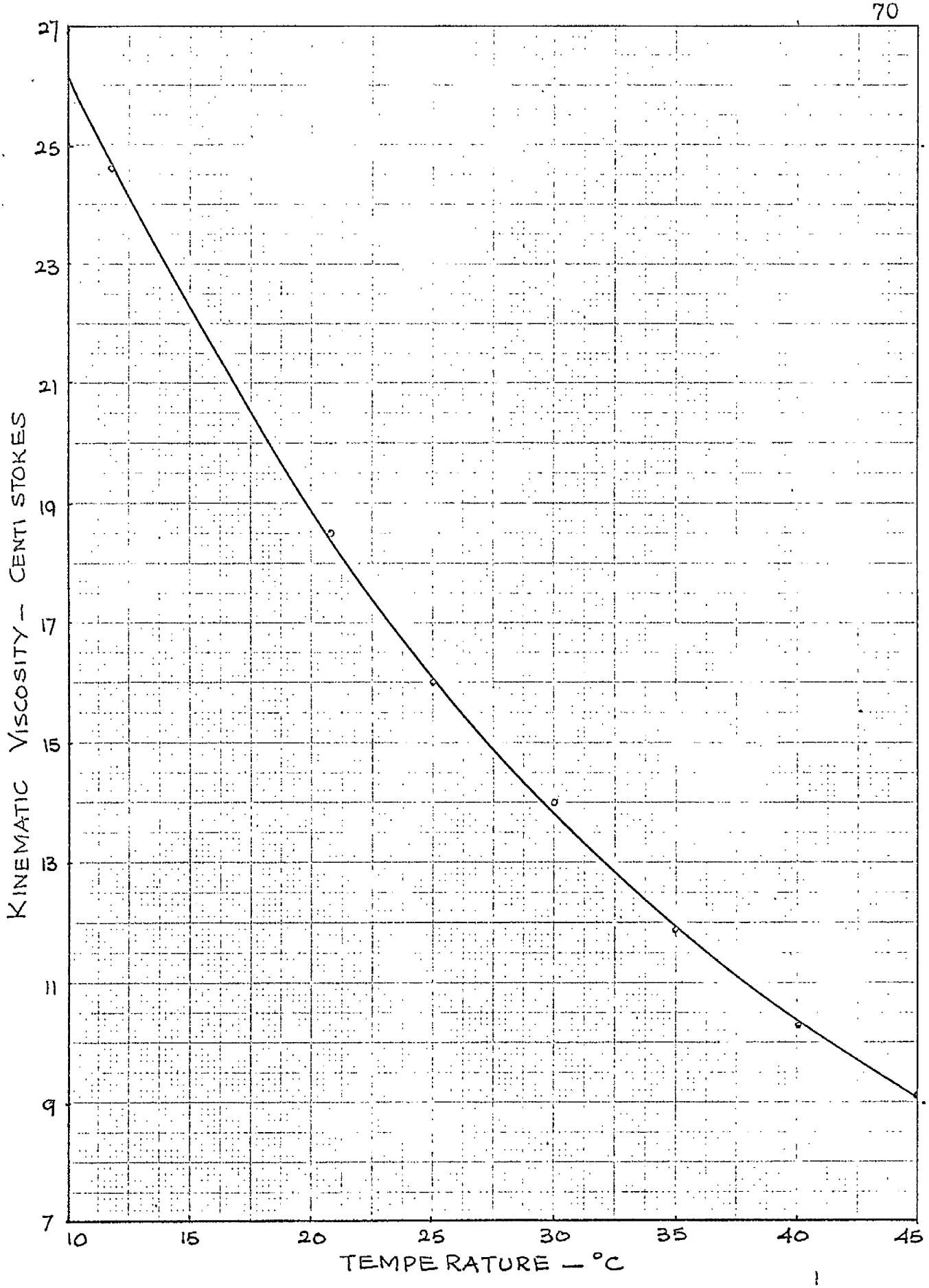

FIG. 4.3.6. KINEMATIC VISCOSITY OF PLURACOL SOLUTION. No: 5.

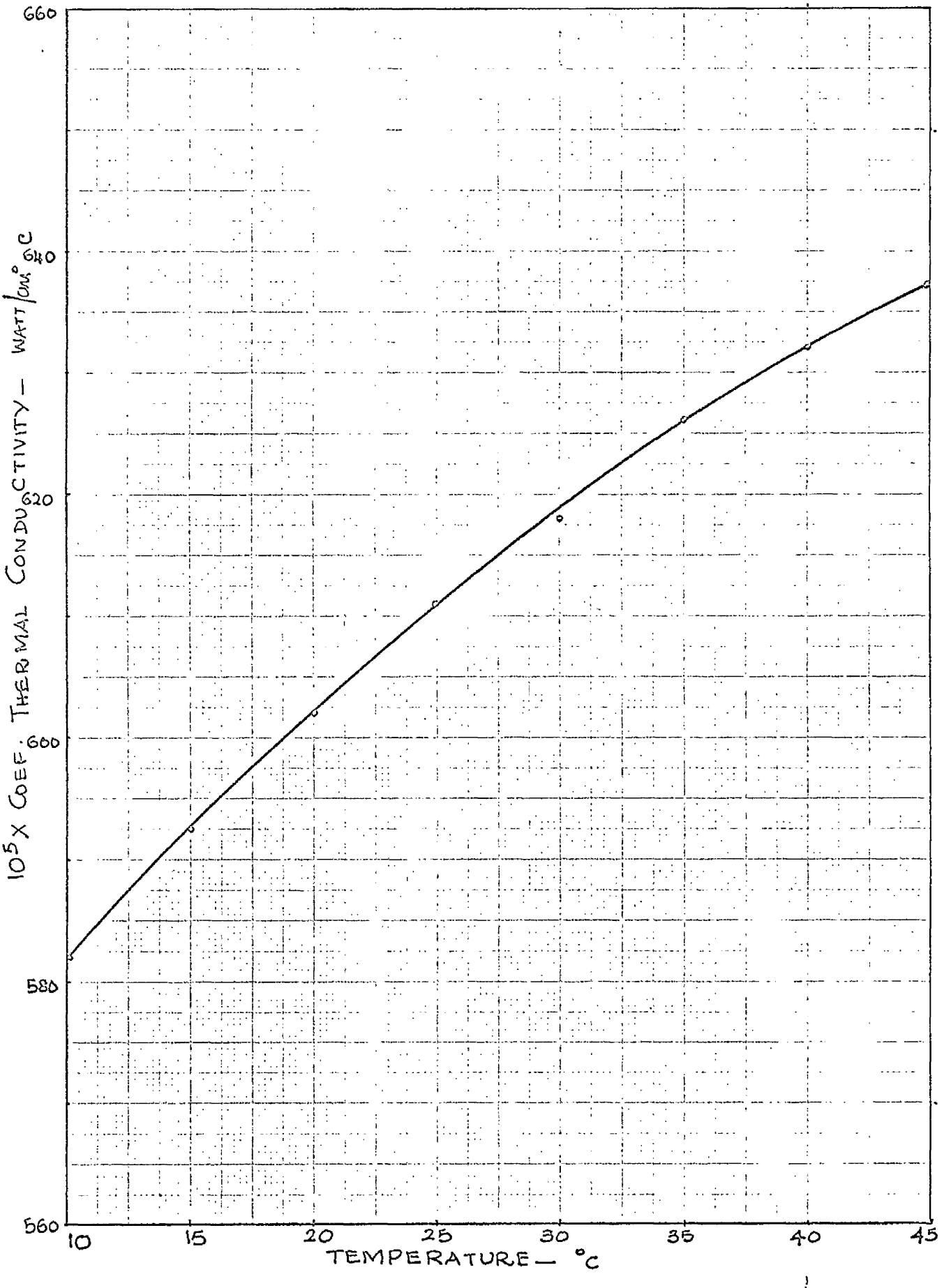

FIG. 4.3.7. THERMAL CONDUCTIVITY OF WATER.

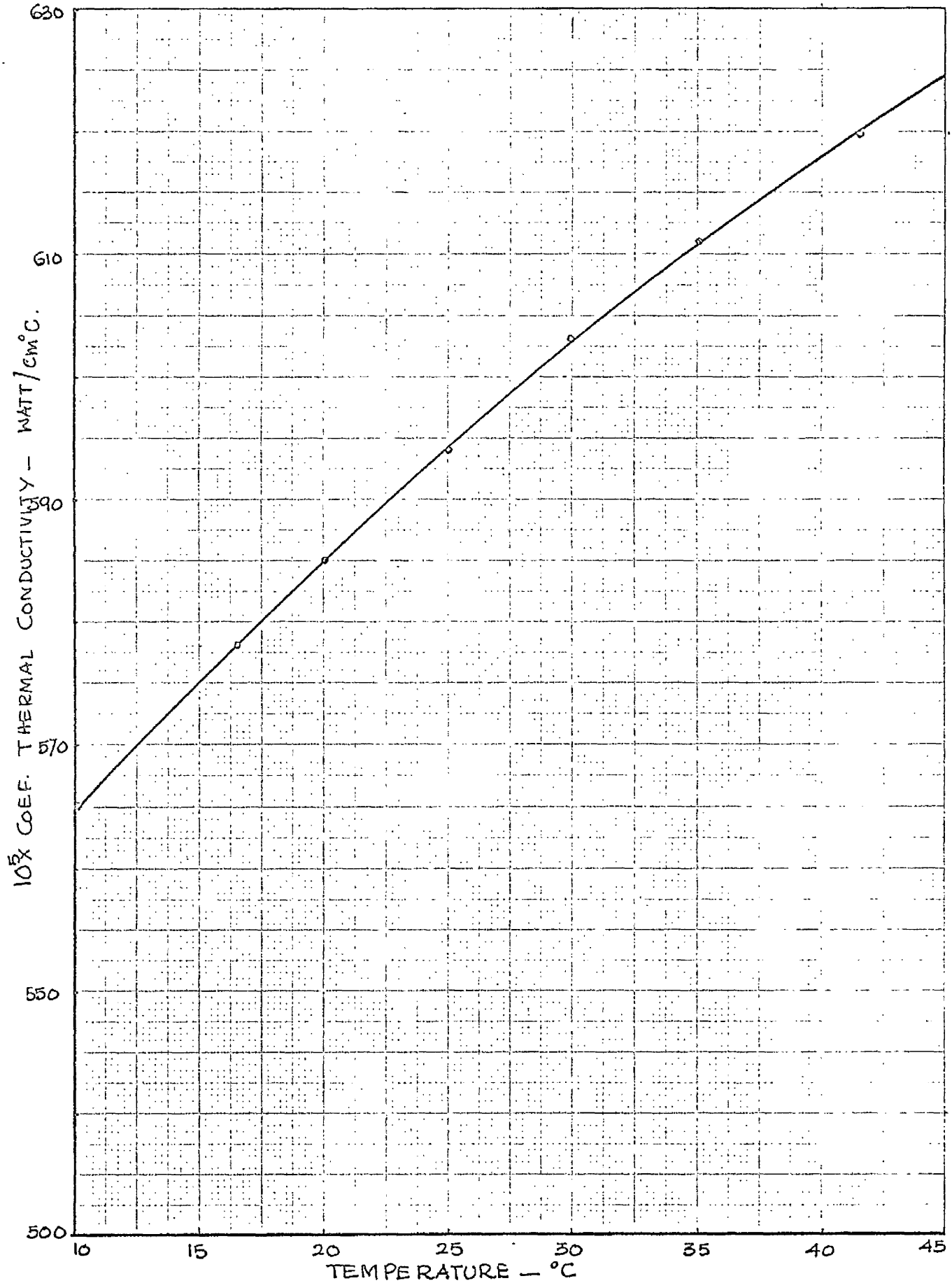

FIG. 4.3.8. THERMAL CONDUCTIVITY OF PLURACOL SOLUTION NO:1.

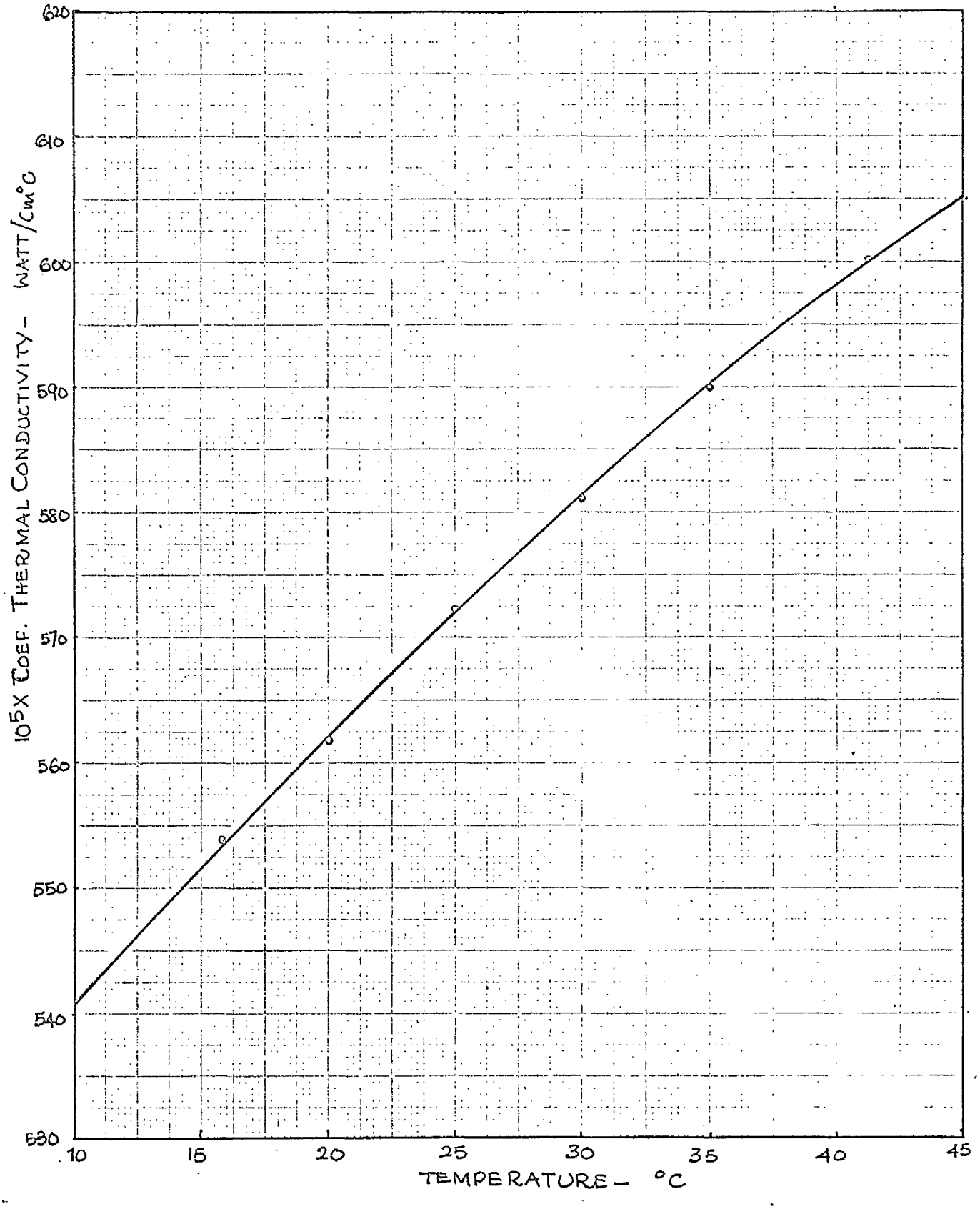

FIG. 4.3.9. THERMAL CONDUCTIVITY OF PLURACOL SOLUTION NO:2.

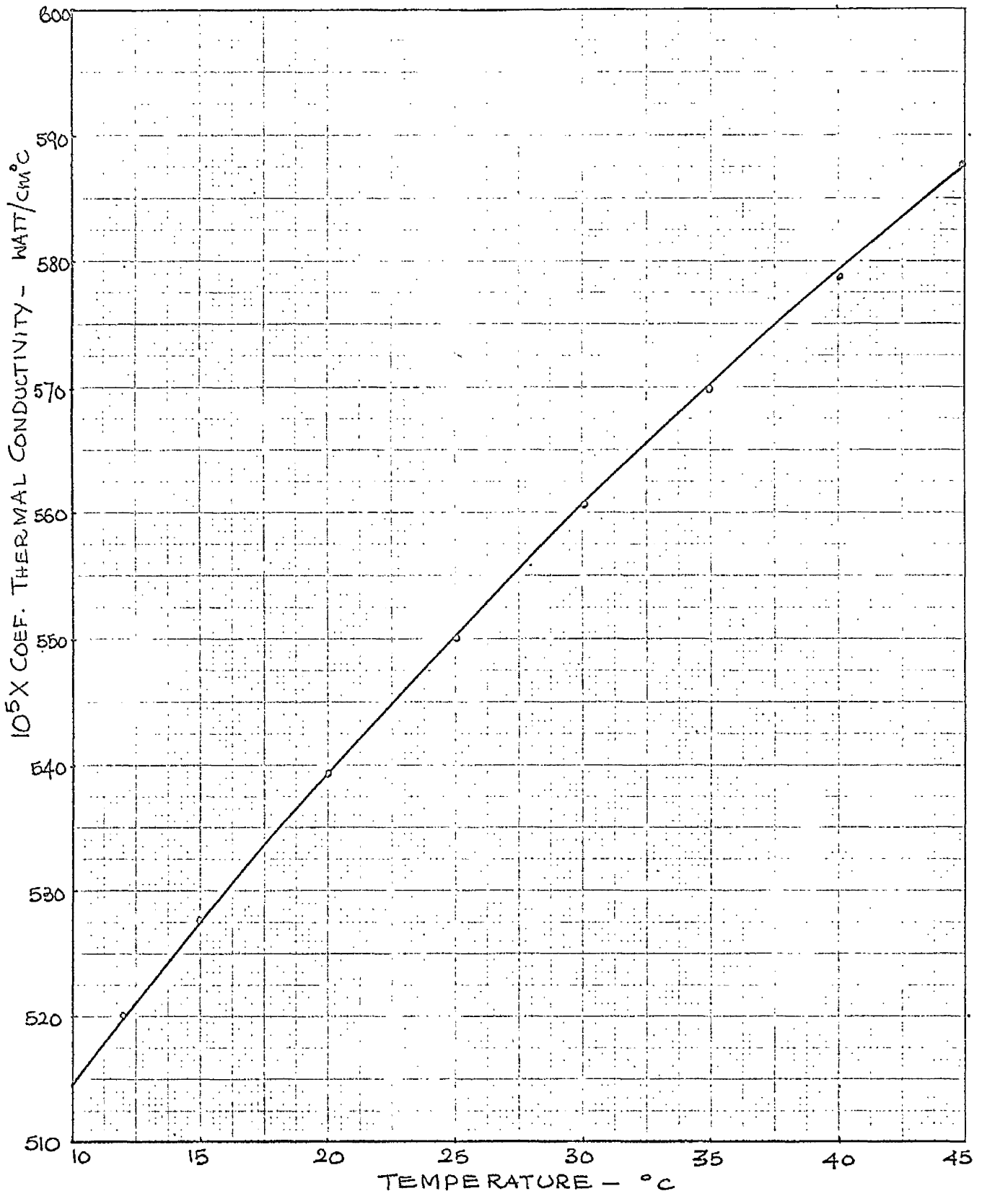

FIG. 4.3.10. THERMAL CONDUCTIVITY OF PLURACOL SOLUTION. NO: 3.

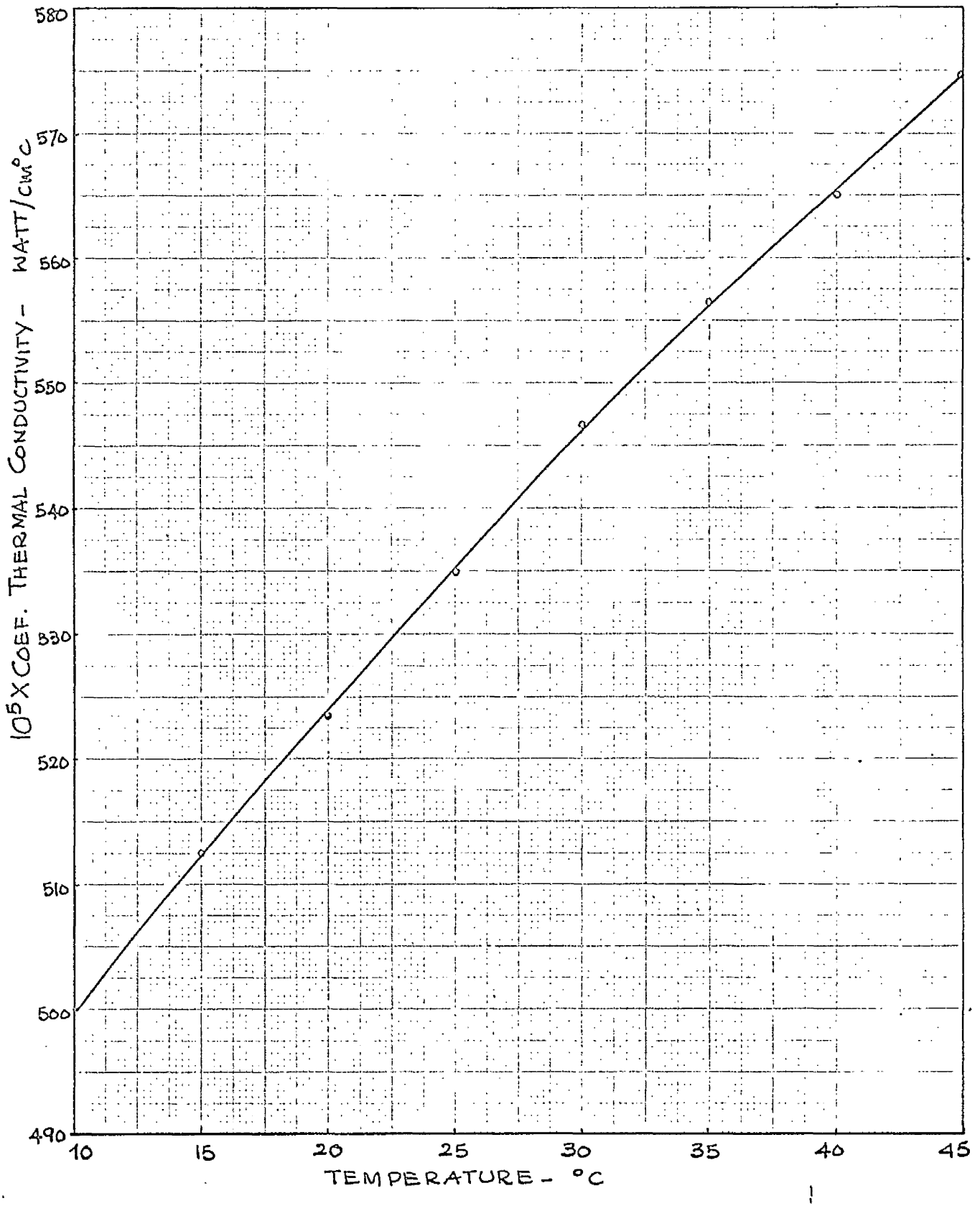

FIG. 4.3.11. THERMAL CONDUCTIVITY OF PLURACOL SOLUTION NO: 4.

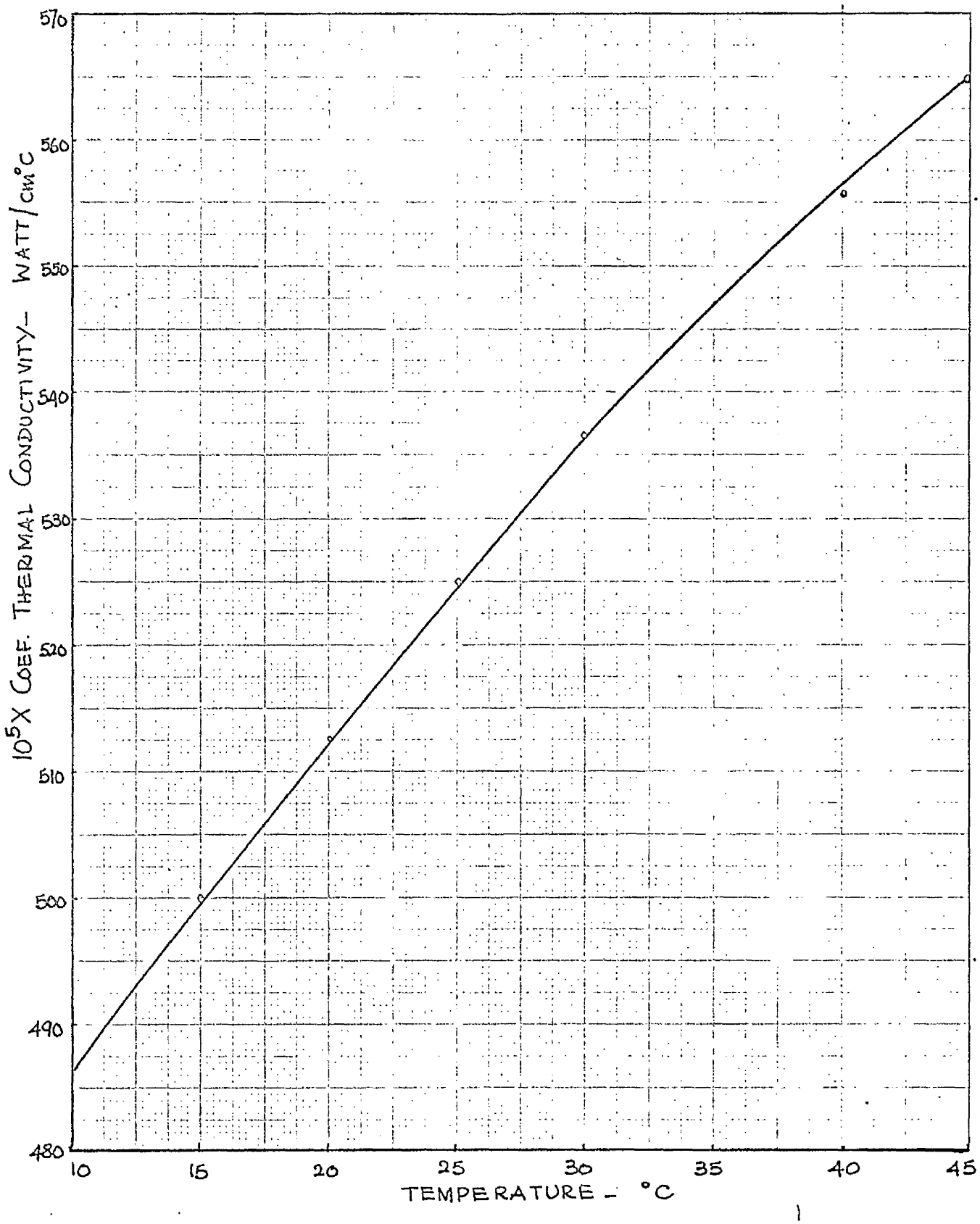

FIG. 4.3.12. THERMAL CONDUCTIVITY OF PLURACOL SOLUTION NO: 5.

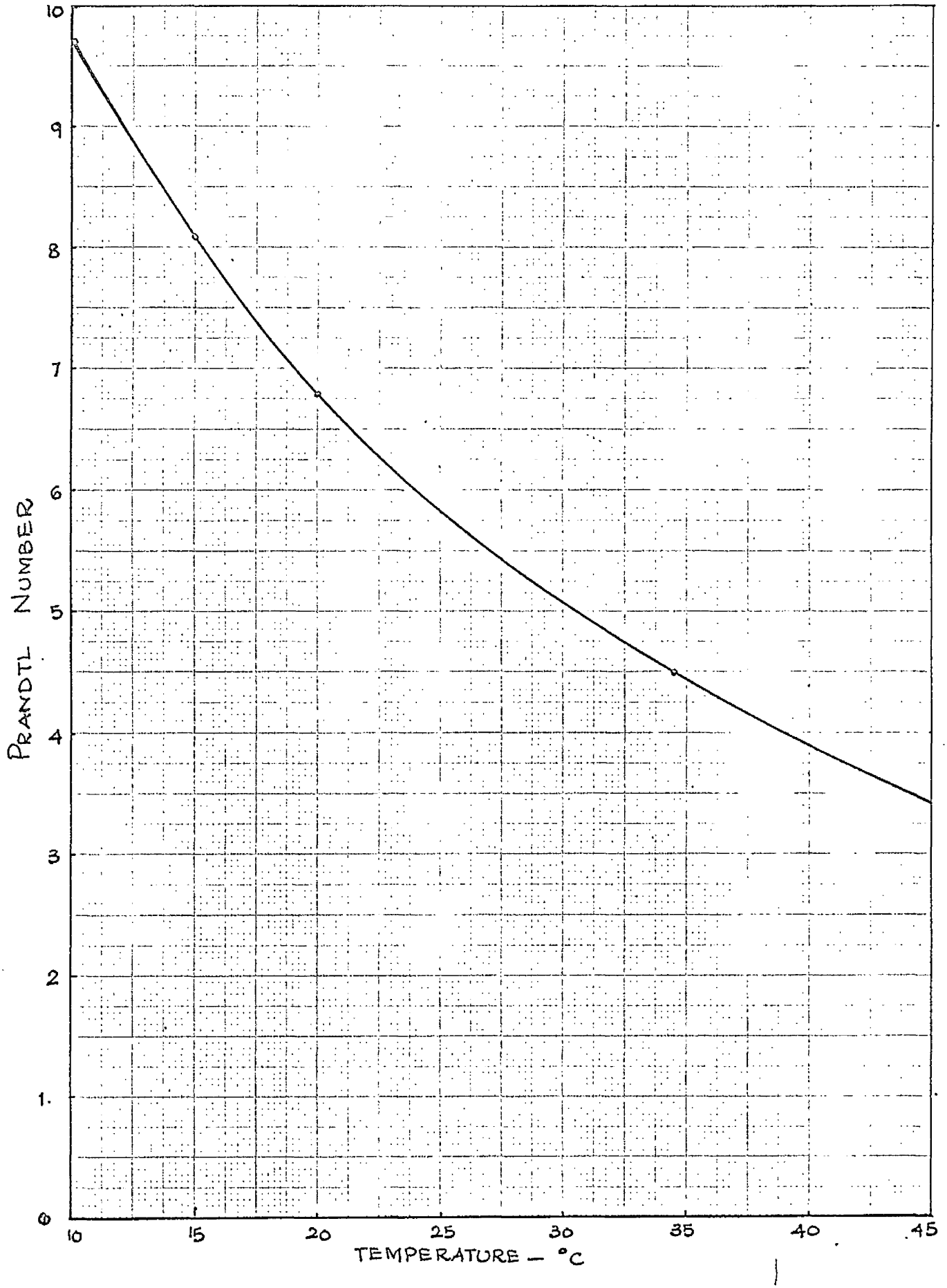

FIG. 4.3.13. PRANDTL NUMBER OF WATER.

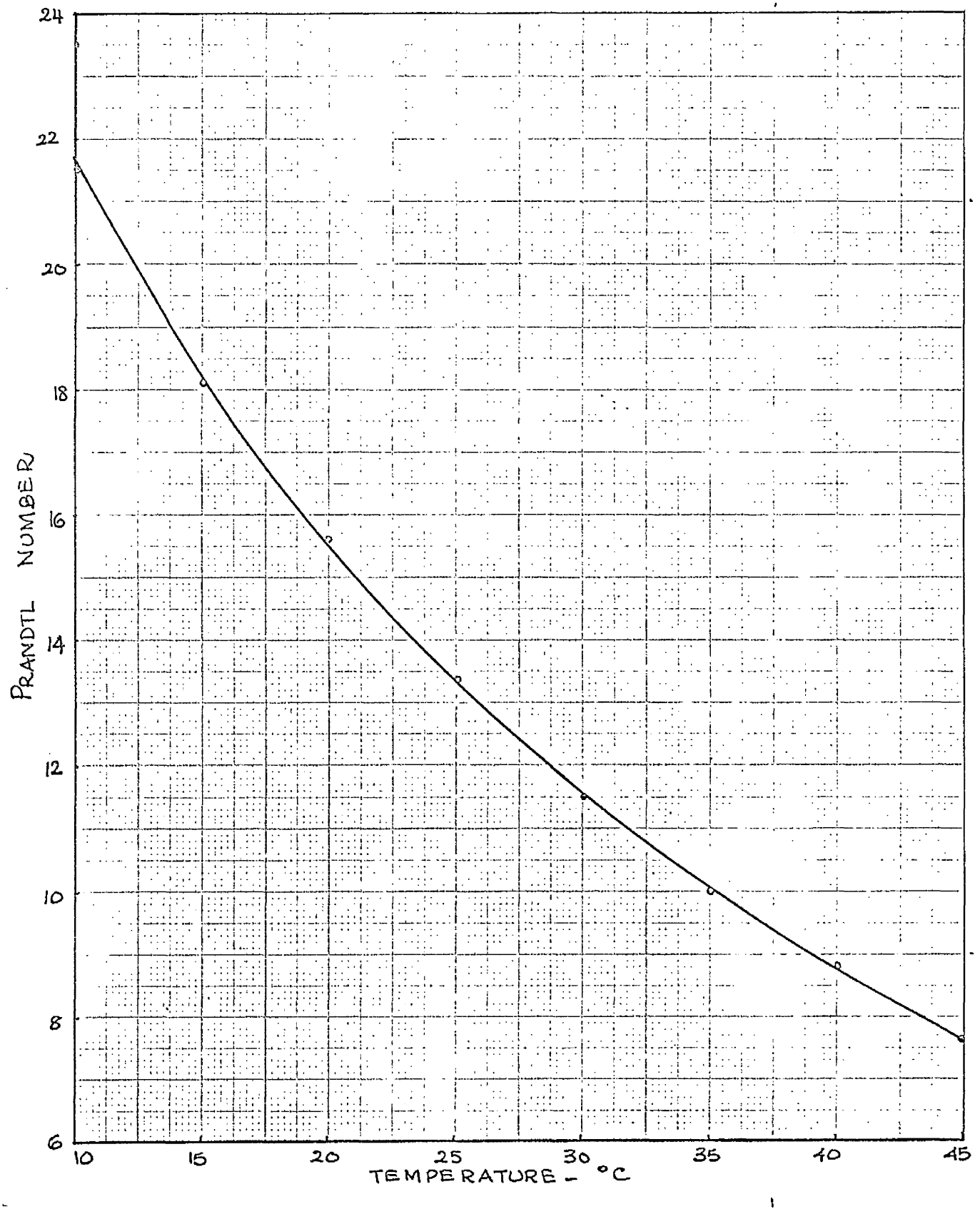

FIG. 4.3.14. PRANDTL NUMBER OF PLURACOL SOLUTION. No.1.

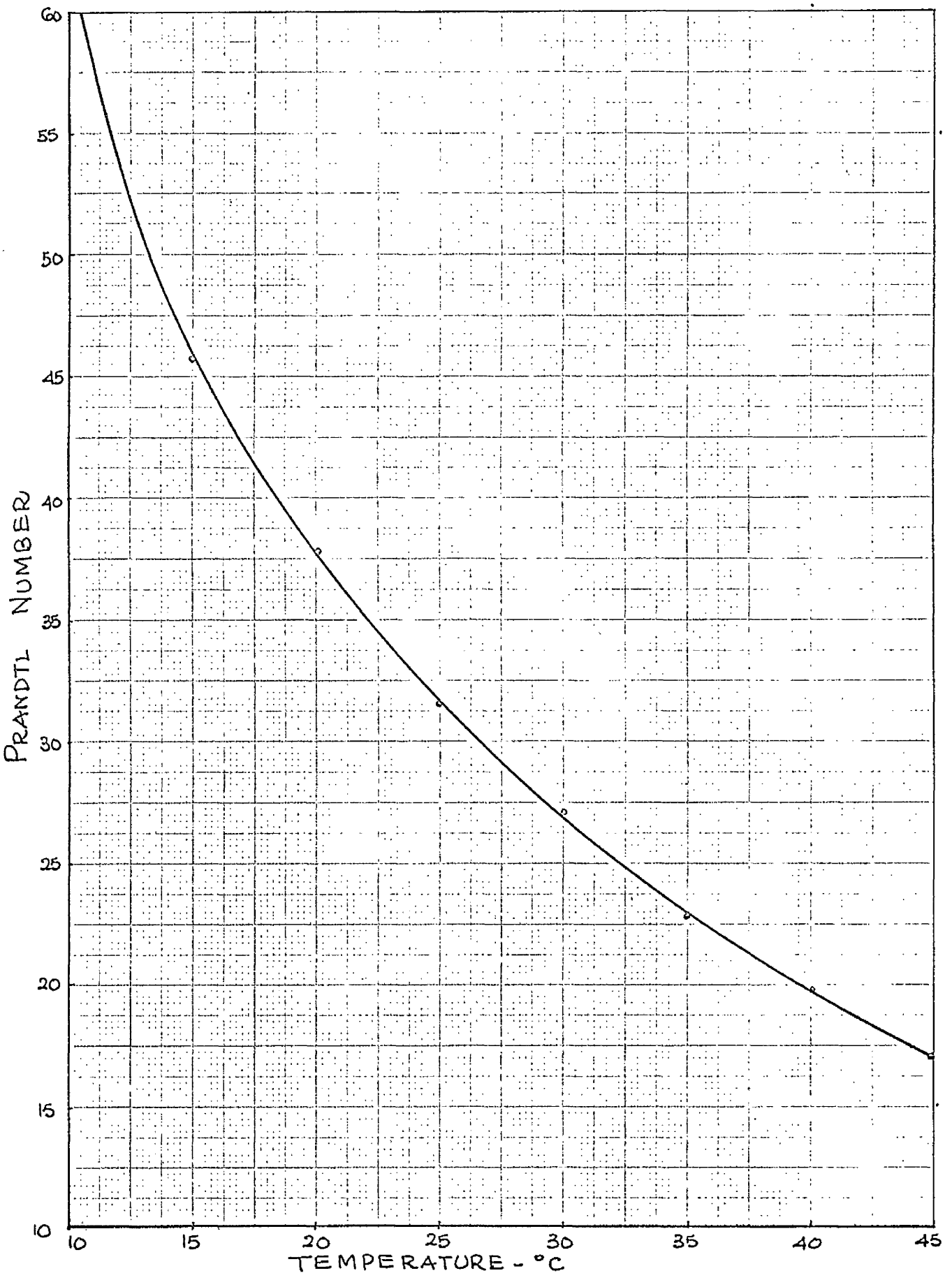

FIG. 4.3.15. PRANDTL NUMBER OF PLURACOL SOLUTION. No:2.

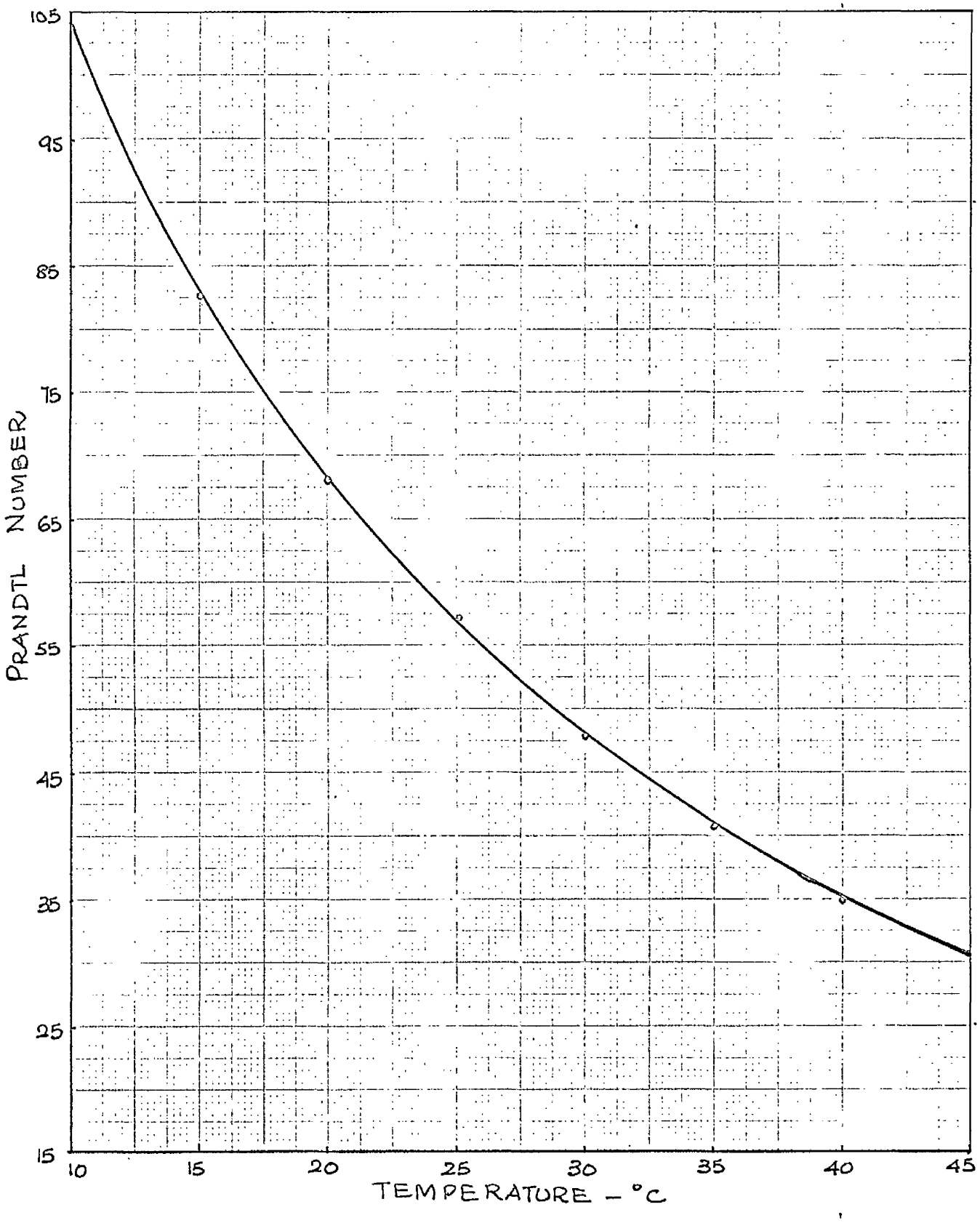

FIG. 4.3.16. PRANDTL NUMBER OF PLURACOL SOLUTION. NO: 3.

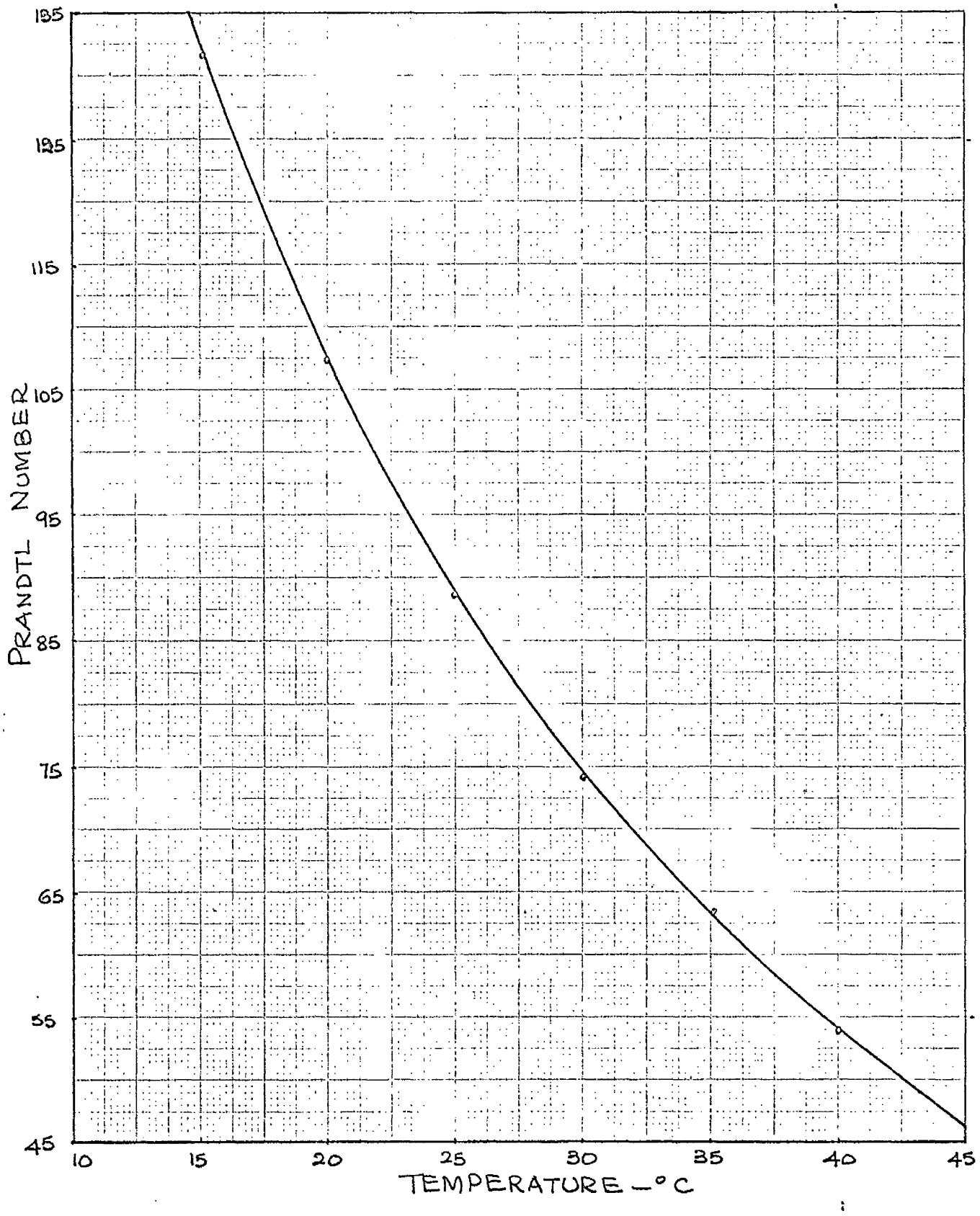

FIG. 4.3.17. PRANDTL NUMBER OF PLURACOL SOLUTION. No: 4.

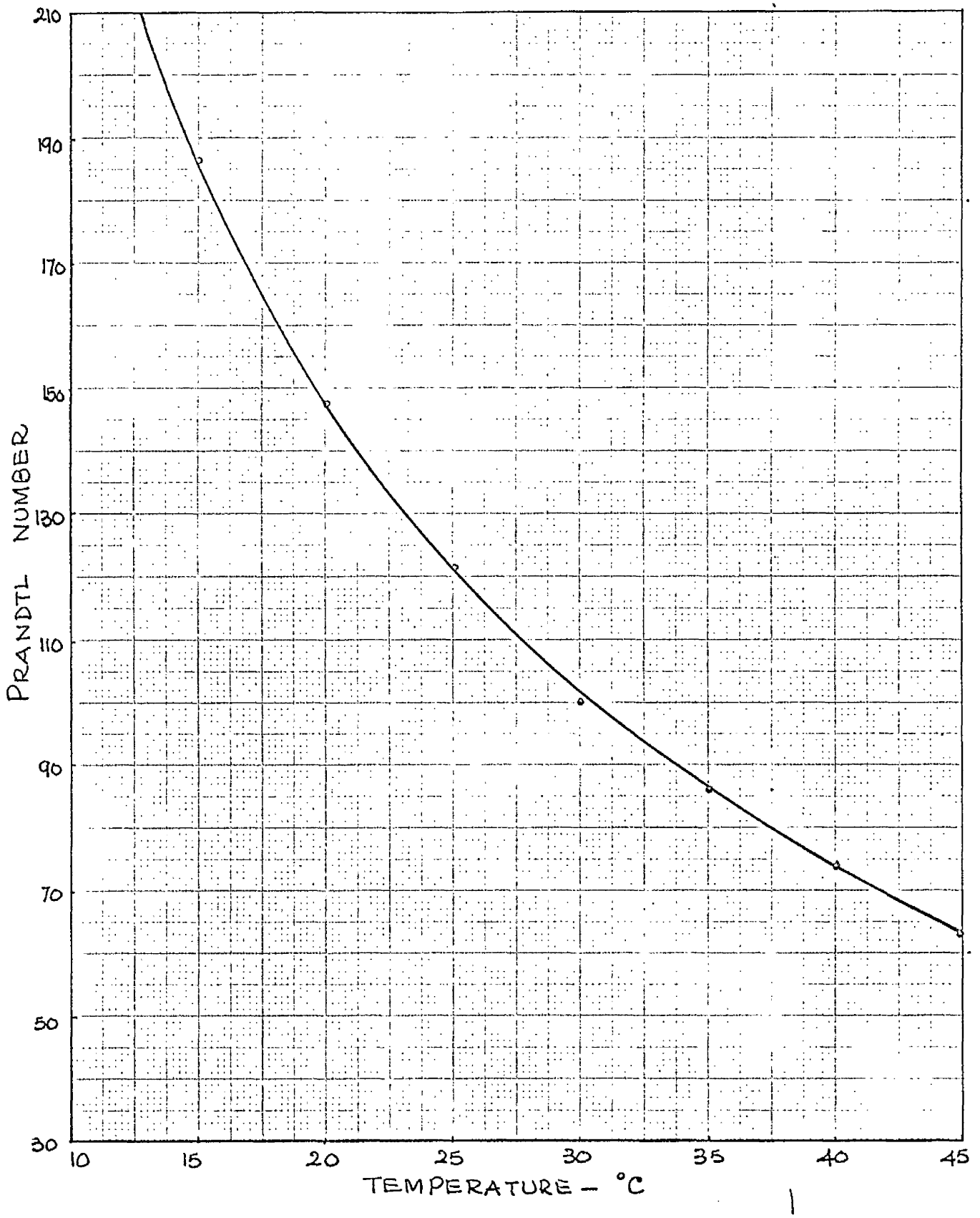

FIG. 4.3.18. PRANDTL NUMBER OF PLURACOL SOLUTION No: 5.

CHAPTER 5

DESCRIPTION OF CAVITATION RIG

5.1 Introduction

A small cavitation rig was designed and erected to primarily conduct experiments on a medium sized centrifugal pump. The cavitation rig consists of a Harland 4 in. monoglide pump, a venturimeter, a non-cavitating valve and a deaerator. The centrifugal pump is driven by a 3-phase 40 h.p. induction motor and the pump is placed at one end of the higher horizontal leg of the circuit. The general layout of the rig is shown in Fig. (5.1.1).

5.2 The Centrifugal Pump

A medium sized centrifugal pump of specific speed 1080 (g.p.m - feet units) was chosen. This Harland 4 in. monoglide centrifugal pump had an impeller of 9.45 in diameter and was capable of delivering 264 g.p.m. at a head of 61 feet at a speed of 1440 r.p.m. It was originally tested at National Engineering Laboratory, East Kilbride and Fig. (5.2.1) shows the pump characteristics with a long straight inlet.

In order to observe the cavitation bubbles and to obtain photographs of the impeller under cavitation some modifications were made to

the impeller and casing of the pump. The impeller was of bronze so as to withstand cavitation damage. The front shroud of the impeller was machined out and replaced by a perspex shroud of similar shape. The perspex front shroud was fixed to the impeller vanes by high tensile screws. Fig.(5.2.2) shows the modified impeller of the pump. The original suction cover of the pump casing was replaced by one made of perspex. A perspex suction pipe 1 foot long was attached to the perspex suction cover, as shown in Fig. (5.2.3).

Fig. (5.2.4) shows the pump characteristics at different speeds and Fig. (5.2.5) shows the pump characteristics while pumping fluids of different viscosities. These were calculated using the results given by Tetlow[39] in his paper.

The original gland of the pump was removed and a rotary mechanical seal was used in its place. However, the mechanical sealing, though more efficient than the ordinary stuffing box type of sealing, did not come up to expectation due to the inherent vibration present in the power transmission side of the rig. The mechanical sealing was satisfactory only down to 20 feet of vacuum suction pressure and below this pressure the atmospheric air started to leak into the circuit through the mating surface of the sealing. This imposed a very sever limitation on the function of the deaerator. It is therefore recommended that the mechanical sealing is replaced by a more efficient sealing in future works. Fig. (5.2.6) shows the complete mounting of the pump.

5.3. The Electrical Motor

The centrifugal pump is driven by a 3-phase, 40 h.p. induction motor provided with a Crofts Variable speed pulley drive consisting of a patent V/S pulley assembly mounted on the shaft of the electric motor. The motor is mounted on an adjustable slide base and the entire speed range which can be varied gradually from 1,000 to 2,000 r.p.m. within the limits of the maximum and minimum diameter of the V/S pulley, can be attained whilst driving, by adjustment of the base wheel. The pulley assembly mounted on the motor shaft consists of the two cone-faced discs, one fixed, the other sliding; when combined they form a V-groove pulley of variable pitch diameter. Rotation of the hand-wheel moves the motor platform and motor towards or away from the driven shaft which in turn automatically increases or reduces the pitch diameter of the variable speed pulley. The motor and the pulley drives were mounted on a platform supported by the wall and a tie-rod. Fig.(5.3.1) shows the motor, the pulley and the driving shaft assembly. Fig.(5.3.2) shows the efficiency of the power transmission assembly.

5.4. Venturi-meter

A standard venturi-meter was installed in the circuit to measure the discharge from the pump. The venturi-meter was designed in accordance with B.S.1042 specifications. The inlet pipe diameter was 4 in. with a $2\frac{1}{4}$ in. diameter throat which produced an "m" ratio of approximately 0.316. The venturi-meter was designed to measure

up to 1.4 cu.ft/sec. with a maximum differential head of 30 in. of mercury and had a 10 degree outlet cone. The resultant head loss was assumed to be about 12% of the applied differential head. A 5 feet long (= 15 D) straight pipe was installed upstream.

The venturi-meter was calibrated, before installing it in the cavitation rig, with exactly the same upstream configuration as that of the main circuit. The calibration curve is shown in Fig. (5.4.1) and the coefficient of discharge of the venturi-meter compares favourably with the B.S.1042 curve.

5.5 The Non-cavitating valve

A valve which is being used as a part of a closed-circuit rig such as the present cavitation rig should necessarily possess the two main qualities given below:

(a) Operation free from fluctuations in pressure or flow since the mass and volume of fluid available in the circuit for damping are small.

(b) Over a wide range of valve opening, the valve must be able to operate free from cavitation.

Such a valve has been successfully designed[40] and used in the National Engineering Laboratory at East Kilbride. This valve essentially consisted of a long tapered plug which could be moved axially in a similarly shaped body. Along the direction of flow the diameter of both plug and body increased and the flow was directed through an annular passage of gradually increasing area. The energy

was therefore dissipated by friction at the solid boundaries and the characteristics of the valve could be altered by moving the plug axially, varying in turn the shape of the boundaries.

The design of the valve used in the present cavitation rig was essentially the same as that of model 7 of the paper by D. Firth and Leslie Young[40]. The valve consisted of a plug of $16\frac{1}{4}$ in. length with 12° taper and a similarly shaped body. The outlet section of the valve body, beyond the diverging conical part, was suitably shaped to fit 6 in. diameter outlet pipe section. Five pressure tappings, equally spaced, were provided along the conical section of the valve body. The valve body was made out of perspex in order to observe cavitation. Fig. (5.5.1) shows the construction of the valve in detail.

Using Bernouilli's equation, we can write that loss of pressure head L through the valve

$$L = (H_1 - H_2) + \frac{V_2^2}{2g}\left[\left(\frac{A_2}{A_1}\right)^2 - 1\right] \qquad (5.5.1)$$

where H is pressure head, V is the velocity, A is the area of cross-section, and suffixes 1 and 2 stand for inlet and outlet sections of the valve respectively. Therefore,

$$\text{Loss Coefficient} = \frac{L}{\left(\frac{V_2^2}{2g}\right)} = \frac{(H_1 - H_2)}{V_2^2/2g} + \left[\left(\frac{A_2}{A_1}\right)^2 - 1\right] \qquad (5.5.2)$$

$$= \frac{H_1 - H_2}{V_2^2/2g} + 4.05, \text{ in the present case.}$$

Fig. (5.5.2) shows the loss coefficient of the valve against valve travel which is expressed as percentage of outlet diameter.

Energy loss taking place in the valve may be divided into two parts: (1) The friction loss which mainly occurs in the annular diverging passage (2) The form loss which takes place mainly beyond the maximum diameter of the plug. Firth and Young[40] give the following formula for the total losses,

$$\text{Total Losses} \quad L = \left(\frac{A_2}{A_e}\right)^2 \left[f.z. \frac{1}{l.\sin\theta} + K\right] \frac{V_2^2}{2g} \qquad (5.5.3)$$

where f is the friction factor, z the length of the equivalent straight annular pipe, A_e its area which is the geometric mean of the areas normal to flow at the beginning and end of the conical section of the plug while z is axial length of that conical section, l valve travel, θ the semi-angle of the cone (plug) and K the form-loss coefficient. By rearranging the above equation, we get

$$\frac{f.z}{\sin\theta} \, l^{-1} + K = \frac{L/(V_2^2/2g)}{(A_2/A_e)^2} \qquad (5.5.4)$$

Fig. (5.5.3) shows the term on the right-hand side of the above equation plotted against the reciprocal of valve travel l. The average values of the friction factor f and the form-loss coefficient were obtained from it.

$$f = 1.29 \times 10^{-2} \qquad \text{and} \quad K = 0.245$$

The value of friction factor f for the valve is of the same order as those found for flow in smooth concentric annular pipes. The value

of form-less coefficient is, however, almost reduced to half the expected value of 0.45. This is probably due to the relatively large size of the outlet section of the body compared to the dimensions of the plug of the valve.

The pressure distribution along the valve body is shown in Fig. (5.5.4) for various valve openings. The cavitation rig was originally designed and erected for testing a centrifugal pump and only five equally spaced pressure tappings were provided along the diverging section of the perspex body of the valve. These pressure tappings were utilised to measure the pressure along the valve body and therefore Fig. (5.5.4) gives only a general idea of the pressure distribution along the valve body. Since the lowest pressure in the valve was not measured, the pressure measured by the tapping No: 2 was used throughout for calculating cavitation parameter K.

Fig. (5.5.5) shows the expected and actual loss-coefficient of the valve. The increase in loss-coefficient may be due to the increase in the value of the friction factor which was assumed to be equal to 1.18×10^{-2}. The pressure distribution curves show that the minimum pressure inside the valve is well below the outlet pressure and that the point of minimum pressure moves gradually towards the nose of the plug as the opening is creased. Further, the pressure drop along the first quarter of the length of the valve is very steep and this pressure distribution is responsible for cavitation occurring first in the valve. In order to avoid cavitation taking place in the valve, it is suggested that the outlet pressure of the valve be

increased by increasing the vertical height of the rig.

5.6 The Deaerator

Fig. (5.6.1) shows the details of the deaerator. It consists of a 4 in. diameter vertical pipe which is provided with a suitable cap. The cap is provided with $\frac{1}{4}$ in. diameter holes to eject the fluid in the form of small jets. The deaerator is connected at its top to a vacuum pump.

Fig. (5.6.2) shows the rate of deaeration of water, by the deaerator. It was not possible to bring down the pressure of the circuit below 20 feet of vacuum since the atmospheric air started to leak into the rig through the mechanical sealing. Hence it was not possible to deaerate the water in the circuit below 28% of total air content at atmospheric conditions. An apparatus designed by Kanellopoulos[42] was used to measure the gas-content of water.

5.7 The Pressure Control Device

Fig. (5.7.1) shows the pressure control device used in the circuit. It consists of a 6 in. diameter brass cylinder with suitably designed cap. A rubber bladder is attached to the tube which passes through the cap. The cylinder is connected to the main circuit through a valve and the rubber bladder is connected to the vacuum pump through an air-vessel which is provided with valves to control the absolute pressure.

5.8 The Circuit in General

Standard steel pipes of 4 in. and 6 in. diameter were used in the circuit. All the metallic parts coming in contact with water were coated with polyurethene, a pitch based compound, to protect them from corrosion. The circuit was connected to the main water supply through a valve and a suitable opening was provided at the pump level to add pluracol V-10 into water in the circuit. A thermometer pocket was provided in the rig.

Fig. (5.8.1) shows the head developed across the pump at two valve openings.

The rig does not have a heat-exchanger, since the preliminary calculations showed that the circuit would attain a steady temperature of 35°C at an input of 15 h.p. However this was proved wrong since the internal coating of polyurethene and the external coating of paint had considerably changed the heat conducted through the surface of the rig. Fig. (5.8.2) shows the increase in temperature of the circuit water against time while the input power was 7 h.p. While conducting cavitation tests with viscous solutions, a temperature increase of as much as 0.1°C per three minutes was noted. It is therefore suggested the circuit be provided with a heat-exchanger, while the valve is used to dissipate energy generated by the pump.

5.9 Pressure Measurements

5.9.1 Pressure transducers are used in the present circuit to measure the suction and outlet pressures of the pump and a differential pressure

transducer is used to measure the differential head across the venturi-meter. These transducers were mounted separately on a panel and were connected to appropriate points in the circuit through polythene tubes.

The pressure transducers have an accuracy of ± 1% of full range output and operate with 10 volts (d.c) input. The electrical outputs from the pressure transducers are fed into an ultra-violet galvano-meter recorder. Figs. (5.9.1) to (5.9.3) show typical calibration curves of the pressure transducers. The suction and the differential pressure transducers were calibrated against mercury manometers and the outlet-pressure transducer (of the pump) was calibrated against a piston gauge[41].

5.9.2 Mercury manometers were used to measure the pressures in the valve. The pressures can be measured accurately to ± 1 mm. of mercury. Fig. (5.9.4) shows the details of the connections to manometers.

5.10 Speed Measurement

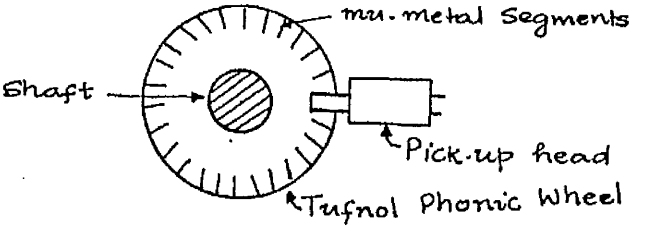

FIG. 5.10.1

A phonic wheel and pick-up head arrangement was used to measure the pump shaft speed, see figure (5.10.1). The electrical output

from the pick-up head was fed into a frequency/D.C. converter. The converter readings were calibrated using a stroboscope. Fig. (5.10.2) shows the calibration curve of the frequency/D.C. converter.

5.11 Power Measurement

Electrical power input to the motor was measured using a watt meter. A mercury thermometer, accurate to $0.1^{o}C$, was used to obtain the temperature of the fluid in the circuit.

5.12 Defects of the present Cavitation Rig

(1) It was found impossible to lower the absolute pressure of the rig below 20 feet of vacuum, since the atmospheric air started to leak into the system through the mechanical seal. It is recommended, therefore that a more suitable sealing of the pump shaft be made before starting any further work on the rig.

(2) The so-called non-cavitating valve started cavitating well before the centrifugal pump. The pressure distribution curves of the valve reveal that a very sharp pressure drop exists along the diverging conical section of the valve. Perhaps the valve cavitation could be prevented by increasing the outlet pressure at the valve by increasing the vertical height of the circuit. A suitably designed turbine could also be used in the place of the non-cavitating valve.

(3) Since the electrical-motor and the pulley mechanisms are mounted on a platform projecting from the wall, vibrations are present in the rig.

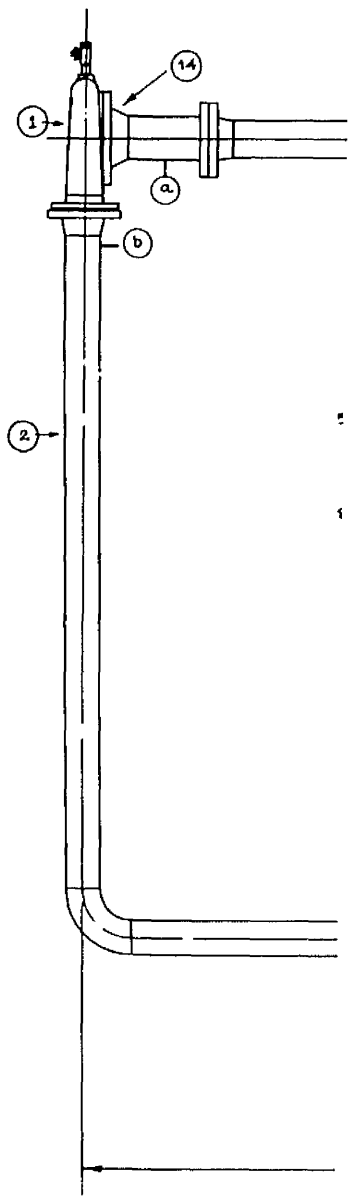

FIG. 5.1.1. GEN

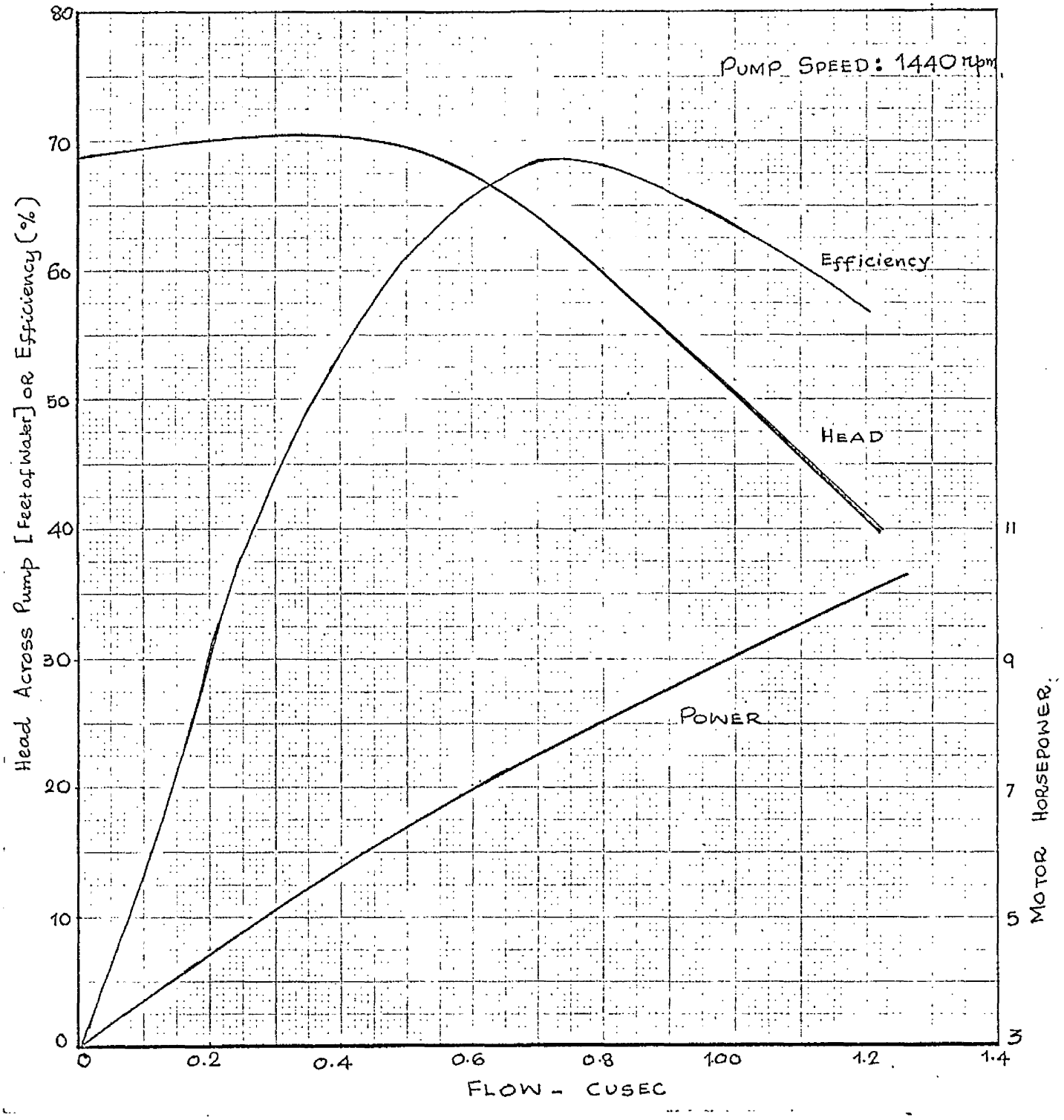

FIG. 5.2.1. PUMP CHARACTERISTICS.

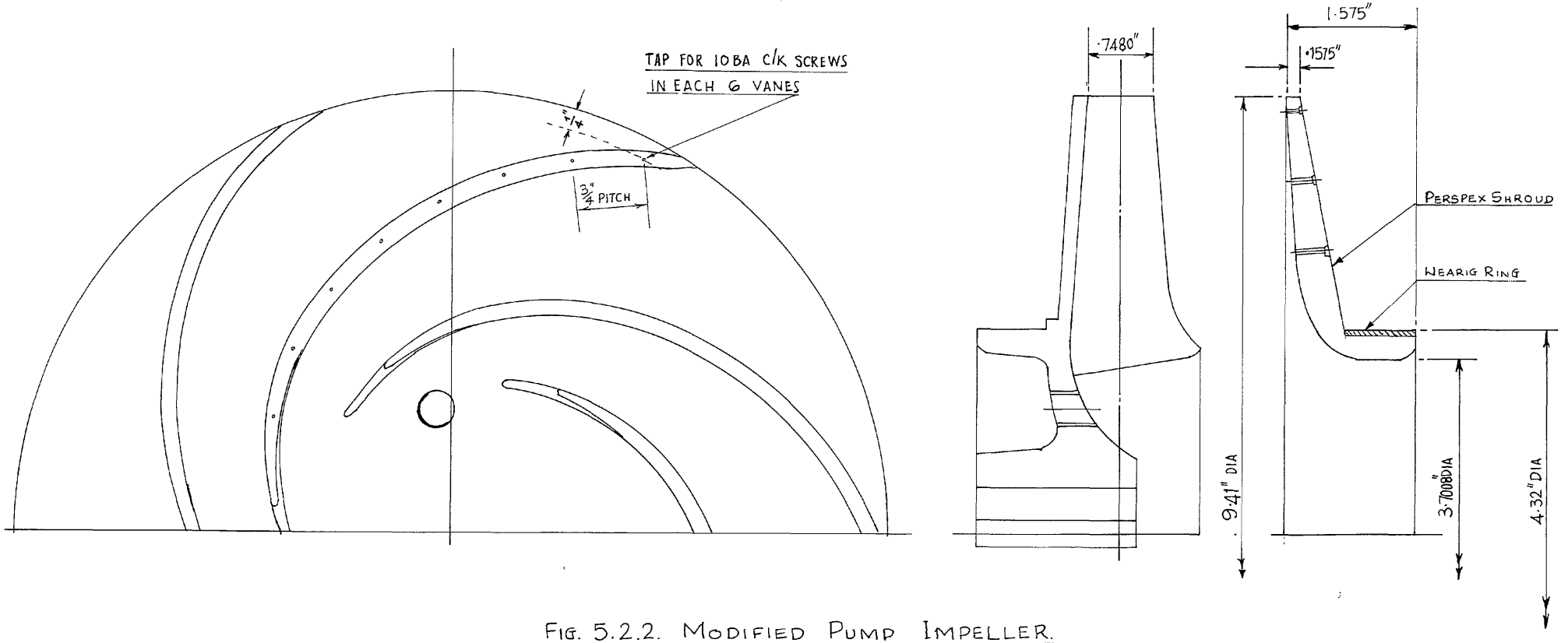

FIG. 5.2.2. MODIFIED PUMP IMPELLER.

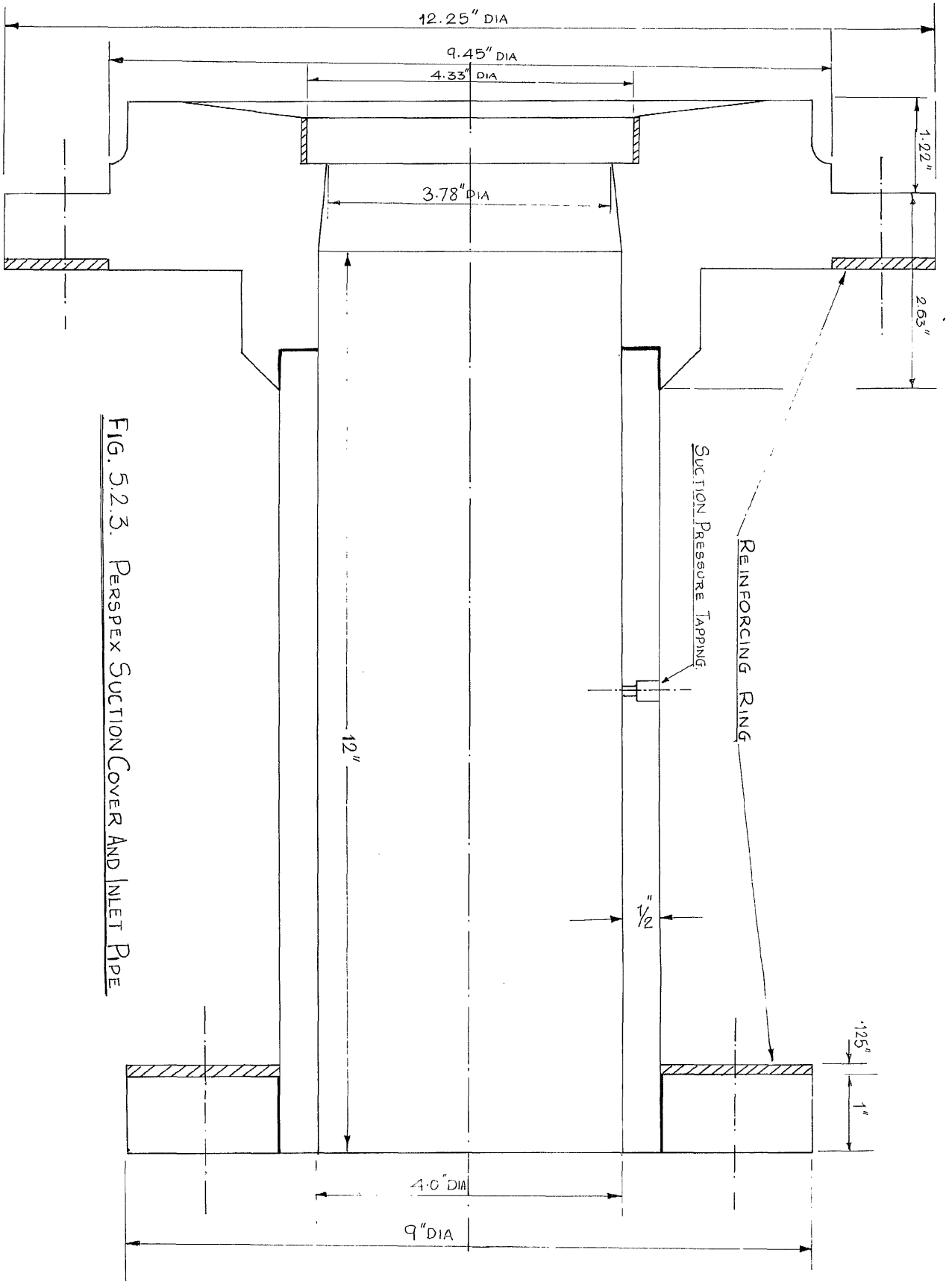

FIG. 5.2.3. PERSPEX SUCTION COVER AND INLET PIPE.

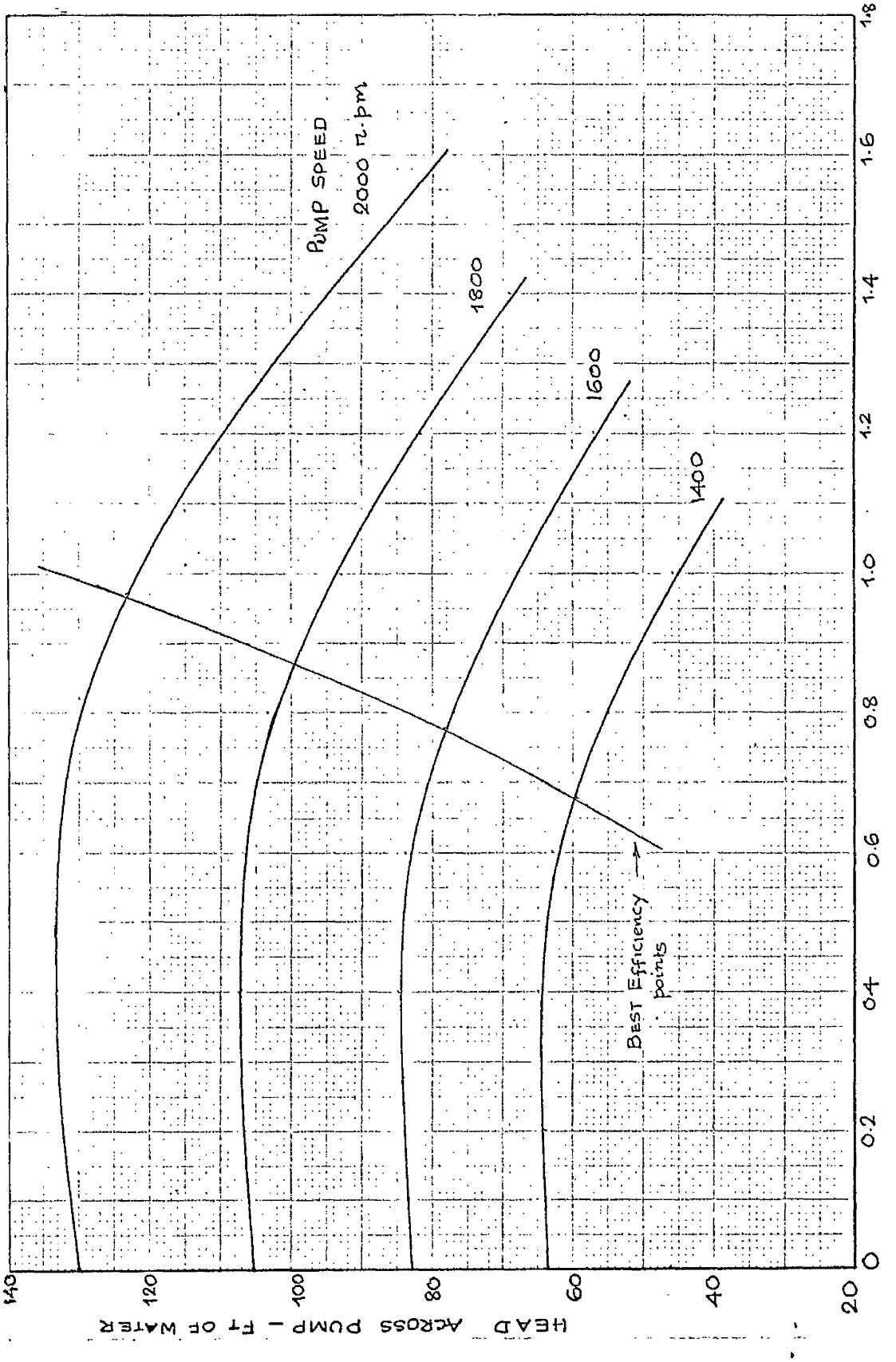

FIG. 5.2.4. PUMP CHARACTERISTICS AT DIFFERENT SPEEDS

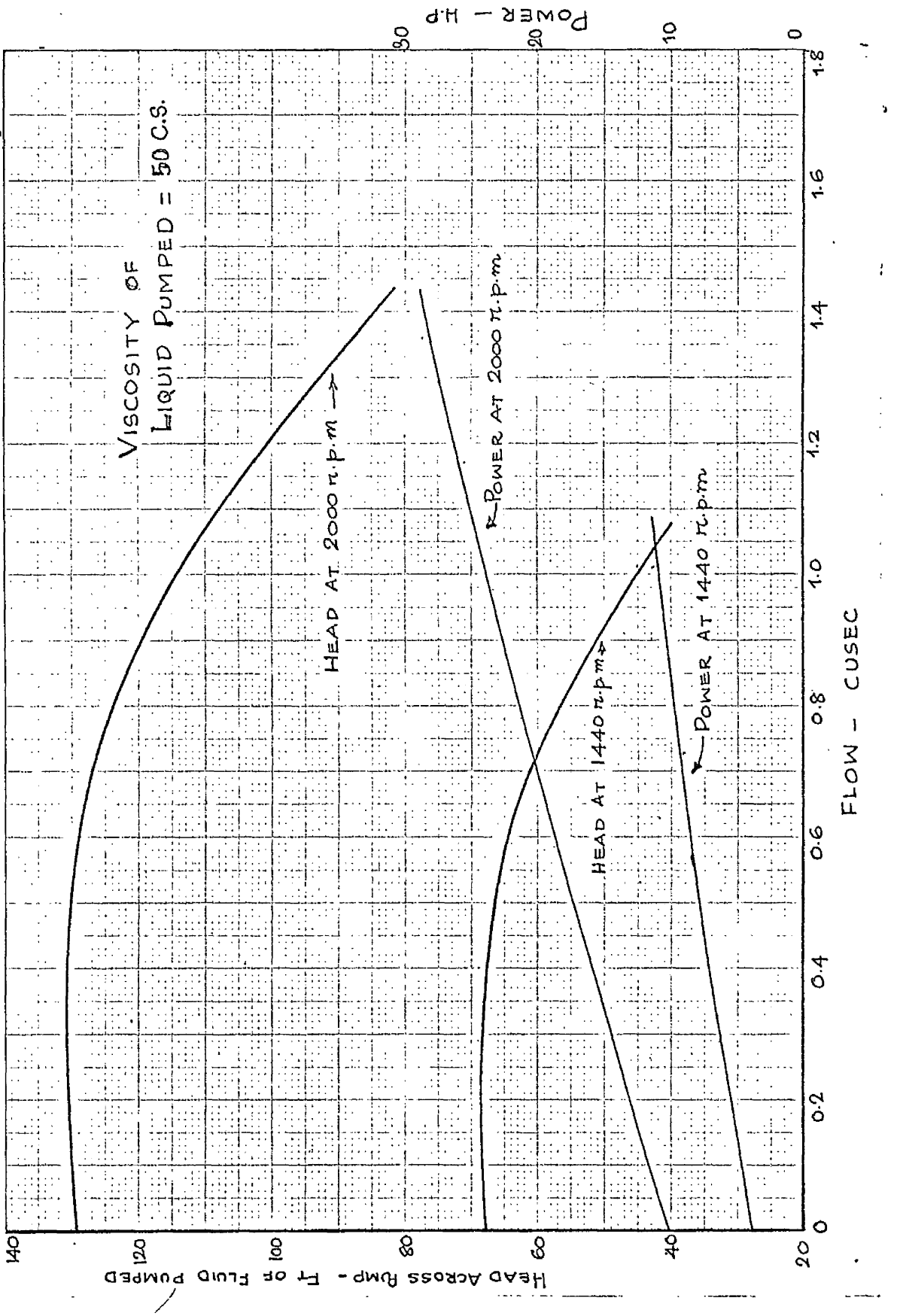

FIG. 5.2.5. Pump Characteristics

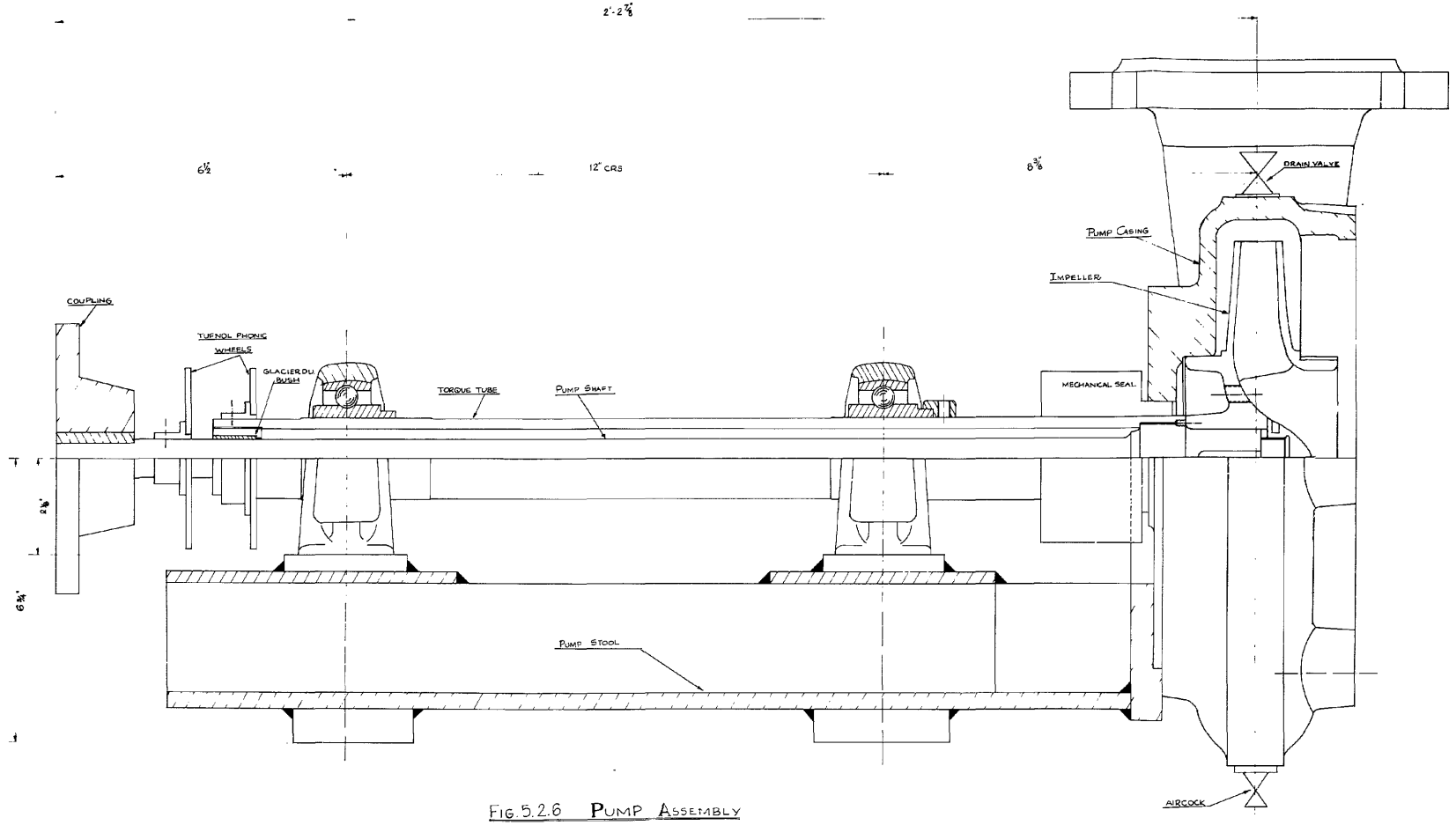

FIG. 5.2.6 PUMP ASSEMBLY

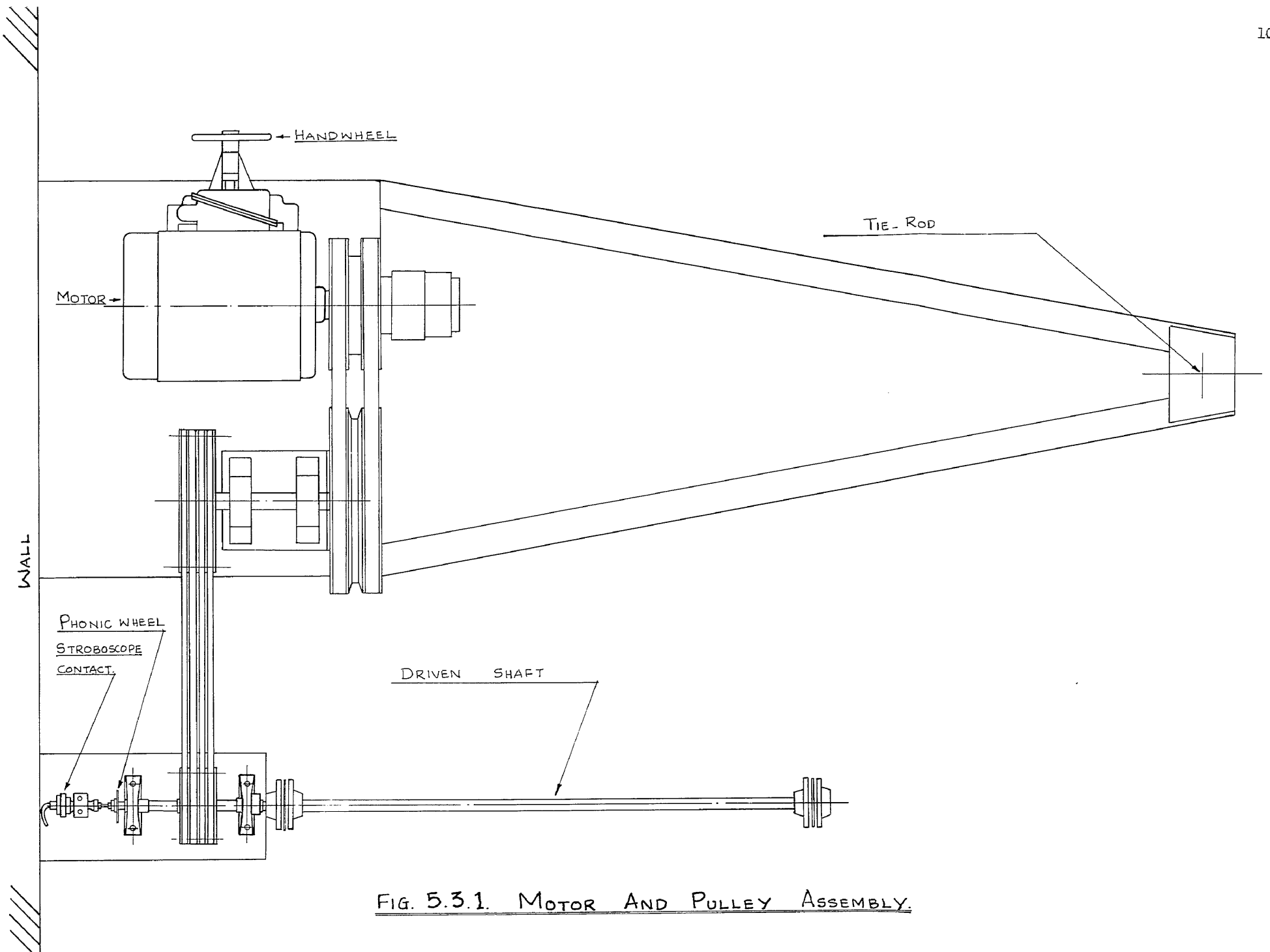

FIG. 5.3.1. MOTOR AND PULLEY ASSEMBLY.

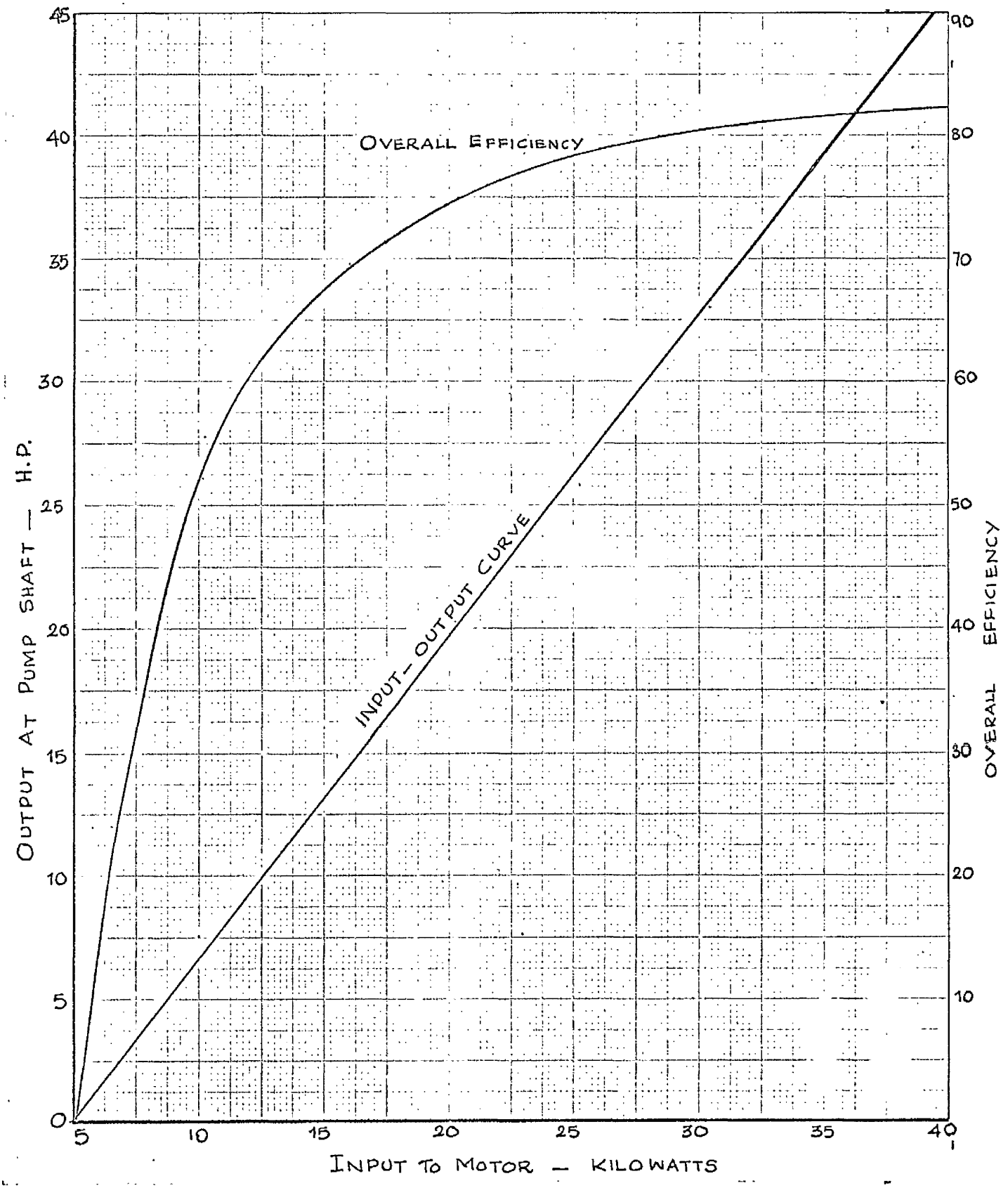

FIG. 5.3.2. Efficiency of Power Transmission System.

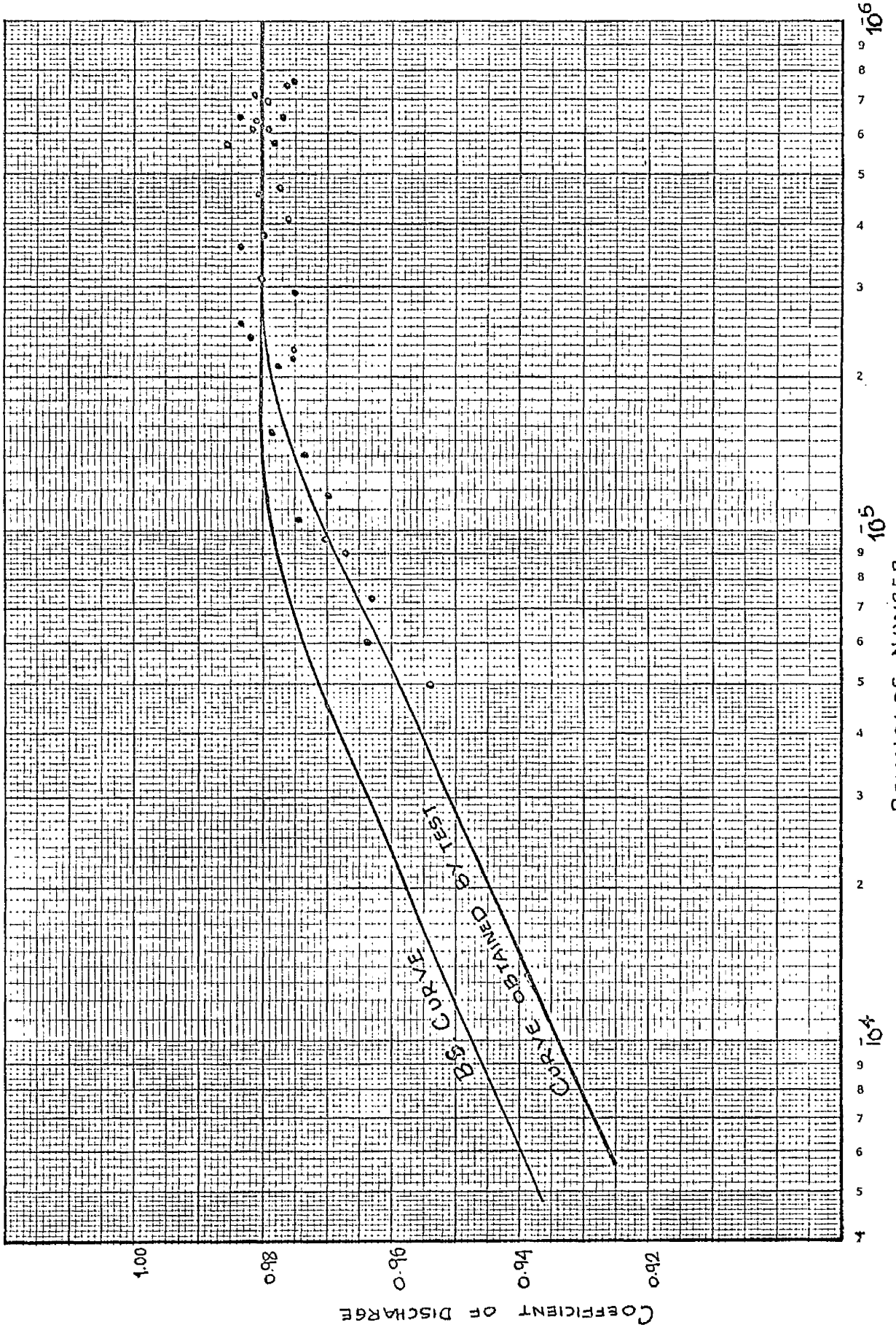

Fig. 5.4.1 Calibration Curve of Venturi meter.

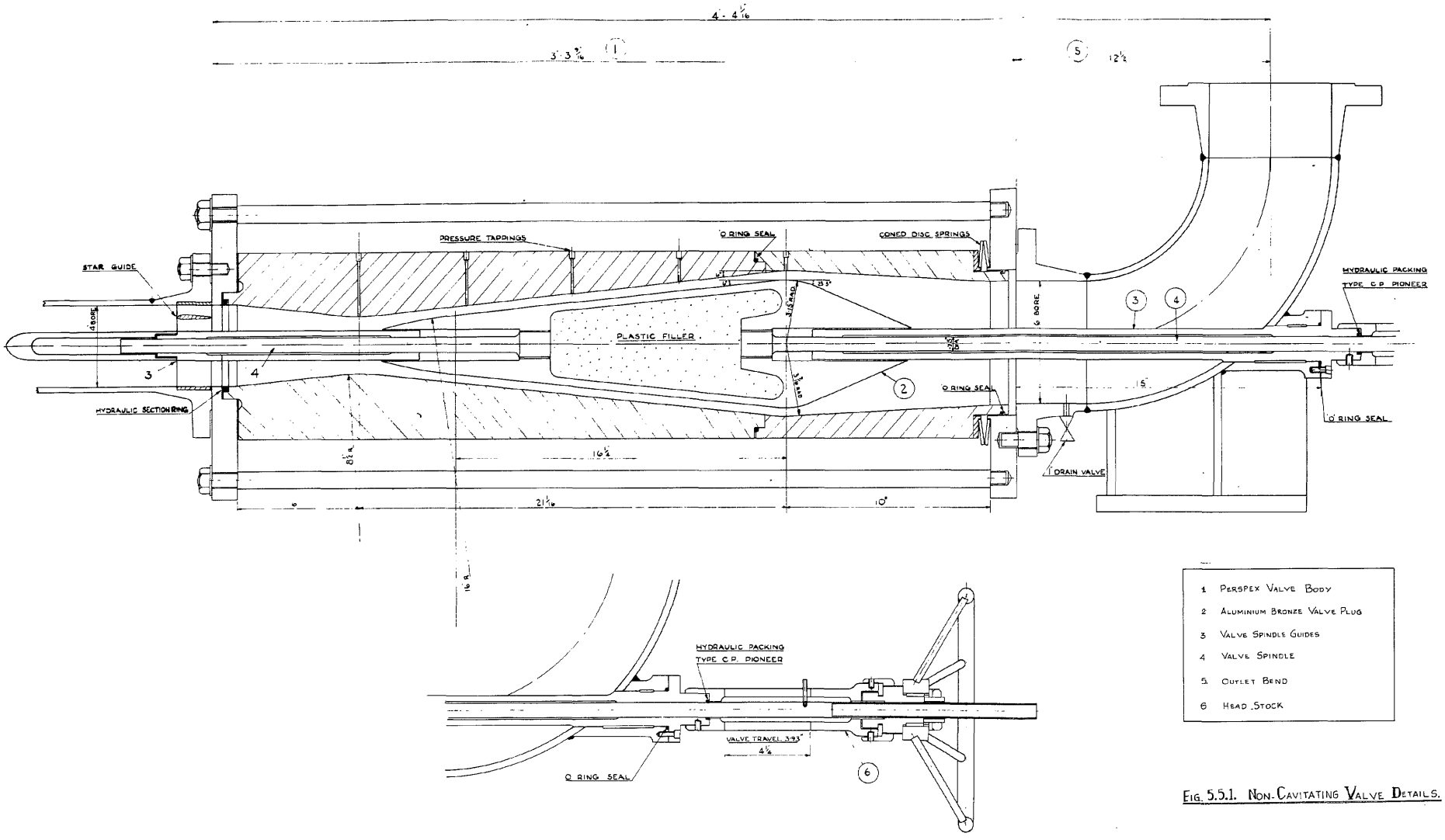

FIG. 5.5.1. NON-CAVITATING VALVE DETAILS.

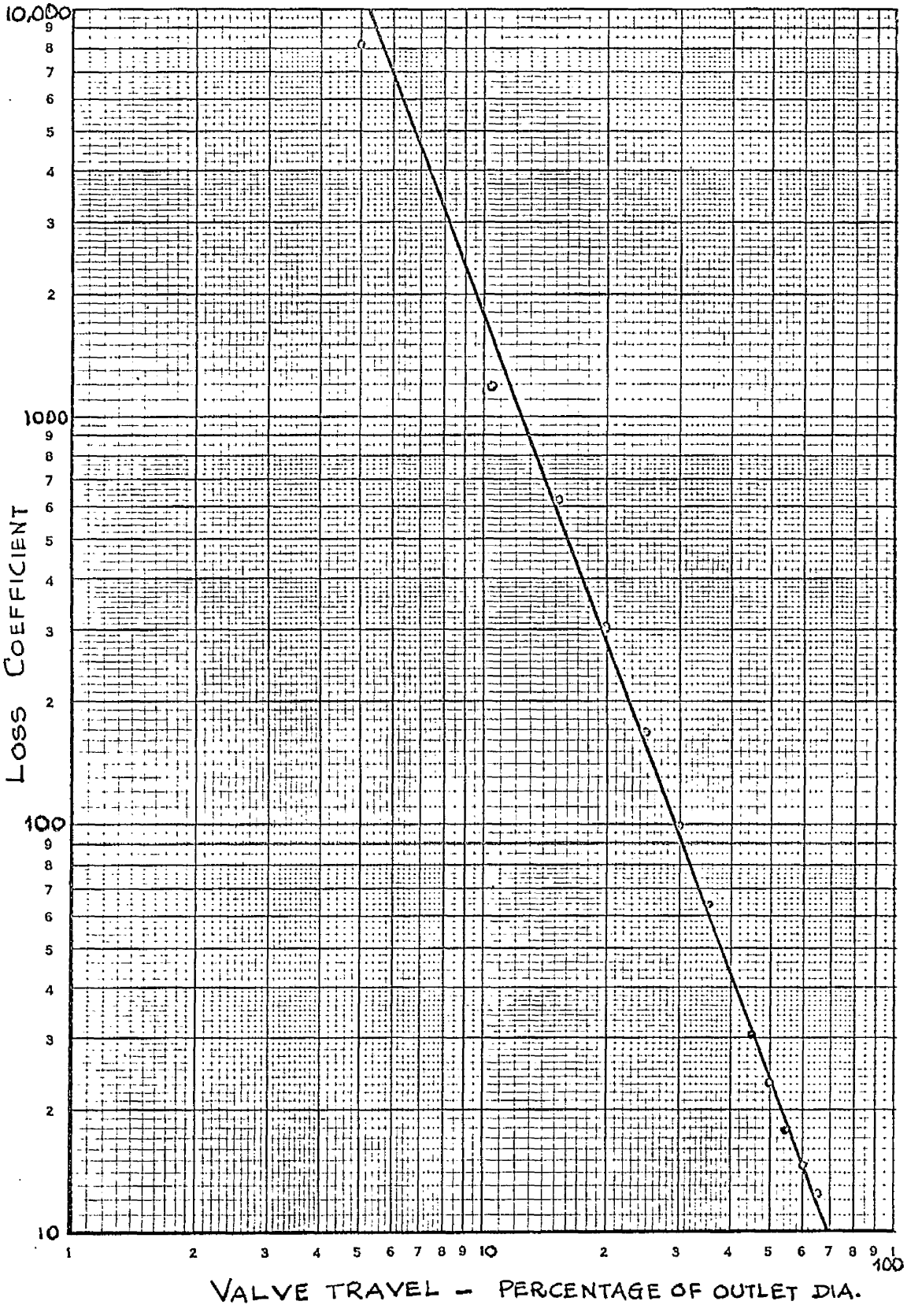

FIG. 5.5.2. LOSS COEFFICIENT OF VALVE.

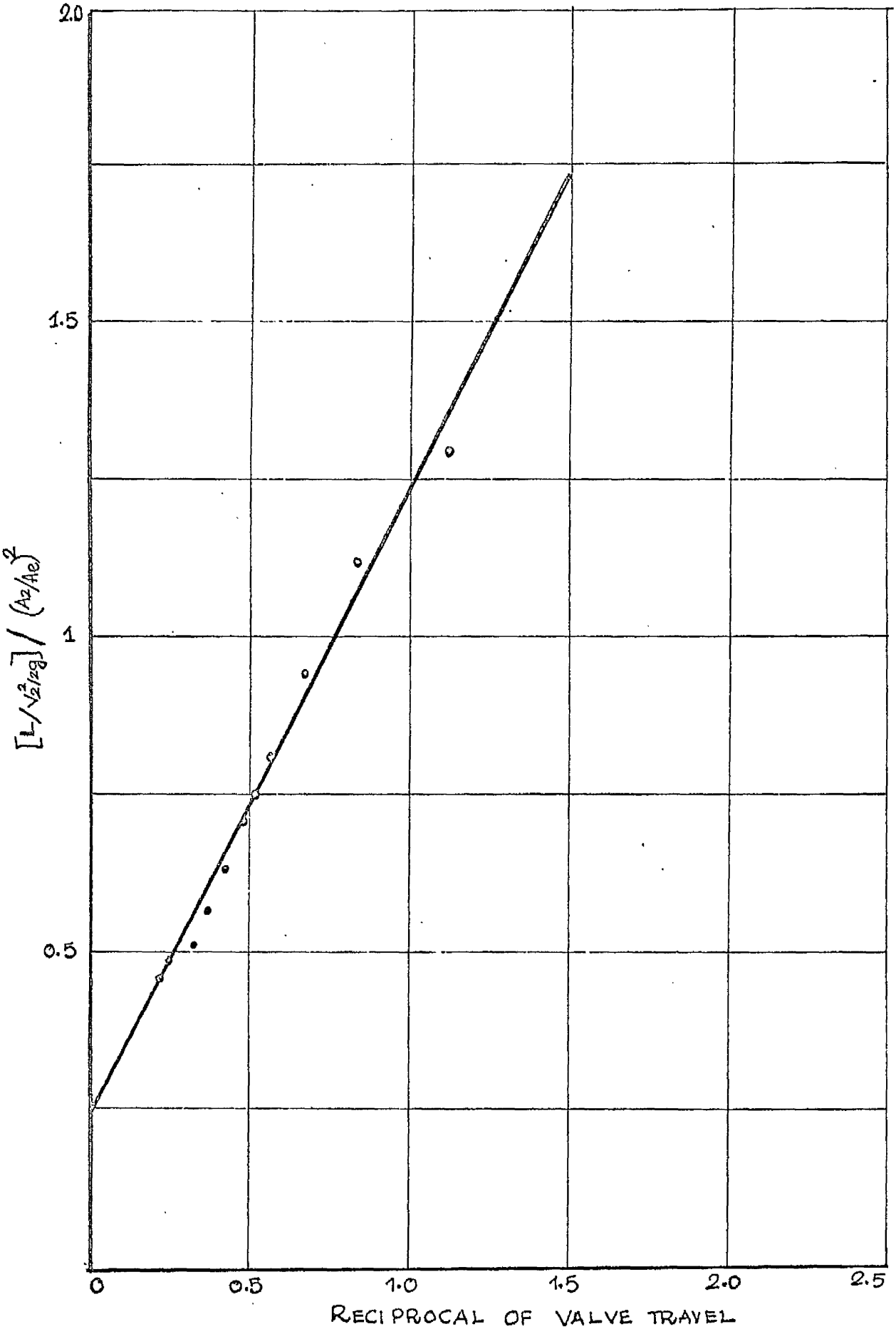

FIG. 5.5.3. FRICTION AND FORM LOSSES.

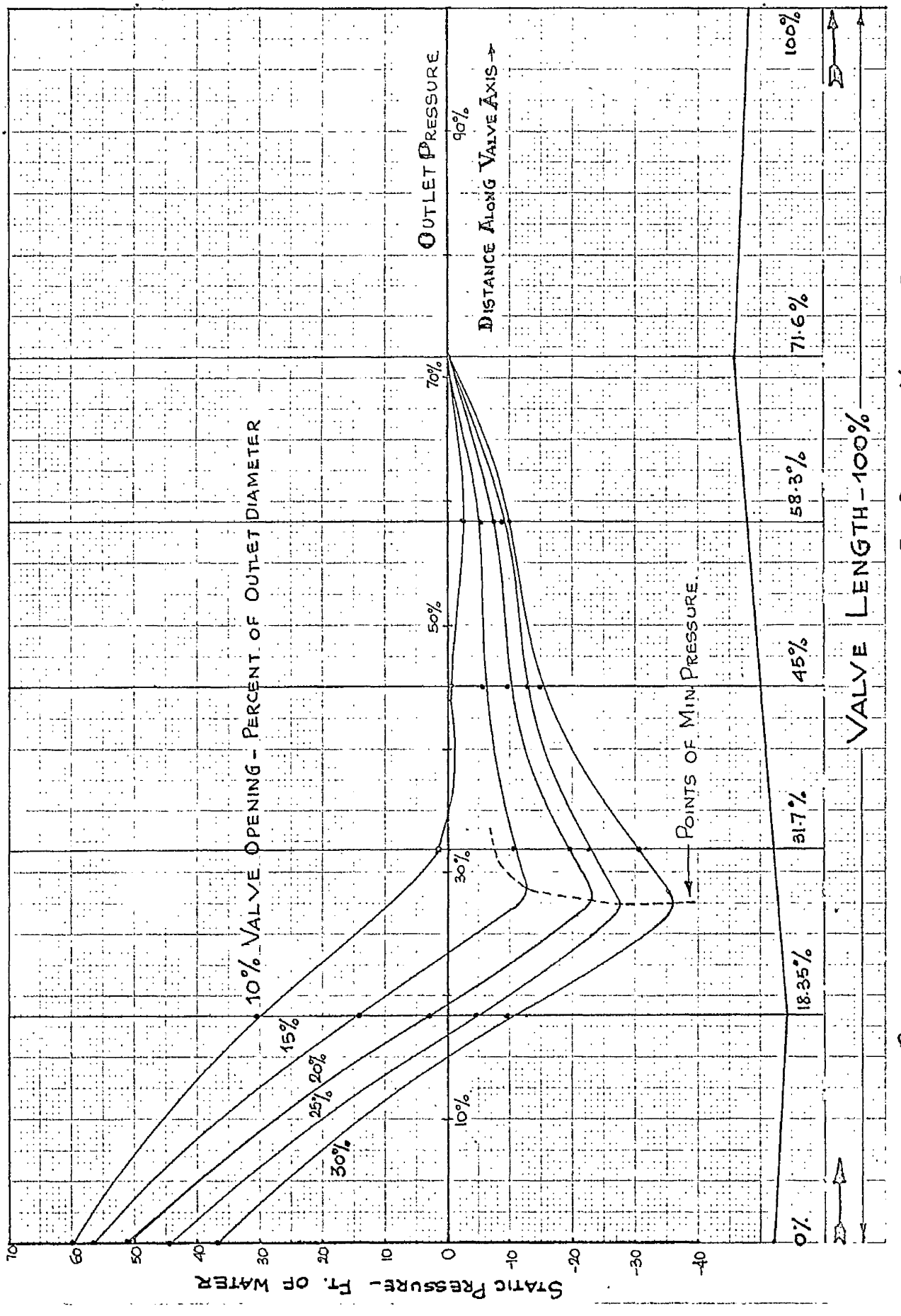

Fig. 5.5.4. Pressure Distribution Along Valve Body For Different Valve Openings.

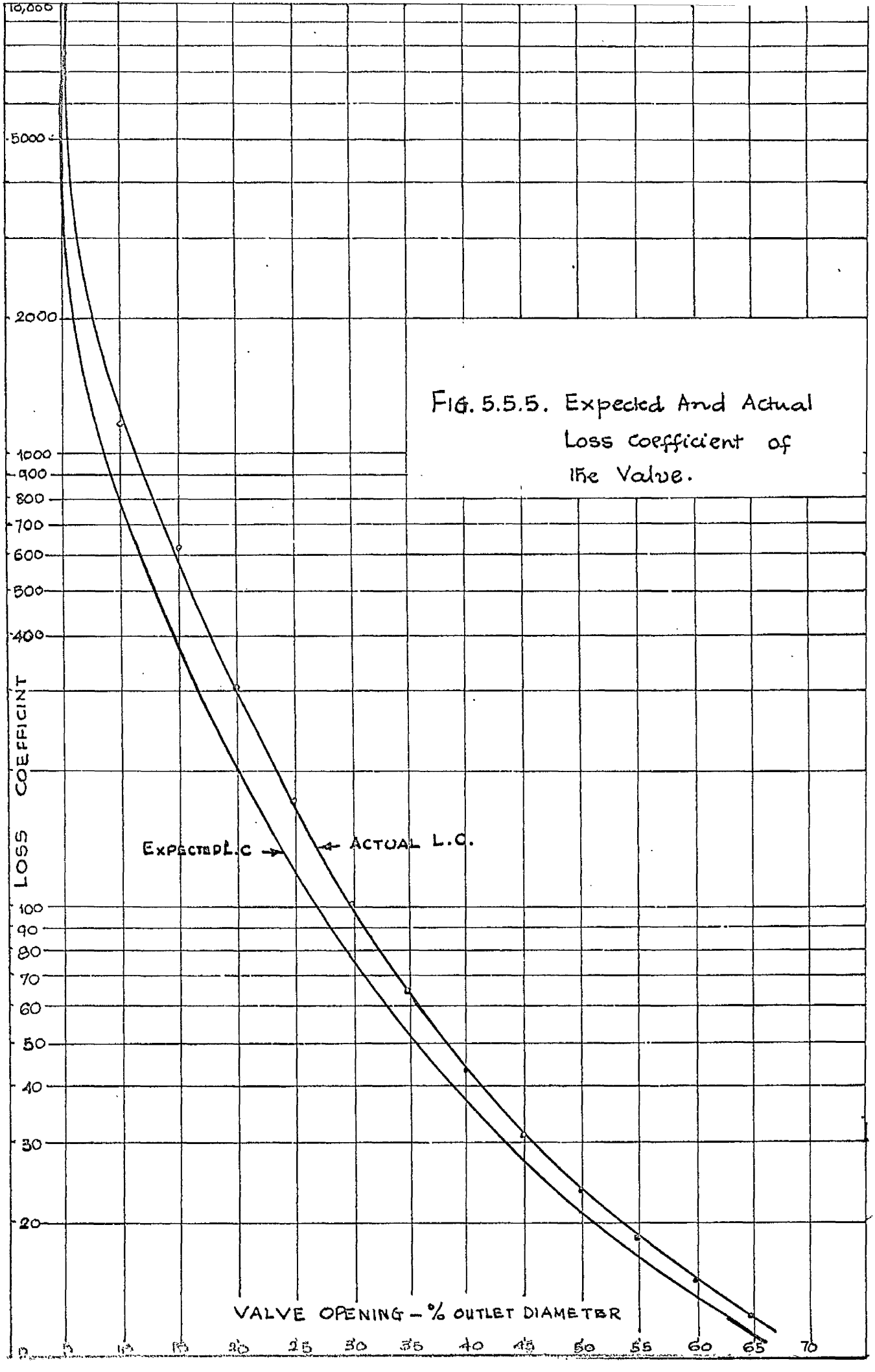

FIG. 5.5.5. Expected And Actual Loss coefficient of the Valve.

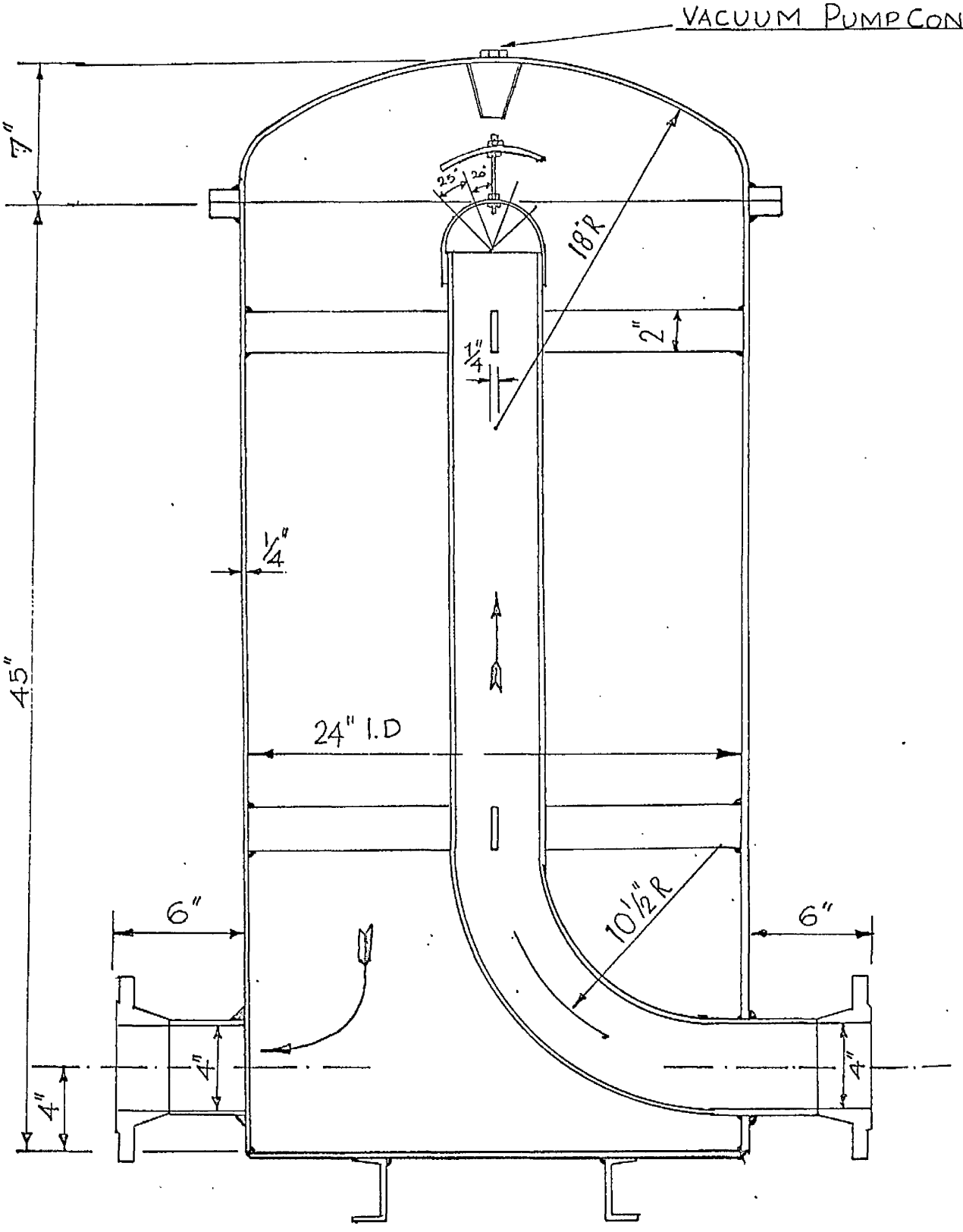

FIG. 5.6.1. DETAILS OF DEAERATOR.

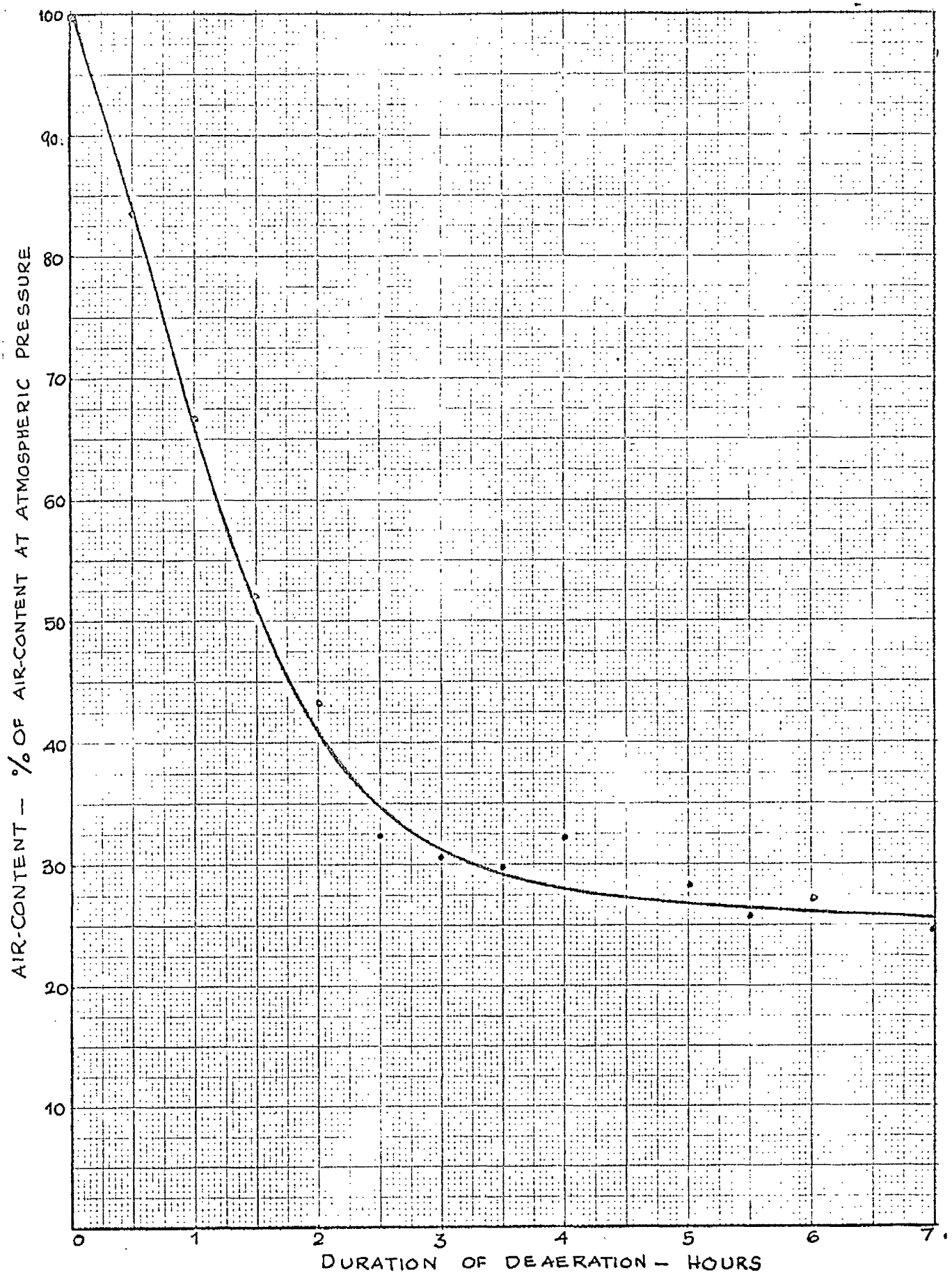

FIG. 5.6.2. RATE OF DEAERATION.

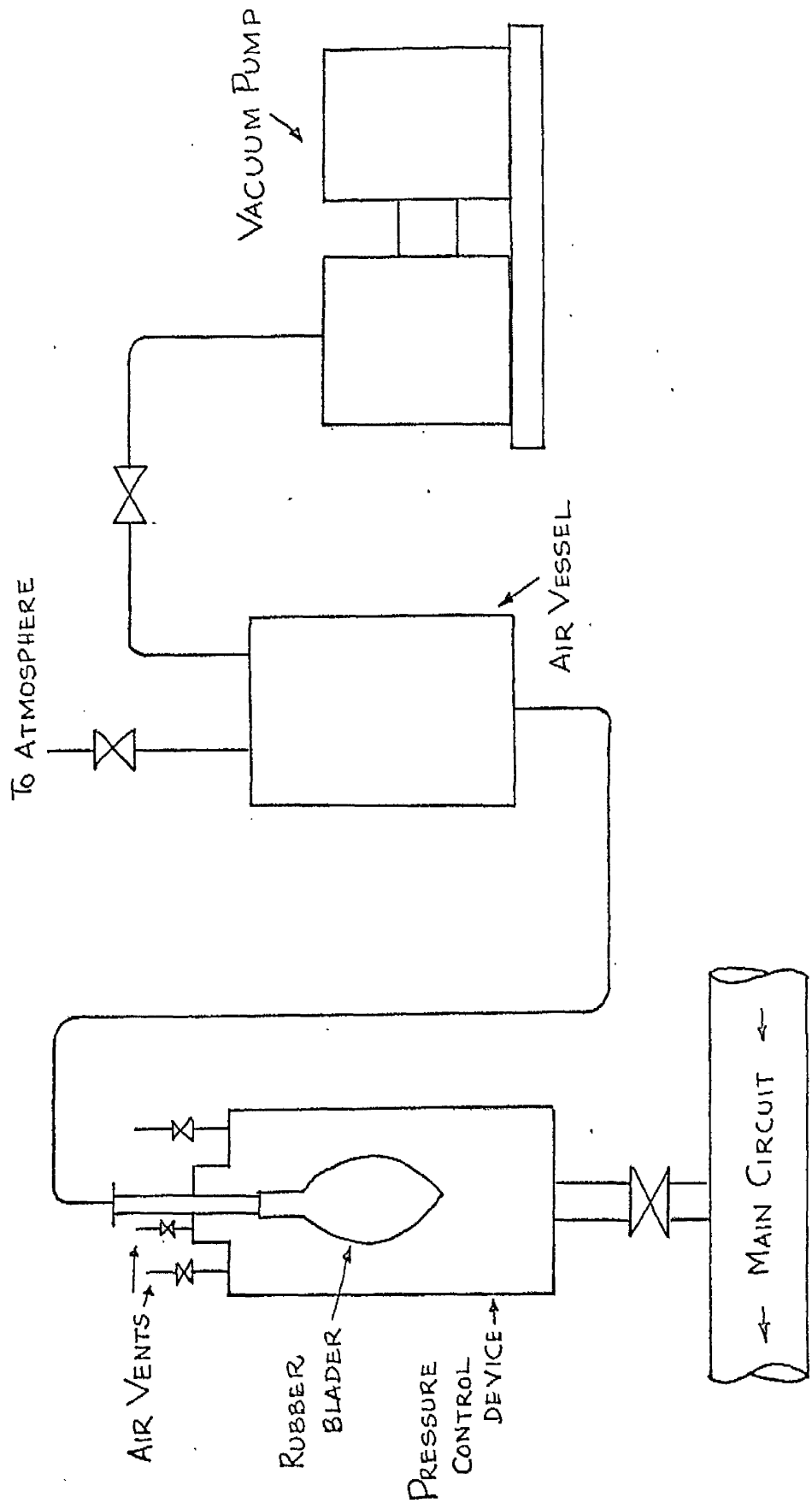

FIG 5.7.1. PRESSURE CONTROL DEVICE

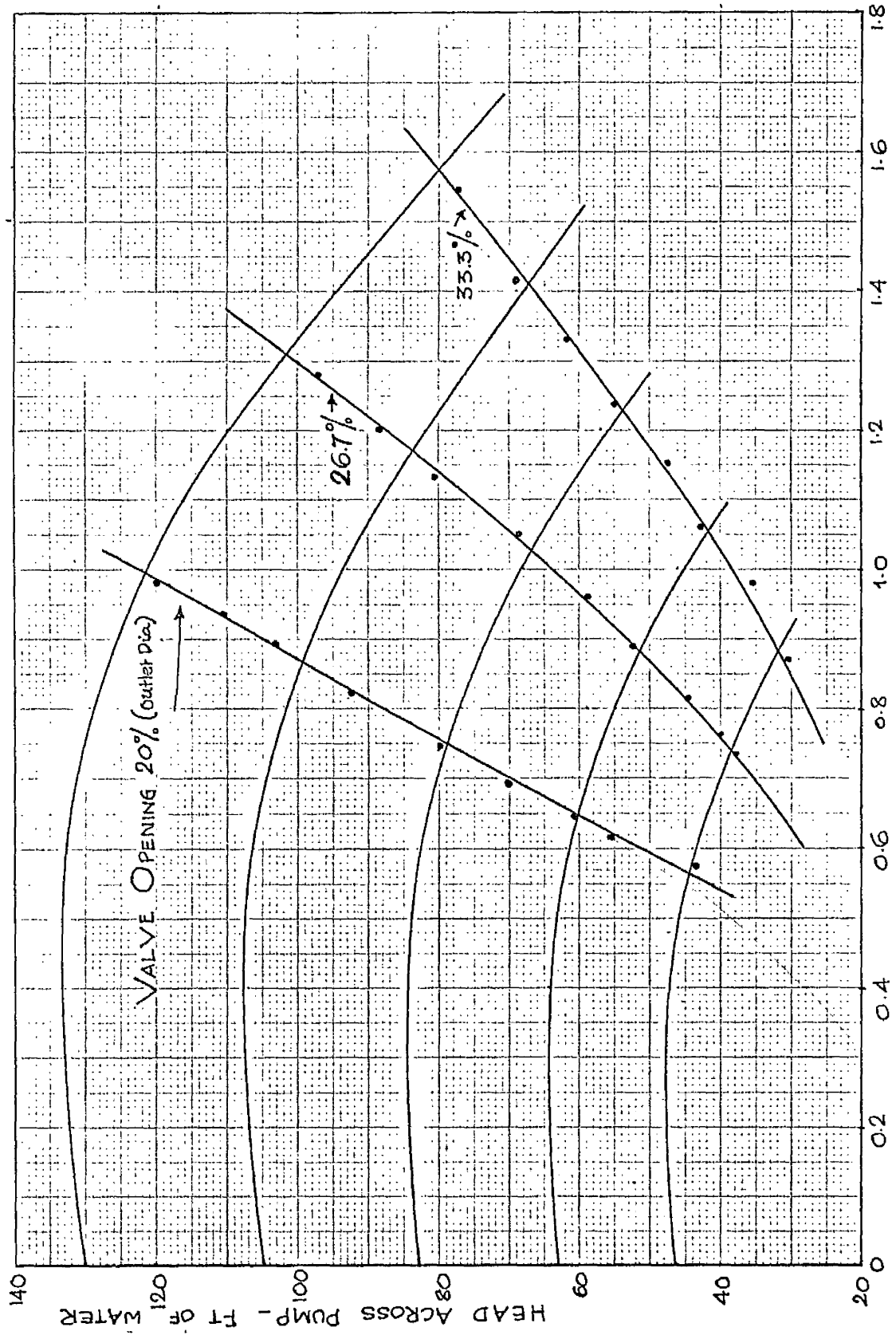

FIG. 5.8.1 HEAD ACROSS PUMP FOR DIFFERENT VALVE OPENINGS.

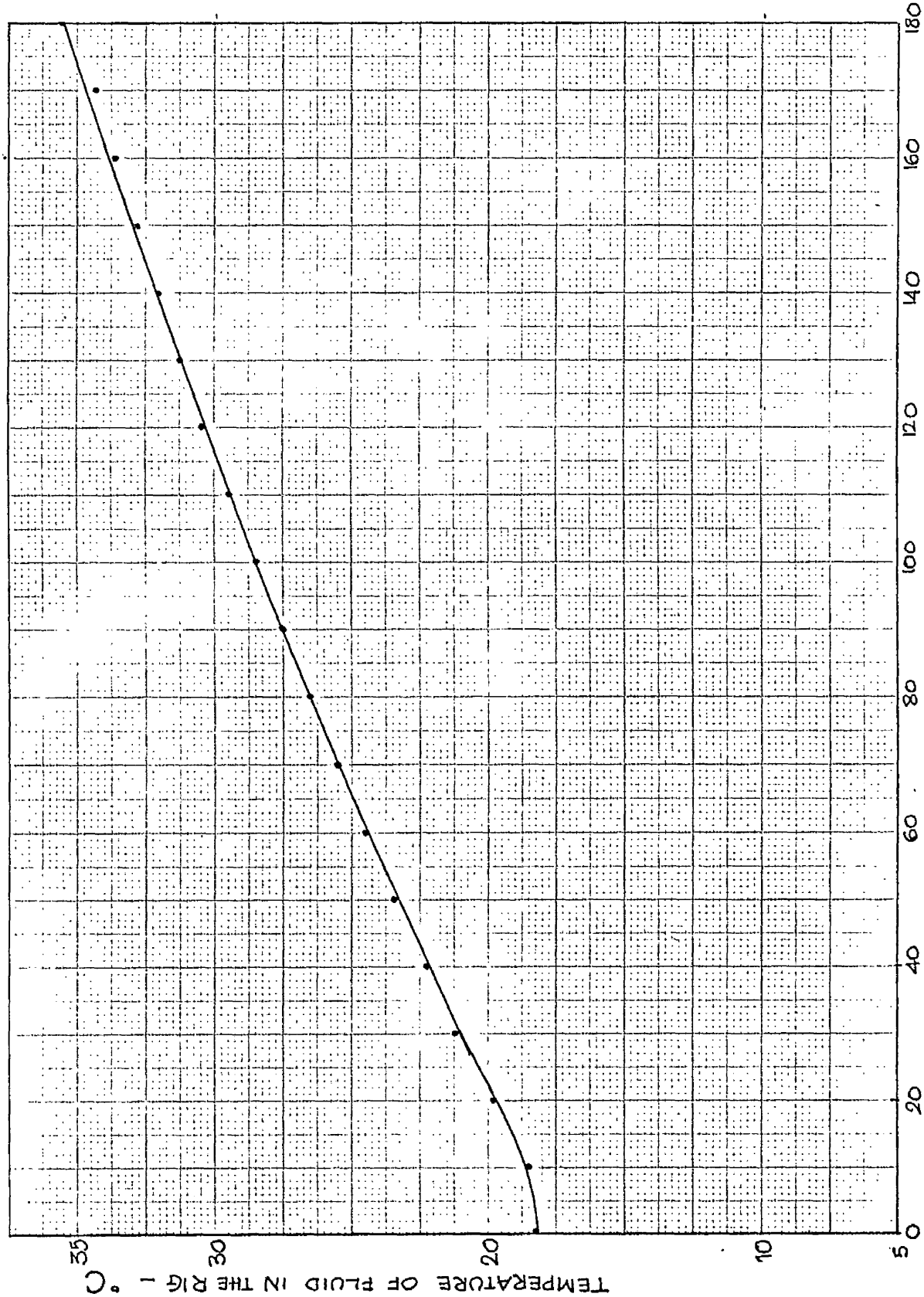

FIG. 5.8.2. Rate of Increase in Temperature of the Fluid in the Rig at an input of 7 H.P.

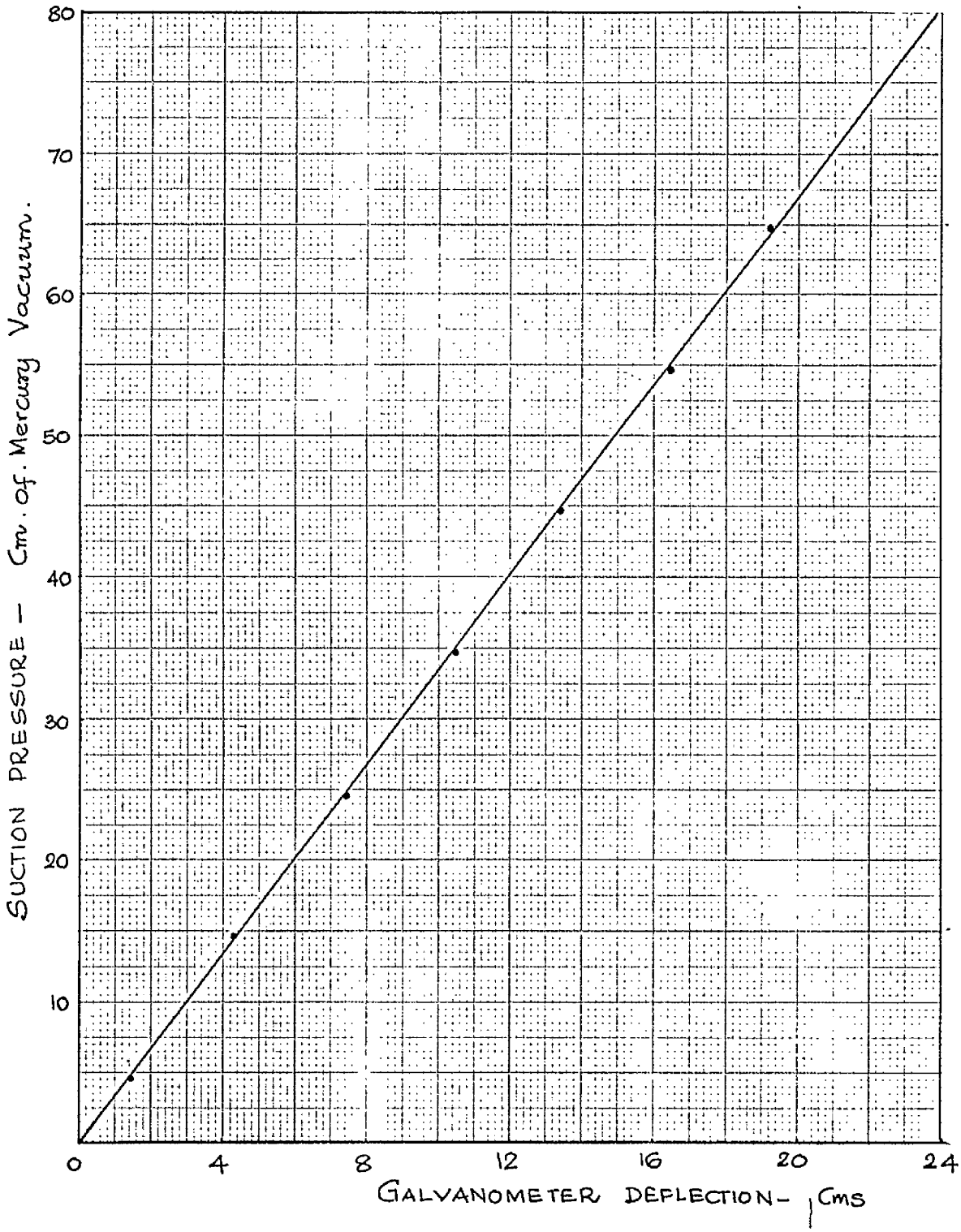

FIG. 5.9.1 CALIBRATION CURVE OF SUCTION PRESSURE TRANSDUCER.

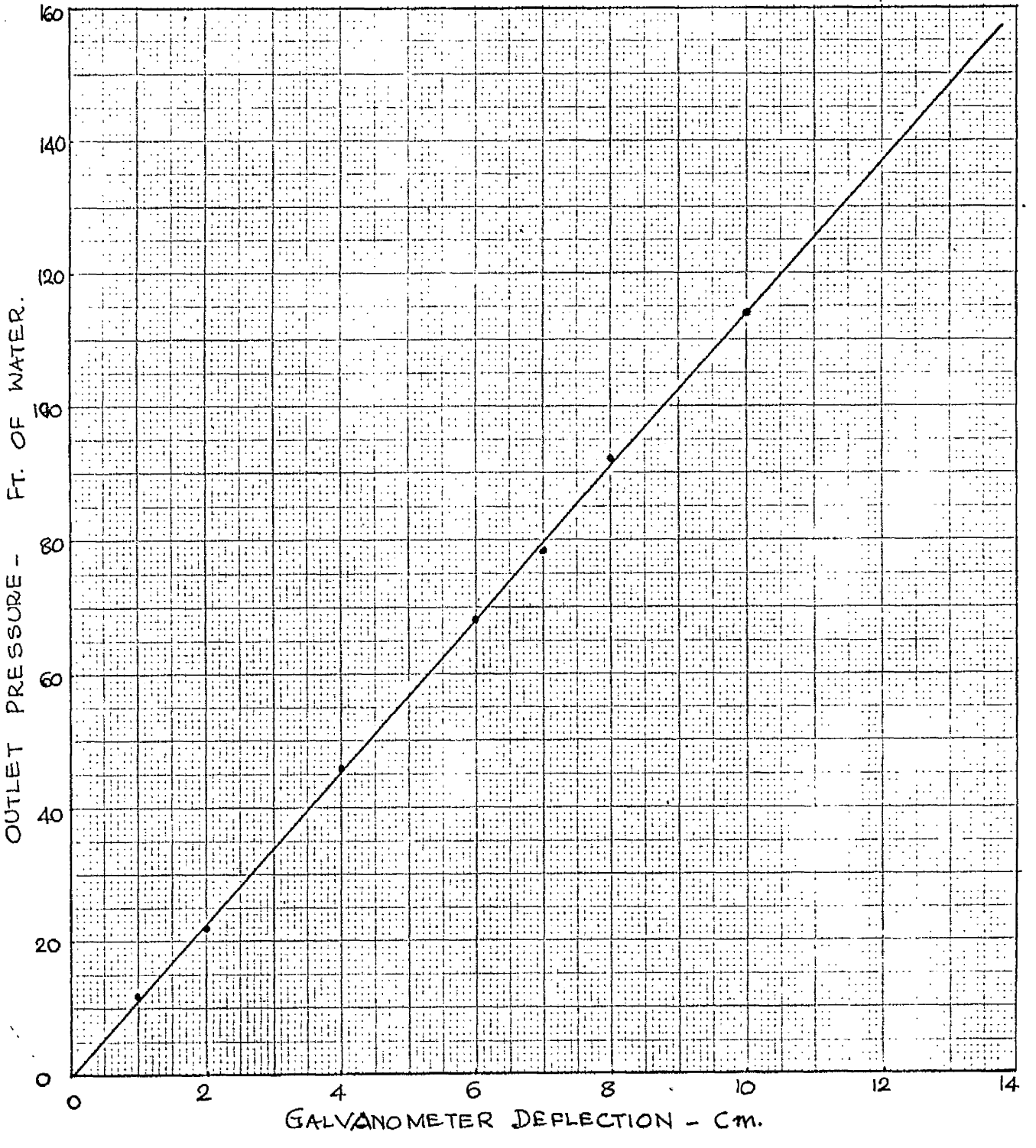

FIG. 5.9.2. CALIBRATION CURVE OF OUTLET PRESSURE TRANSDUCER.

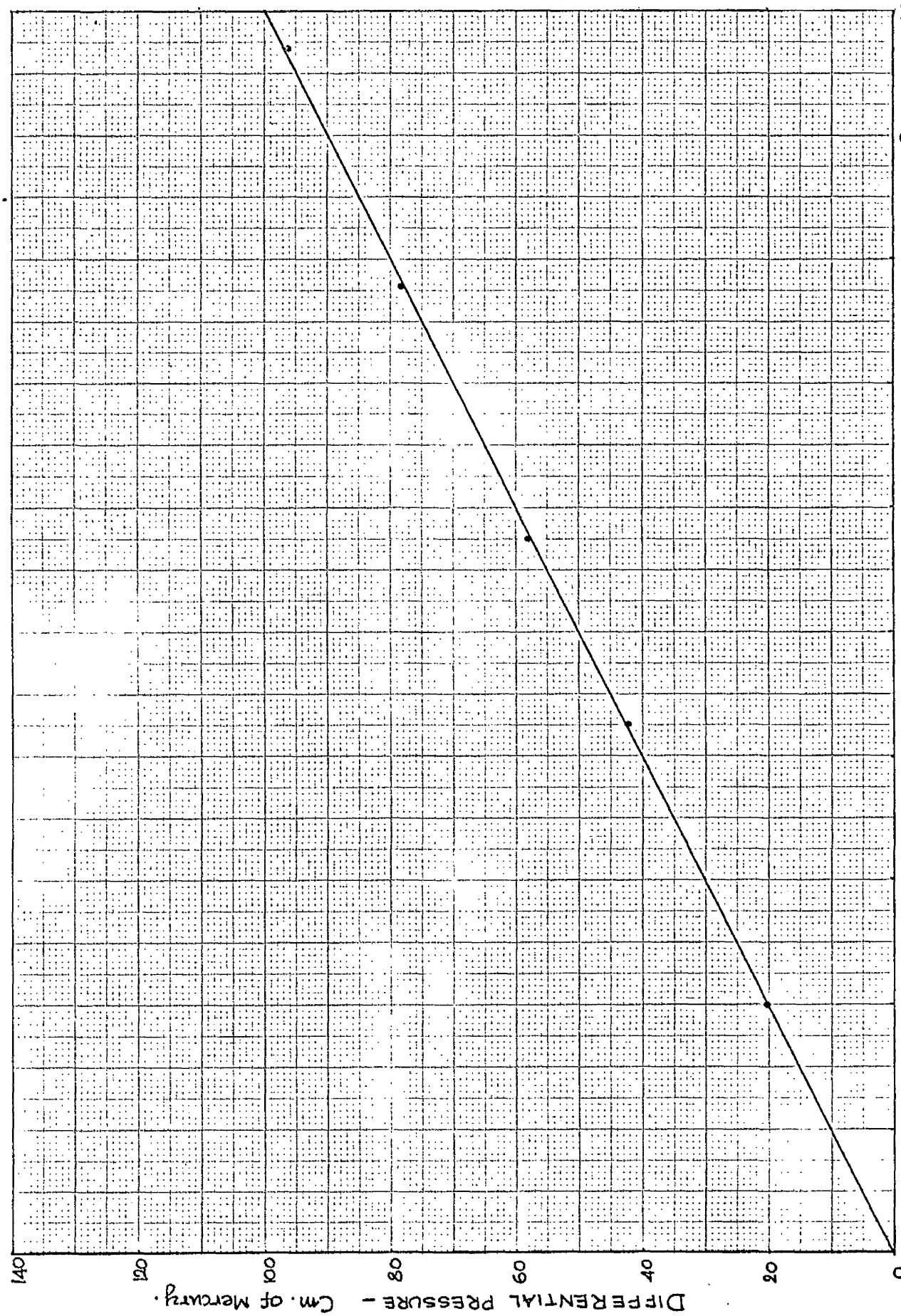

FIG. 5.9.3. CALIBRATION CURVE OF DIFFERENTIAL PRESSURE TRANSDUCER.

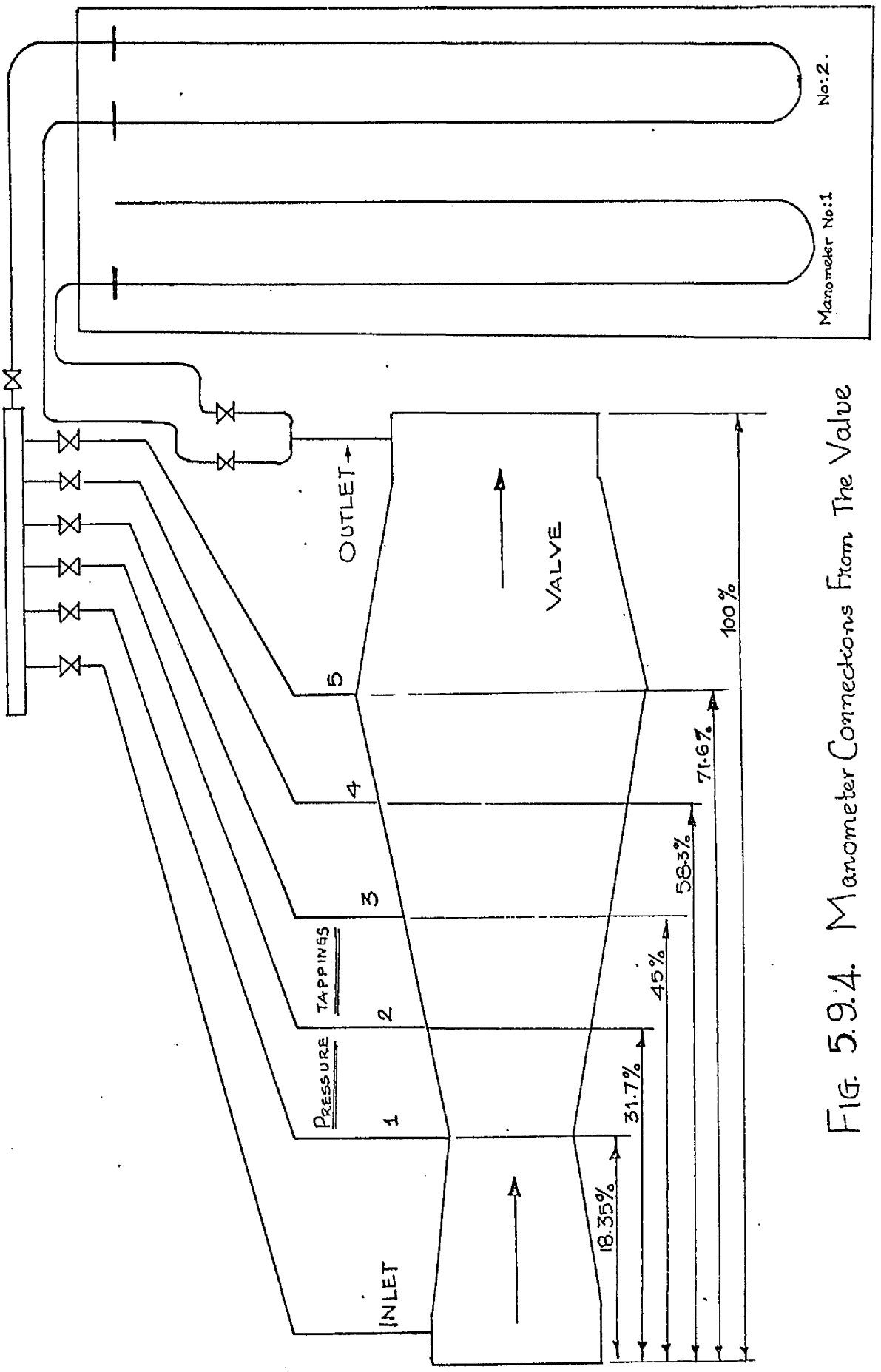

FIG. 5.9.4. Manometer Connections From The Valve

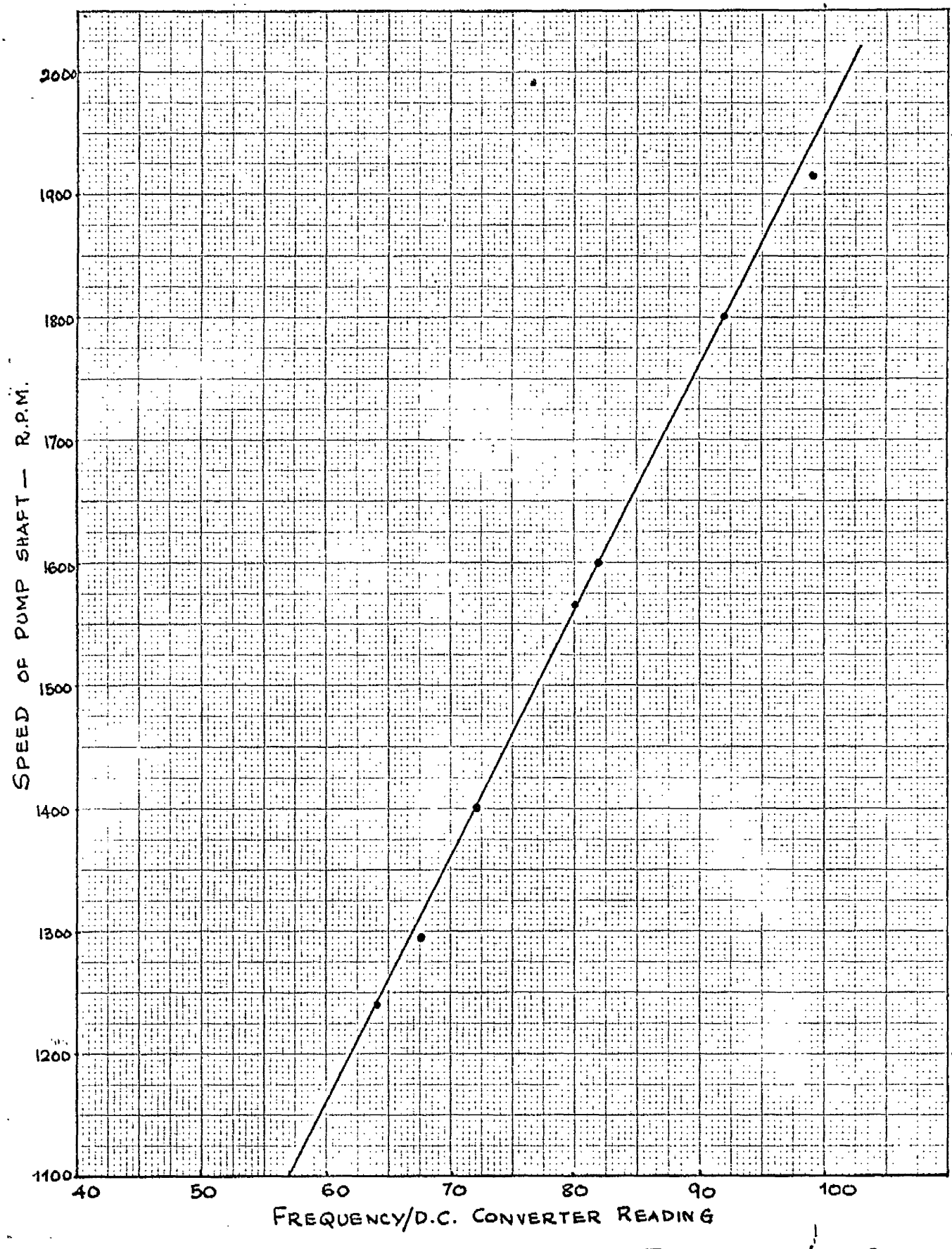

FIG. 5.10.2. CALIBRATION CURVE FOR FREQUENCY/D.C. CONVERTER

CHAPTER 6

TEST PROCEDURE AND RESULTS

6.1 Pressure-Distribution along Valve Body

The perspex body of the valve has five pressure tappings, equally spaced, along the conical diverging section as shown in Fig. (5.5.1). In addition it also has inlet and outlet pressure tappings. The connections to mercury manometers are shown in Fig. (5.9.4) and the manometers can be read accurately to 1 mm. of mercury.

The pump speed was adjusted to 1,400 r.p.m. and the valve travel was kept at 5% of outlet diameter. The venturi manometer reading was noted and the outlet pressure of the valve was observed by using the manometer No.1. The differences in pressure between the outlet and the inlet pressures, the pressures at various tappings 1 to 5, were noted by using the differential manometer No.2. This experiment was repeated by increasing valve travel by 5% in steps up to 65%. Fig. (6.1.1) shows the typical pressure distribution for valve openings of 25% and 30% of outlet diameter.

The number of pressure tappings along the valve body was not sufficient to locate exactly the point of minimum pressure. The points of minimum pressure shown in Fig. (6.1.1) are purely speculative and it is suggested that in future works more closely spaced pressure

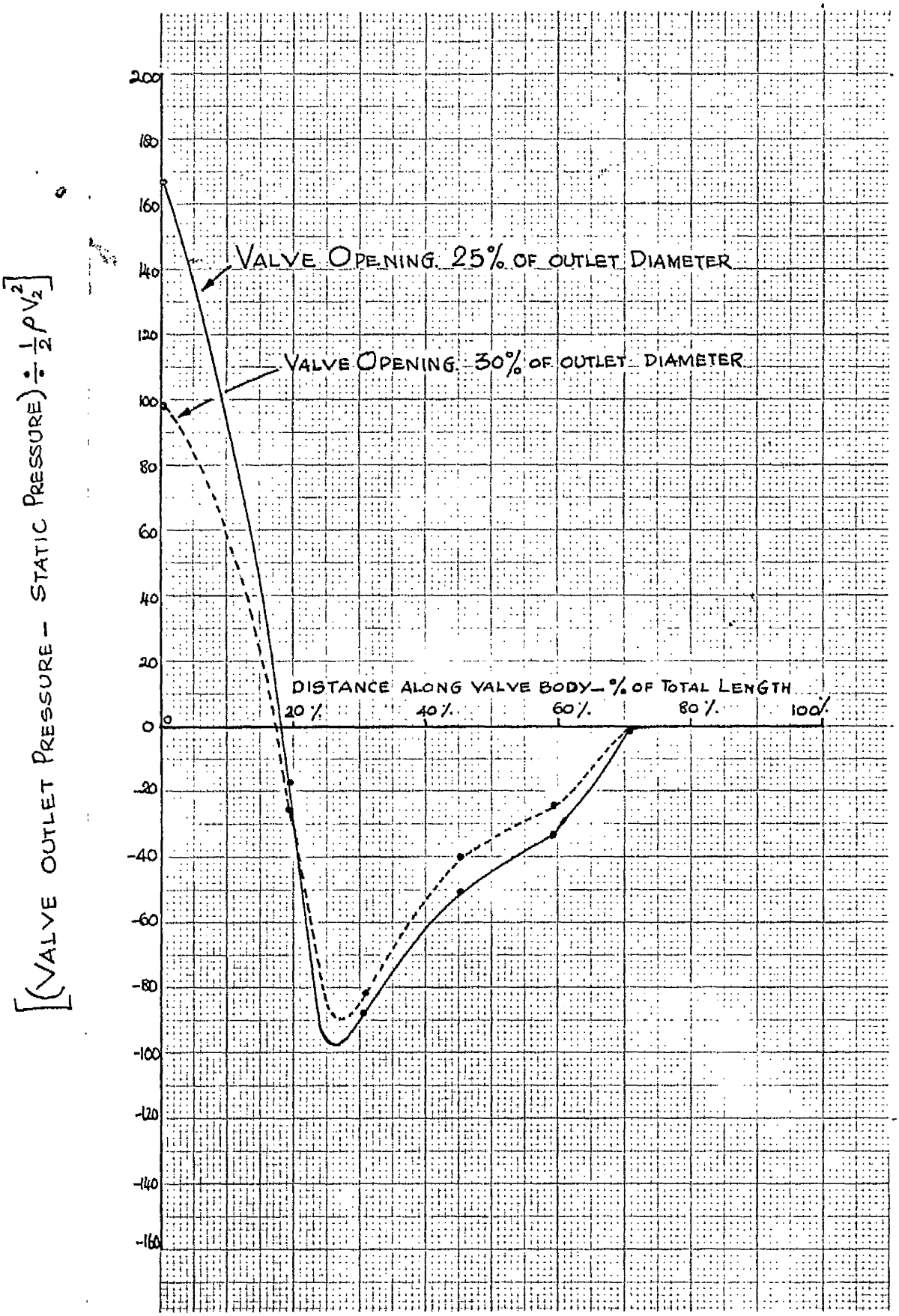

FIG. 6.1.1. Pressure Distribution Along Valve body for two valve openings.

tappings be used. In the present work, for calculating cavitation parameter K, the pressures measured at tapping number 2 were used throughout.

6.2 Deaeration

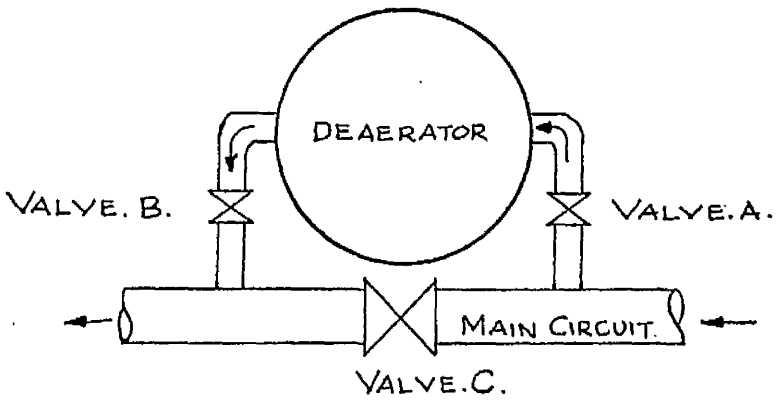

Fig. (6.2.1)

For deaerating the water in the main circuit, the 6 in. ball valve C was closed and the 4 in. ball valves A and B were kept open thereby making the water flow through the deaerator. The flow was adjusted to a desired rate, in the present case to about 0.6 cusecs at a pump speed of 1,400 r.p.m. and the pressure inside the deaerator was slowly reduced to about 20 feet of vacuum using the vacuum pump. It was not possible to lower the absolute pressure of the system below the above mentioned value since atmospheric air started to leak into the system through the mechanical seal.

Water samples were periodically drawn into air-content measuring apparatus and the air-content of each sample was determined. Fig. (5.6.2) shows the rate of deaeration. It was however, not possible to deaerate the water in the circuit completely, due to the limitation

imposed upon the absolute pressure of the circuit by the mechanical seal used on the pump shaft.

6.3 Choice of Suitable Valve Opening

Fig. (5.5.4) shows the pressure distribution along the valve body. It indicates that the point of lowest pressure is located at or near the maximum diameter of the plug for a small valve opening. For instance we find that for a valve opening of 10% of outlet diameter the minimum pressure occurs at a point which is located at a distance of 60% of the total valve length. For larger valve openings the point of lowest pressure is found midway along the plug or at the nose. Initial experiments were therefore carried out to find a suitable valve opening for which the minimum pressure would occur exactly at the point which is at 31.7% of the valve total length, since the pressure tapping number 2 is located at this point. It was found, see Fig. (5.5.4) that for a valve opening of about 14% the pressure tapping number 2 was registering the lowest pressure occurring in the valve. For this particular valve opening, it was found that the flow varied by only about 0.2 cusec for pump speed variation from 1,200 to 2,000 r.p.m. This variation of flow was not sufficient to produce the desired change in Reynolds number and hence 14% valve opening had to be rejected.

Referring to Fig. (5.8.1), we find that at 33.3% valve opening, flow varied from 0.85 cusec to about 1.6 cusec. This particular valve opening was found unsuitable for cavitation tests since the

valve plug started vibrating thereby producing pressure and flow fluctuations. A valve opening of 26.7% of outlet diameter was finally chosen for which the flow varied from 0.7 cusec to about 1.4 cusec.

6.4 Cavitation Tests

6.4.1 All cavitation experiments were conducted on the valve with a fixed opening of 26.7% of outlet diameter.

During cavitation tests, the deaerator was isolated from the main circuit by closing the 4 in. ball valves A and B, and keeping 6 in. ball valve C, shown in Fig. (6.2.1), open completely. Flow in the main circuit was controlled only by varying the speed of the pump from 1,200 to 2,000 r.p.m. Reduction of the flow by closing the 6 in. ball valve was not possible since this caused cavitation in it. Therefore the upper and lower limits of flow in the circuit were essentially controlled by the pump speed.

6.4.2 Throughout the cavitation experiments, only "desinent cavitation" pressures were measured.

The circuit was filled with fresh water from the supply mains to a depth of 2 feet in the deaerator. Special care was taken to eliminate the trapped air pockets in the main circuit. The pressure control device was filled with water from the main and all the air trapped in it was removed by using the vents provided. Attention was paid to removing air bubbles from manometers and pressure connections.

The deaerator was isolated from the main circuit and the 6 in. ball valve was kept completely open. Pump speed was adjusted to 1,200 r.p.m. and the venturi-meter differential pressure was noted. The absolute pressure of the system was then gradually decreased by using the pressure control device which was connected to the vacuum pump through an air vessel with valves. Pressure was lowered until cavitation began at the valve. Since the valve body is made of perspex, cavitation can be clearly seen with the unaided eye. The pressure was then gradually increased till the cavitation just disappeared. Particular attention was paid here to note exactly the point of diappearance of cavitation. The pressure at this point was held constant. The temperature of the fluid in the circuit, the pressure at the valve outlet and the difference between the pressures at outlet and tapping number 2 were noted. This whole operation could be done in less than 2 minutes and in this interval the change in temperature of the fluid was never more than 0.05°C depending upon the input of the pump.

Flow was then increased by changing the pump speed and the above described cavitation experiment was repeated. Tests were continued up to the maximum flow that could be obtained by changing the speed of the pump.

It was observed that the cavitation always started to occur first on the valve plug near its nose. It was noted further that the cavitation always began on very small irregularities on the surface of the plug. Throughout the present work, the same area of the surface

of the plug was observed for disappearance of cavitation.

Results of the cavitation experiments for water fully saturated with air are given in Table 3.

6.4.3 The water in the circuit was deaerated to an air-content of 40.5% of full saturation and cavitation tests were carried out as before at different flow rates; results are given in Table 4.

6.4.4 A measured quantity of pluracol V-10 was then added to the water in the rig, through the opening specially provided. Since pluracol V-10 is a very viscous substance, it was initially mixed with water to make it flow easily and then added to the water in the rig.

Pluracol V-10 thus added and the water in the rig were thoroughly mixed by running the pump for about 30 minutes.

Five solutions of different concentration were used at testing media and the various properties of these solutions are given in article (4. 3.).

Cavitation experiments were done using these solutions and results are given in Tables 5. to 9.

6.5 Discussion

6.5.1 The initial cavitation experiments were carried out with water fully saturated with air at atmospheric pressure and 40.5% air-content. These tests were done with a view to finding out whether the amount of dissolved gases in water has any particular effect on the inception

TABLE. 3.

VALVE OPENING: 26.7% OF OUTLET DIA

Atmospheric pressure: 34 ft. water.

LIQUID: Water, fully saturated with air at atm. Condn.

Sl. No:	Temp. of fluid in rig °C	Rate of flow Cusec	Valve outlet pressure P_2 FT. WATER	Pressure at tapping No:2 below P_2 FT. WATER	Cavitation number K	Reynolds number $R \times 10^{-3}$	Froude Number F	Prandtl number P_r
1.	19.9	0.756	13.26	24.90	0.443	65.47	75.86	6.75
2.	21.6	0.815	23.34	28.60	0.493	72.50	81.76	6.50
3.	23.6	0.895	35.83	34.20	0.508	84.32	89.75	6.25
4.	26.0	0.959	45.43	36.45	0.534	95.37	96.18	5.80
5.	29.5	1.053	60.59	49.60	0.462	112.36	105.61	5.25
6.	22.0	1.129	83.51	56.95	0.551	102.56	113.29	6.50
7.	27.5	1.201	100.63	65.46	0.553	123.48	120.49	5.75
8.	17.5	0.789	20.06	26.31	0.511	64.45	79.14	7.40
9.	17.8	0.762	15.23	23.79	0.500	62.85	76.44	7.30
10.	22.0	0.826	24.47	28.96	0.487	74.98	82.83	6.50
11.	20.5	0.891	34.92	33.79	0.507	78.07	89.38	6.70
12.	24.0	0.931	43.92	37.59	0.533	88.53	93.39	6.25
13.	27.0	0.977	51.50	42.01	0.520	99.33	98.01	5.75
14.	25.0	1.047	67.37	48.13	0.559	101.79	104.98	6.25
15.	27.5	1.109	82.06	54.61	0.574	114.10	111.33	6.30
16.	32.0	1.154	92.08	59.98	0.569	130.28	115.72	5.00
17.	30.0	1.216	101.53	66.51	0.537	131.81	121.96	5.20
18.	20.5	1.205	95.93	64.24	0.525	105.56	120.86	6.70
19.	20.0	1.146	81.07	57.50	0.508	99.22	114.95	6.80
20.	23.0	1.078	72.89	51.84	0.547	100.14	108.10	6.30

Calculations Common to Tables 3 to 9.

$$\text{Velocity } Vm = \frac{\text{Rate of flow}}{0.0135} \quad \text{ft/sec.}$$

$$\text{Velocity } Vv = \frac{\text{Rate of flow}}{0.0149} \quad \text{ft/sec.}$$

$$l.\sin\theta = 0.0139 \quad \text{ft.}$$

$$\text{Cavitation Number } K = \frac{\text{Valve outlet pressure head} - \text{Differential pressure head between outlet and tapping No.2} - (\text{Vapour pressure})}{Vm^2/2g}$$

$$\text{Reynolds Number } R = \frac{Vv\,(l.\sin\theta)}{\nu}$$

$$\text{Froude Number } F = \frac{Vv}{\sqrt{g\ l.\sin\theta}}$$

$$\text{Prandtl Number } Pr = \frac{Cp\,l\,\mu}{k} \quad \text{(See appropriate graphs)}$$

TABLE. 4.

VALVE OPENING: 26.7% OF OUTLET DIA

Atmospheric pressure: 34 ft of Wate

LIQUID : Water with 40.5% air content.

Sl. NO:	Temp. of fluid in rig °C	Rate of flow cusec	Valve outlet pressure P_2 FT. WATER	Pressure at tapping No:2 below P_2 FT. WATER	Cavitation number K	Reynolds number $R \times 10^{-3}$	Froude Number F	Prandtl number P_r
1.	21.0	0.834	25.61	29.91	0.489	73.98	83.68	6.60
2.	22.5	0.878	32.61	34.33	0.479	80.77	88.06	6.40
3.	24.2	0.956	49.99	40.90	0.542	91.29	95.86	6.20
4.	28.6	1.008	60.72	46.18	0.547	105.90	101.14	5.50
5.	27.6	1.106	81.43	55.31	0.566	113.74	110.92	5.70
6.	17.5	1.156	90.02	59.57	0.561	94.47	115.99	7.40
7.	23.0	1.209	99.77	66.80	0.531	112.37	121.29	6.25
8.	20.0	0.755	14.20	24.08	0.482	65.41	75.78	6.70
9.	22.6	0.767	17.16	25.08	0.504	70.60	76.93	6.40
10.	24.5	0.798	21.87	27.43	0.507	76.85	80.03	6.20
11.	25.9	0.810	25.52	28.83	0.531	80.53	81.27	6.00
12.	27.5	0.883	37.41	34.20	0.543	90.76	88.56	5.70
13.	29.1	0.930	44.45	38.21	0.529	98.63	93.30	5.50
14.	17.5	0.973	52.65	41.10	0.558	79.48	97.58	7.40
15.	21.3	1.023	66.79	46.43	0.601	91.31	102.66	6.50
16.	20.4	1.032	64.35	46.64	0.562	90.40	103.51	6.75
17.	24.7	1.096	80.26	53.91	0.581	106.15	109.93	6.20
18.	30.2	1.151	90.23	60.73	0.551	125.38	115.42	5.10

TABLE. 5.

VALVE OPENING: 26.7% OF OUTLET DIA

Atmospheric pressure: 33.90 ft/WATE

LIQUID : PLURACOL SOLN. NO: 1.

Sl. NO:	Temp. of fluid in rig °C	Rate of flow cusec	Valve outlet pressure P_2 FT. WATER	Pressure at tapping NO:2 below P_2 FT. WATER	Cavitation number K	Reynolds number $R \times 10^{-3}$	Froude Number F	Prandtl number P_r
1.	17.0	0.761	10.47	20.63	0.469	27.48	76.29	17.10
2.	18.7	0.793	17.24	22.99	0.512	30.23	79.56	16.20
3.	20.7	0.845	24.12	26.87	0.498	34.28	84.81	15.30
4.	23.3	0.898	33.53	31.29	0.512	39.16	90.13	14.10
5.	25.0	0.967	43.50	37.29	0.490	44.27	96.98	13.38
6.	28.1	1.040	58.66	45.23	0.500	52.57	104.35	12.18
7.	18.5	1.108	65.66	48.24	0.484	41.99	111.13	16.30
8.	23.5	1.155	73.11	53.99	0.458	50.32	115.82	14.00
9.	15.8	0.709	11.05	18.79	0.596	24.63	71.20	17.70
10.	17.7	0.756	15.61	22.06	0.549	28.06	75.88	16.70
11.	19.4	0.789	19.95	24.25	0.545	30.90	79.11	15.85
12.	21.1	0.825	25.30	27.18	0.539	33.83	82.73	15.10
13.	22.9	0.855	30.88	30.03	0.544	37.04	85.77	14.20
14.	25.7	0.897	34.08	34.12	0.477	41.44	90.00	13.00
15.	24.4	0.961	48.62	39.41	0.535	43.54	96.44	13.60
16.	27.6	1.006	57.47	44.37	0.531	49.42	100.94	12.35
17.	27.8	1.081	73.38	52.59	0.537	53.47	108.43	12.28
18.	16.9	1.160	86.13	57.59	0.539	41.78	116.35	17.10
19.	23.0	1.070	69.45	49.70	0.540	46.66	107.38	14.20
20.	26.8	1.016	59.39	45.44	0.530	48.88	101.95	12.60

TABLE. 6

VALVE OPENING: 26.7% OF OUTLET DIA

Atmospheric pressure: 33.30 FT/WA

LIQUID : PLURACOL SOLN.NO: 2

Sl. NO:	Temp. of fluid in rig °C	Rate of flow cusec	Valve outlet pressure P_2 FT. WATER	Pressure at tapping No:2 below P_2 FT. WATER	Cavitation number K	Reynolds number $R \times 10^{-3}$	Froude Number F	Prandtl number P_r
1.	14.5	0.658	4.68	11.73	0.696	9.18	66.04	46.60
2.	15.9	0.734	10.26	15.62	0.596	10.82	73.59	44.20
3.	18.0	0.780	15.05	18.88	0.555	12.36	78.25	40.75
4.	20.0	0.819	21.73	21.77	0.569	13.89	82.14	37.60
5.	22.2	0.863	28.28	25.24	0.558	15.76	86.59	34.90
6.	25.1	0.907	34.47	28.99	0.538	18.01	90.98	31.50
7.	28.1	0.955	45.28	34.20	0.554	22.03	95.84	28.50
8.	17.0	1.076	58.97	40.44	0.519	16.46	107.96	42.30
9.	24.0	1.147	78.20	49.53	0.544	22.09	115.04	32.75
10.	20.1	0.727	7.07	16.19	0.520	12.42	72.90	37.50
11.	21.8	0.755	10.83	18.22	0.516	13.63	75.73	35.30
12.	23.8	0.782	15.97	20.20	0.539	14.98	78.47	33.10
13.	25.5	0.816	19.93	22.84	0.516	16.51	81.88	31.20
14.	27.7	0.870	28.52	26.60	0.527	19.96	87.26	29.00
15.	30.2	0.914	37.97	30.78	0.549	21.11	91.68	26.75
16.	16.2	0.959	37.87	30.89	0.506	14.29	96.19	43.80
17.	21.5	1.002	47.28	35.53	0.517	17.82	100.47	35.80
18.	25.7	1.047	56.27	40.15	0.517	21.23	105.55	30.80
19.	30.0	1.085	63.96	45.11	0.506	24.89	108.85	31.85
20.	16.2	1.139	67.78	46.72	0.486	16.98	114.27	43.80

TABLE. 7

VALVE OPENING: 26.7% OF OUTLET DIA

Atmospheric pressure: 33.7 FT/WATER

LIQUID : PLURACOL SOLN. NO: 3

Sl. NO:	Temp. of fluid in rig °C	Rate of flow Cusec	Valve outlet pressure P_2 FT. WATER	Pressure at tapping No:2 below P_2 FT. WATER	Cavitation number K	Reynolds number $R \times 10^{-3}$	Froude Number F	Prandtl number P_r
1.	17.9	0.628	10.02	13.18	0.874	5.66	63.03	73.50
2.	19.7	0.799	25.53	16.98	0.762	7.66	80.16	69.00
3.	22.9	0.897	33.09	23.34	0.619	9.52	90.02	61.30
4.	18.1	0.974	41.77	27.14	0.589	8.84	97.73	73.30
5.	22.7	1.041	55.27	33.38	0.593	10.97	104.38	61.80
6.	28.6	1.115	65.50	42.88	0.519	13.98	111.80	50.60
7.	22.8	0.689	7.81	12.23	0.700	7.28	69.15	61.60
8.	24.6	0.759	21.93	15.82	0.790	8.46	76.14	57.80
9.	26.7	0.865	31.19	22.10	0.652	10.26	86.81	53.50
10.	28.2	0.946	38.00	28.46	0.551	11.78	94.86	51.10
11.	16.2	0.931	35.39	23.50	0.609	7.91	93.35	79.00
12.	20.0	1.009	43.71	29.95	0.539	9.68	101.18	68.20
13.	24.6	1.062	54.43	36.06	0.532	11.83	106.48	57.80
14.	30.4	1.109	62.42	42.47	0.498	14.69	111.25	47.40
15.	25.0	0.721	8.99	14.21	0.619	8.12	72.34	57.00
16.	26.9	0.772	18.57	16.89	0.674	9.22	77.48	53.20
17.	28.5	0.843	24.39	21.07	0.590	10.58	84.58	50.80
18.	30.7	0.907	33.01	25.94	0.561	12.16	90.96	47.80
19.	22.7	0.989	42.23	29.41	0.547	10.43	99.22	61.80
20.	27.0	1.055	51.17	36.23	0.500	14.65	105.83	53.10

TABLE. 8.

VALVE OPENING: 26.7% OF OUTLET DIA

Atmospheric pressure: 33.25 FT/WATER

LIQUID : PLURACOL SOLN. NO: 4

Sl. No:	Temp. of fluid in rig °C	Rate of flow Cusec	Valve outlet pressure P_2 FT. WATER	Pressure at tapping No:2 below P_2 FT. WATER	Cavitation number K	Reynolds number $R \times 10^{-3}$	Froude Number F	Prandtl number P_r
1.	15.4	0.666	1.86	17.80	0.443	3.52	66.78	129.0
2.	17.0	0.743	7.17	21.32	0.393	4.15	74.55	121.0
3.	19.6	0.784	13.89	22.76	0.451	4.81	78.67	108.8
4.	21.9	0.828	22.69	22.64	0.560	5.44	82.68	98.4
5.	21.1	0.871	24.65	24.41	0.505	5.62	87.36	101.8
6.	24.6	0.937	35.81	24.33	0.584	6.75	94.03	89.2
7.	29.6	0.980	44.04	27.31	0.594	8.31	98.30	75.0
8.	31.5	1.069	54.73	34.24	0.536	9.61	107.24	70.5
9.	15.0	0.630	-3.36	15.62	0.406	3.27	63.15	131.70
10.	16.5	0.670	0.48	17.97	0.397	3.68	67.16	123.30
11.	18.3	0.714	4.71	19.58	0.407	4.19	71.62	114.50
12.	20.1	0.754	10.45	20.74	0.458	4.71	75.62	106.5
13.	22.6	0.801	16.51	21.10	0.508	5.43	80.31	96.0
14.	24.3	0.778	21.93	20.45	0.654	5.56	78.03	90.0
15.	27.8	0.880	27.22	20.12	0.593	7.06	88.23	79.60
16.	23.5	0.949	36.93	24.70	0.580	6.59	95.18	93.0
17.	28.3	0.997	44.56	28.17	0.5707	8.12	100.04	78.20
18.	21.9	0.679	0.55	16.81	0.410	4.49	68.13	98.4
19.	22.4	0.687	5.89	17.93	0.505	4.62	68.94	96.8
20.	25.1	0.770	12.86	18.75	0.520	5.65	77.33	87.80

TABLE. 9

VALVE OPENING: 26.7% OF OUTLET DIA

Atmospheric pressure : 33.25 FT/WATER

LIQUID : PLURACOL SOLN. NO: 5

Sl. NO:	Temp. of fluid in rig °C	Rate of flow cusec	Valve outlet pressure P_2 FT. WATER	Pressure at tapping No:2 below P_2 FT. WATER	Cavitation number K	Reynolds number $R \times 10^{-3}$	Froude Number F	Prandtl number P_r
1.	17.3	0.594	-7.84	12.60	0.405	2.42	59.55	166.0
2.	19.0	0.651	-3.80	15.78	0.359	2.85	65.27	154.5
3.	21.3	0.732	4.66	20.57	0.361	3.49	73.42	141.0
4.	23.6	0.778	11.66	23.17	0.402	4.04	78.07	131.0
5.	26.8	0.832	18.31	24.37	0.441	4.79	83.49	113.0
6.	15.3	0.802	13.98	24.99	0.395	3.01	80.48	183.4
7.	19.5	0.900	26.77	30.98	0.409	4.03	90.33	151.5
8.	24.0	0.965	36.27	31.60	0.465	5.07	96.83	126.5
9.	22.1	0.642	-0.76	16.15	0.440	3.15	64.42	136.5
10.	24.0	0.761	10.71	22.27	0.420	3.99	76.30	126.5
11.	16.7	0.794	11.89	25.41	0.355	3.18	79.69	171.0
12.	21.0	0.858	22.14	28.75	0.410	4.07	86.10	142.8
13.	26.2	0.929	32.79	28.92	0.489	5.25	93.27	116.0
14.	24.4	1.023	44.58	32.02	0.502	5.44	102.68	124.5
15.	17.6	0.747	6.15	22.39	0.344	3.10	74.95	164.1
16.	21.0	0.808	14.82	25.98	0.382	3.83	81.07	142.8
17.	24.4	0.856	22.57	28.17	0.426	4.55	85.86	124.5

of cavitation.

The cavitation parameter K was calculated using the following formula:

$$\text{Cavitation parameter} \quad K = \frac{pm - pv}{\frac{1}{2}\rho Vm^2} \qquad (6.5.1)$$

where pm is the absolute static pressure measured at tapping number 2 of the valve, pv is the vapour of water at the ambient temperature and Vm is the average velocity of fluid at the section where the pressure pm is measured. Velocity Vm was calculated from the flow rate and area Am normal to direction of flow.

During these experiments, the temperature of water varied from 17° to 32°C, thereby producing variations in kinematic viscosity from 0.77 to 1.07 centistokes and from 5 to 6 in Prandtl number. The result is shown in Fig. (6.5.1.1), in which the cavitation parameter K is plotted against Reynolds number for the valve. Reynolds number was obtained using the formula given below

$$\text{Reynolds number} \quad R = \frac{V_v\,(1.\sin\theta)}{\nu} \qquad (6.5.2)$$

where $(1.\sin\theta)$ is the mean hydraulic radius and V_v is the velocity at a section of area A_θ.

In Fig. (6.5.1.1) the results using water fully saturated with air and of water with 40.5% air-content are plotted on the same graph.

The results do not show any noticeable effect of the amount of air-content of water on the inception of cavitation. Two possible reasons can be extended for this conclusion as follows. (1) The

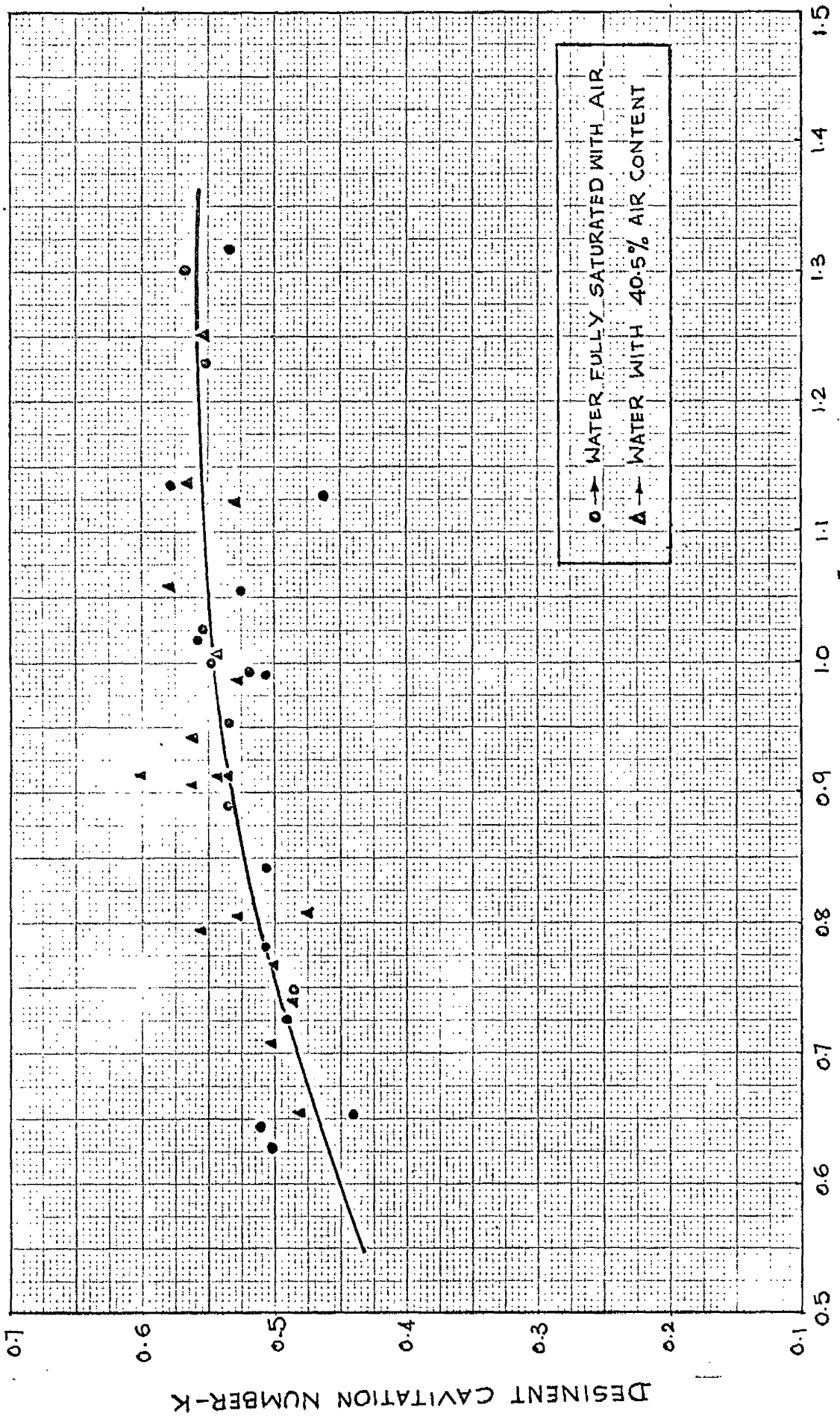

FIG. 6.5.1.1. CAVITATION NUMBER AS A FUCTION OF REYNOLDS NUMBER.

cavitation rig used for the present work does not have a resorber. The water discharged by the valve is directly fed into the centrifugal pump where it is subjected to pressure rise. It is therefore concluded that the water flowing through the valve had always a sufficient number of nuclei to trigger cavitation. (2) It was observed during the tests that the cavitation started initially on the surface of the valve plug. It is therefore concluded that the surface on which the cavitation occurred had a sufficient number of nuclei present or stabilized on the crevices and minute cracks on the surface of the valve plug.

6.5.2 The results of cavitation tests with water and pluracol solutions of different concentration are shown in Fig. (6.5.2.1), with a view to finding out whether there exists a relation between Reynolds and Prandtl numbers with respect to cavitation parameter K. On the graph, the results for various average Froude numbers are represented in different symbols, to show whether Froude number has any special effect on the inception of cavitation. It was not, however, possible to find the effect of Froude number due to the limited number of points. Due to the restrictions of the apparatus, it was not possible to cover an adequate area in the Fig. (6.5.2.1). Therefore, the results in Fig. (6.5.2.1) are divided into three groups as shown. The results in the block 1 have an average Prandtl number of 5.5, while the results in block 3 have an average Reynolds number of 5×10^3. The results in block 2 are neglected since Reynolds and Prandtl numbers vary by

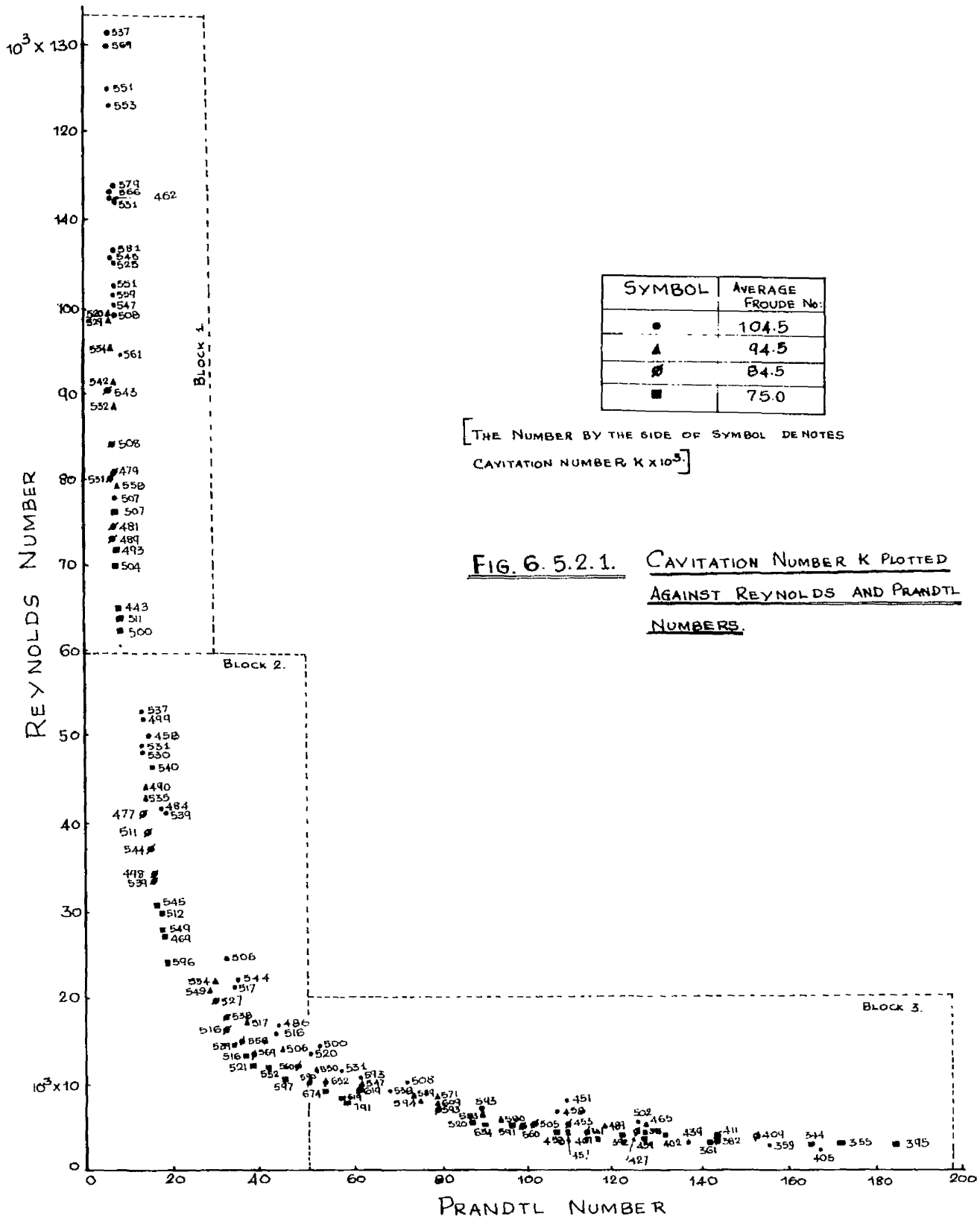

SYMBOL	AVERAGE FROUDE No:
●	104.5
▲	94.5
⌀	84.5
■	75.0

[THE NUMBER BY THE SIDE OF SYMBOL DENOTES CAVITATION NUMBER K X 10^5.]

FIG. 6.5.2.1. CAVITATION NUMBER K PLOTTED AGAINST REYNOLDS AND PRANDTL NUMBERS.

almost equal amounts.

The results in block 1 are shown in Fig. (6.5.2.2). The large scatter of results reflects the complexity of cavitation phenomenon and its physical instability. It must be said however, in connection with the present work that the pressure used in calculating the cavitation parameter was not really the lowest pressure that occurred in the valve and further that the pressure distribution along the surface of the plug might have been entirely different from that along the valve body. It can be observed from Fig. (6.5.2.2) that the cavitation parameter K tends to increase with increasing Reynolds number.

The results in block (3) are shown in Fig. (6.5.2.3). The average Reynolds number for these points is 5×10^3. In this graph the points having average Froude number of 75, 84.5, 94.5, 104.5 are represented in different symbols in order to find out the effect of Froude number, if any, on the inception of cavitation. Due to large scatter of results it is not possible to draw any specific conclusion regarding Froude number effect.

From Fig. (6.5.2.3), however we can conclude in general that the cavitation parameter tends to decrease with increasing Prandtl number. As thermal conductivity k decreases, Prandtl number increases and therefore with increasing Prandtl number the amount of heat transferred to, and causing nuclei to grow, decreases. Since cavitation is essentially on evaporation process, the tendency to cavitate decreases with Prandtl number. This tentative conclusion contradicts the cavitation test results for cold and hot water obtained by other workers in this field, and it is found that tendency for

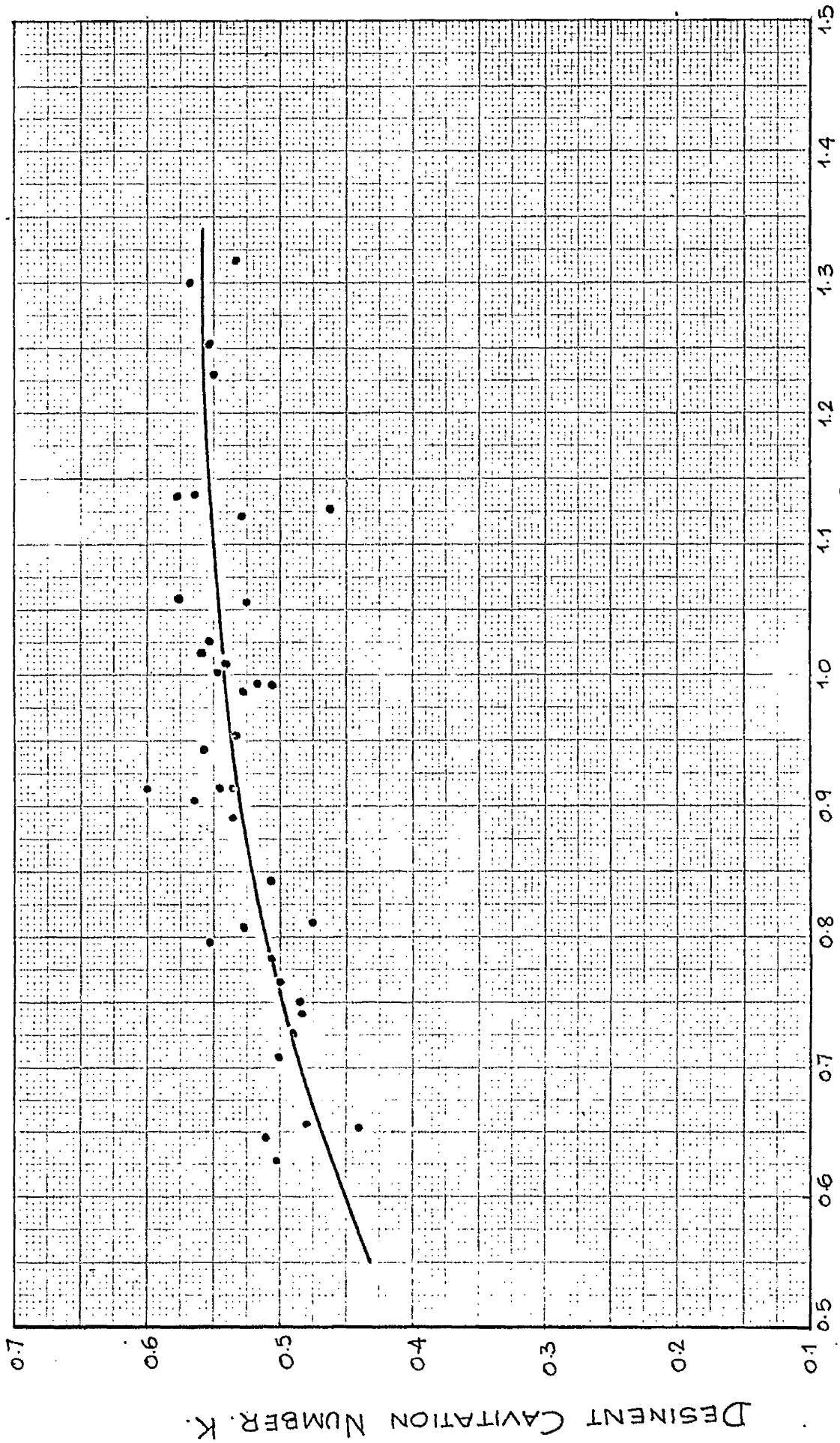

Fig. 6.5.2.2. Cavitation Number As A Function of Reynolds Number.

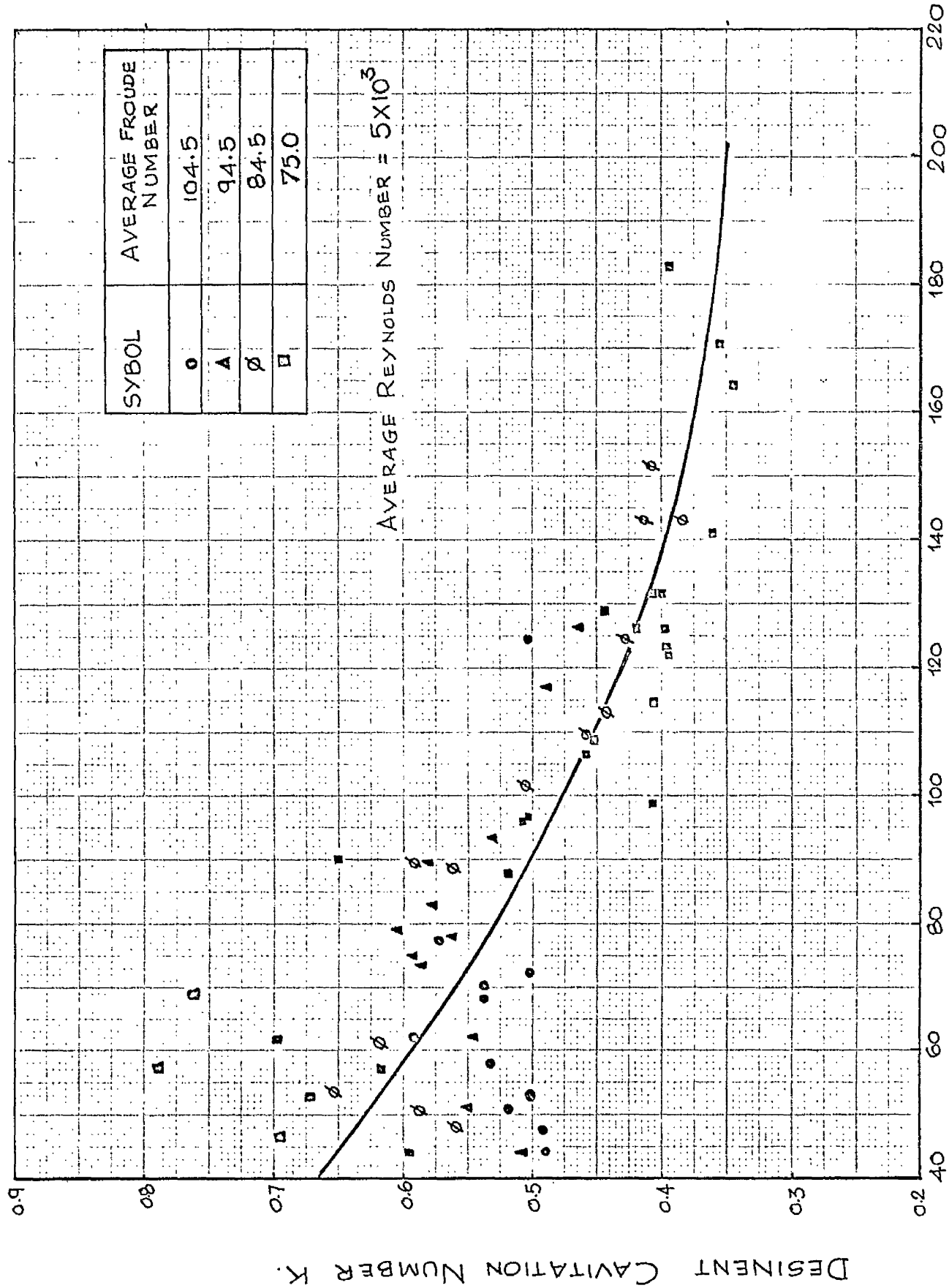

FIG. 6.5.2.3 CAVITATION NUMBER AS A FUNCTION OF PRANDTL NUMBER.

water to cavitate decreases with increasing temperature (Prandtl number decreases). Perhaps the change in Prandtl number is not big enough and the effect of $\left(\frac{\lambda^2}{V^2/2g C_{pl} T}\right)$ becomes important.

6.6 Suggestions for further works

The present cavitation rig has a few defects as mentioned in article (5.12). It is therefore suggested that these draw-backs be eliminated before commencing any further work on the rig. We found the results obtained by the present work were limited. So it is suggested that the present work be continued further so as to obtain more variation in Reynolds number with Prandtl number, in order to cover more area in Fig.(6.5.2.1).

BIBLIOGRAPHY

1. Robertson, J.M. — "Water tunnels for hydraulic investigation", Trans. of A.S.M.E., 78(1): 95-104, 1956.

2. Straub, L.G., Ripken, J.F., Olson, R. — "The six-inch water tunnel at the St. Anthony Falls Hydraulic Laboratory and its experimental use in cavitation design studies," Proceedings of a symposium held at the Ntl. Phy. Lab. on Sep.1955, London.

3. Dailey, J.W. — "The water tunnel as a tool in Hydraulic Research", State University of Iowa, Studies in Engg. Bulletin 31, 1947.

4. Temperely, H.N.V. and Chambers, L.L.G. — "The behaviour of water under hydrostatic tension", Proceedings of Phy. Soc., Vol.58, 1946.

5. Harvey, Newton, E., McElroy, W.D., and Whittey, A.H. — "On cavity formation in water", Jl. of Appl. Phys. 18, 1947.

6. Davies, R.M., Trevena, D.H., Rees, N.J.M., and Lewis, G.M. — "The tensile strength of liquids under dynamic stressing", Proceedings of a symposium held at Ntl. Phy. Lab. Sep. 1955, London.

7. Eisenberg, P. — "On the mechanism and prevention of cavitation" David Taylor Model Basin, Report 712, July 1950

8. Knapp, R.T. — "Cavitation and Nuclei", Trans. of A.S.M.E. Vol.80, 1958.

9. Fisher, C.J. — "The Fracture of Liquids", Jl. of Appl. Phys. 19, 1948.

10. Strasberg, M. — "The influence of air-filled nuclei on cavitation inception", David Taylor Model Basin, Report 1078, May 1957.

11. Epstein, P.S. and Plesset, M.S. — "On the stability of gas bubbles in liquid-gas solution", Jl. of Chemical Phys.18, 1950.

12. Noltingk, B.E. and Neppiras, E.A. — "Cavitation produced by ultrasonics", Proceeding of Royal Society (London), B63, 195(

13. Plesset, M.S. and Zwick, S.A. — "The growth of vapour bubbles in superheated water", Jl. of Appl. Phys.,

14. Plesset, M.S. — "Bubble Dynamics", California Institute of Technology, Report No: 85-23, Feb. 1963.

15. Dergarabedian, P. — "The rate of growth of vapour bubbles in superheated water", Jl. Appl. Mechanics, 20, 1954.

16. Holl. J.W. and Wislicenus, G.F. — "Scale effects on cavitation", Proceedings of A.S.M.E., Jl. of Basic Engg., Sep.1961.

17. Kermeen, R.W., McGraw, J.T. and Parkin, B.R. — "Mechanism of cavitation inception and the related scale-effects problem", Trans. of A.S.M.E., Vol.77, 1955.

18. Gerber, H. — "Some reflections on model scale formulae for cavitation phenomena", Proceedings of a symposium held at Ntl. Phy. Lab. on Sep. 1955.

19. Shal'ner, K.K. — "Cavitation of surface roughnesses", David Taylor Model Basin, Translns. 259, Dec. 1955.

20. Holl. J.W. — "The inception of cavitation on isolated surface irregularities", Trans. of A.S.M.E. Series D, Jl. of Basic Engg., Vol.82, 1960.

21. Danel, P., Duport, J. — "The selection of length and head scales for cavitation tests", Trans. of A.S.M.E., Jl. of Basic Engg., Vol.82, 1960.

22. Dailey, J.M. and Johnson V.E. — "Turbulence and boundary layer effects on cavitation inception from gas nuclei", Proceedings of a symposium held at Ntl. Phy. Lab on Sep.1955, London.

23. Milne-Thomson, L.M. — "Theoretical Hydrodynamics", MacMillan & Co.Ltd. 1955.

24. Holl, J.W. and Treaster, A.L. — "Cavitation Hysteresis", Trans. A.S.M.E., Paper No.65-FE-9.

25. Crump, S.F. — "Determination of critical pressure for the inception of cavitation in fresh and sea water as influenced by air content of the water", David Taylor Model Basin, Report 575, Oct.1949.

31. Williams, E.E. and McNulty, P. "Some factors affecting the inception of cavitation", Proceedings of a symposium held at Ntl. Phys. Lab., on Sep. 1955, London.

32. Kanellopoulos, E.V. "Cavitation Tests on a small centrifugal pump", Ntl. Engg. Lab., Fluid Mechanics Division, Report No.95, Dec.1960.

33. Stahl, H.A. and Stepanoff, A.J. "Thermodynamic aspects of cavitation in centrifugal pumps", Trans. of A.S.M.E., Vol.78, 1956.

34. Jacobs, R.B. "Prediction of symptoms of cavitation", Jl. of Research of the Ntl. Bureau of Standards, Engg. and Instrn, Vol.65C, No.3, July,-Sep.1961.

35. Boretz, J.E. "Use of cavitation tendency ratio for predicting suction specific speed, AIAA Journal, Vol.1, No.2, Feb.1963.

36. Reilly, J. and Rae, W.N. "Physico-Chemical Methods", Volume I., Fifth Edition, Methven & Co. Ltd., London.

37. Lawrie, J.W. "Glycerol and the glycols, Production, Properties and Analyses", American Chem. Society Monograph, No.44 (1928).

38. Glasstone, S. "Text book of Physical Chemistry".

39. Tetlow, N. "A survey of Modern Centrifugal Pump Practice for oilfield and oil refinery services", Proce. of Institution of Mech. Engrs. 1942.

40. Firth, D. and Young, L. "Some model experiments on special control valves", Proc. of Institution of Mech. Engrs. Vol.168, No.13, 1954.

41. Singh, D.N. "A manometric piston gauge", Fluids Report No.66 Mech. Engg. Research Lab., D.S.I.R. (London), Feb.1958.

42. Kanellopoulos, E.C. "New method for measuring the gas content of water", Mech. Engg. Research Lab., Fluids Report No.69, 1958.

LIST OF TABLES AND FIGURES